UCLouvain

École polytechnique de Louvain

Optimization methodology to dimension a CCU (carbon capture and utilisation) chain by maximizing the cost efficiency of the infrastucture

Author: **Julien Duquenne**
Supervisor: **Emmanuel De Jaeger**
Readers: **Emmanuel De Jaeger, Jim Gripekoven, Patricia Luis Alconero**
Academic year 2021–2022
Master [120] in Electro-mechanical Engineering

Contents

Abstract

Carbon capture and utilisation (CCU) technologies will likely become an important approach for CO_2 emissions mitigation in the heavy industry sector. However, due to the high investment risk and cost, the technology has not yet been commercialised. The more established technology of CCS, rather similar to the one of CCU, is nowadays already proposed thanks to a higher R&D background. Therefore, CCU still needs more research in order to unlock its full potential. Actively mitigating the CO_2 emissions, as done by the CCS, while going a step further by utilising this carbon dioxide as carbon source in various sectors (e-fuels synthesis, construction materials, chemical industry, etc.).

The document, here, focuses on the use of CCU for Power-to-Fuel applications, more specifically it compares several production routes and their different components to determine the advantages and drawbacks of each, focusing on their global efficiency, selectivity and operability. Simulations have been also realised. They allow to compare the previously studied routes on their yearly production capabilities when powered only by renewable (PV).

The goal of this document is to provide a preliminary study, based on the literature, of different CCU routes for Power-to-Fuel application in order to extract those that would be most conducive to potential future research as well as the one to avoid. The final results of the research and simulations are available in tables at the end of the document: Table III for the table resuming the different characteristics of efficiency, selectivity and operationability and Table 25 the simulation results.

Introduction

Today, no one can deny the harmful effects of global warming on the planet. The Paris Agreement (December 2015) reported the importance to limit anthropogenic global warming to well below 2°C and to pursue efforts towards 1.5°C. To do so, stepping away from fossil fuel in favor renewable energy sources seems to be the solution.
Although, in the last decade, the share of renewable energy has increased significantly. It still remains minor compared to the use of fossil fuels. In the coming years, CO_2 will remain a dominant topic since there is still a long way towards our independence from fossil fuels (in the transportation and electricity generation sector mostly). Besides, some of the heavy industry sector could not be able to totally avoid CO_2 production based on the nature of their activities (cement and steel manufacturing, for example). Therefore, the renewable alternative alone will not be sufficient to reach the target set by the Paris Agreement; other solutions, in the short and medium term, must be found to deal with unavoidable CO_2 emissions.

Among numerous solutions, CCU/S (Carbon Capture and Utilisation/Storage) can be an essential technology to decarbonise the sectors of heavy industry that emit hard-to-abate CO_2 emissions and reach CO_2 emissions targets.
Often, terms of CCS and CCU are often confounded, but Carbon Capture and Storage (CCS) and CCU are two distinct concepts; CCS technologies capture CO_2 and store it into geological formations for long-term storage underground. CCU does not store CO_2 but utilises it as a raw material to produce other goods or services. The two main CCU pathways are, first, the direct use which does not alter the CO_2 molecule which is, for example, used in CO_2-enhanced oil recovery or in fertilisers and, after, the indirect use or conversion of CO_2 which recycle it into products such as low-carbon fuels and building materials (utilisation), or permanently sequestering it in deep underground geologic formations (storage). Therefore, CCUS achieves mitigation via emissions reductions, avoidance, and/or negative emissions.
In general, however, CCU is less advanced in its deployment and maturity than CCS, and therefore requires continuing R&D support.

It is with that purposing mind that this document was written. This document will focus on the CCU chains for a Power-to-Fuel application. This type of chain is composed of two main elements:

- CO_2 capture and syngas production part
- Syngas conversion to hydrocarbon and upgrading part

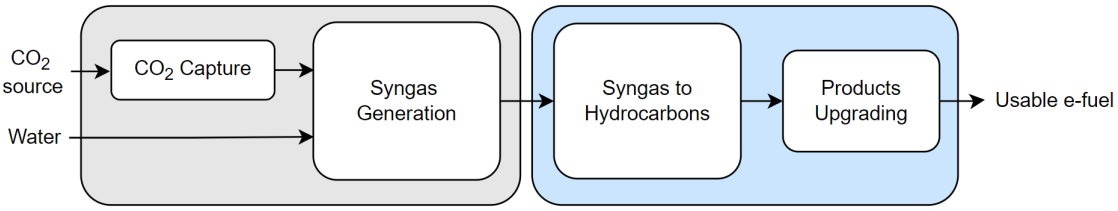

In the study of Power-to-Fuel, different production ways are possible. This document was written with the objective of evaluating some of these ways of e-fuel synthesis based on their respective energetic efficiency, products selectivity, and operability. Therefore, this report will go through the different technologies available for the syngas (mixture of H_2 and CO_2) generation and e-fuel synthesis and how the different parameters involved in these processes influence their performances. This document will also present a simulation of those Power-to-Fuel pathways comparing their production capabilities over a year, based on renewable sources.

Part I

Syngas generation

1 Carbon dioxide (CO_2) capture

Carbon dioxide (CO_2) is a significant greenhouse gas that is largely blamed for global warming. Its main sources of production come from fossil fuels (for electricity generation, transportation, etc) and from large industries (cement production, iron factory, etc). In the foreseeable future, those sources are still expected to play an important role, releasing still more and more CO_2 in the atmosphere. Therefore, solutions to reduce the CO_2 concentration in the atmosphere are necessary to limit the overall global warming and its consequences [1] [2]. A step in this direction can be made by the implementation of carbon capture technologies. Their implementation to existing power plants or facilities can be considered a possible way for short to medium term interventions to reduce CO_2 emissions.

In this section, several techniques of carbon dioxide capture will be presented, this capture can either be operated from industrial waste gas stream, in which case it called point source capture, or it can be operated directly from the atmosphere by a process of direct air capture. Capturing from point source is, in general, easier and cheaper than directly capturing from air since the concentration of CO_2 is way higher (around 0.04% [3] compared to several percent in industrial processes flues gases). However, although it is more expensive and difficult, the direct air capture would allow to operate in a carbon positive way, actively removing CO_2 from the atmosphere where the point-source capture method may only achieve at best carbon neutrality.

1.1 Different approaches to CO_2 capture

There are three major approaches for carbon capture in the industry sector: pre-combustion capture, oxy-fuel process, and post-combustion capture [2].

The *pre-combustion capture* involves the non-complete combustion of a fuel with oxygen or air to produce a gas mainly composed of carbon monoxide (CO) and hydrogen (H_2), also called syngas. The syngas reacts then with steam in a catalytic reactor (shift converter) to produce CO_2 and more hydrogen. At the outlet of the reactor, the CO_2 rich mixture can pass through a separator to produce, on one side, a hydrogen-rich gas and, on the other side, the separated CO_2.

For the *capture in oxy-fuel combustion*, nearly pure oxygen is used for the fuel combustion instead of ambient air. Resulting flue gases are therefore mainly composed of CO_2 and water which can be easily separated using a condenser. Besides having only CO_2 and water in the exhaust stream, another advantage of this combustion is that the resulting flame temperature is higher than when using air since the heat released is less diluted in the process. However, the major disadvantage of oxy-fuel combustion is the large electric power requirement and cost associated to the separation of oxygen from air, using an electrolysis process or buying the oxygen.

In *post-combustion capture*, the separation of CO_2 from the rest of the flue gases is operated after the air-based combustion. This capture approach is interesting since it requires no change to the initial combustion process and can also be used in other sectors like the cement or steel industry, producing large amount of CO_2, most of which not from a combustion process. The major drawback however is the relatively low concentration of CO_2 present in the exhaust gases. Indeed, in most cases, CO_2 is diluted with inert gases such as nitrogen, argon, and water in addition to oxygen. Its concentration varies depending on the process upstream [2]:

- air/coal combustion: 12-15 mol-% CO_2
- air/natural gas combustion: 3-4 mol-% CO_2
- oil refining: 8-9 mol-% CO_2
- cement production: 14-33 mol-% CO_2
- iron and steel production: 20-44 mol-% CO_2

1.2 Separation technologies

When comparing the three approaches for CO_2 capture, it is clear that post combustion capture is the most important to alleviate the CO_2 production in the industry since it offers the most flexibility and does not impact the combustion/production cycle upstream of the separation. If the capture plant shuts down, the plant can still operate. The major disadvantage of this method is the poor state at which the flues gases enter the separation unit (in terms of pressure and CO_2 concentration).
Four primary approaches aimed at CO_2 separation from flue gases are currently available: absorption (including chemical and physical absorption), adsorption, separation membranes and cryogenic processes.

1.2.1 Membranes

Membrane separation methods for CO_2 recovery represent a continuous, steady-state, clean and simple process with a low energy requirement. This separation process is driven by pressure, to push the gases through the different separation membranes.
In post-combustion capture, the driving force for the separation process using membrane is often low (low pressure and low CO_2 concentration). To increase the performance of the separation process, membranes are usually stacked with recycling streams to compensate the low CO_2 separation capabilities. This leads to higher complexity and energy consumption since the pressure, at which the gas enters the process, must be higher (or a re-compression stage must be added to overcome the pressure losses). The energy required by the membrane separation process depends on several parameters: the targeted CO_2 purity, the flue gases composition (concentration of CO_2), and the membrane selectivity (hence the number of membranes to use then the amount of head loss to compensate).
Membrane separation processes have several advantages over other CO_2 separation technologies; the equipment used for the separation is very simple, compact, easy to operate and can easily be scale-up. However, this process is not very useful for large flow rate application and could require a lot of energy depending in the flue gases composition and the purity of CO_2 wanted. Also, depending on the membrane used, the process may not be very efficient to filter out the SO_x and NO_x.
Required specifications for membrane in the use case of post combustion are the following:

- High CO_2 permeability,
- High selectivity for CO_2 from flue gases,
- High thermal and chemical stability
- Resistant to aging

Many efforts have been made to find the right material for post-combustion membrane separation. For now, several membranes are used: the inorganic membranes (porous and dense), the polymeric membranes, the mixed matrix membranes and the hollow fiber membranes (example of membranes operating point and selectivity are listed in the table 6 of [2]).

1.2.2 Absorption

CO_2 absorption refers to the uptake of CO_2 into the bulk phase of another material. In a post combustion capture absorbent process, the flue gases are dissolved in a solvent (bulk phase). The solvent typically contains a reagent that selectively reacts with CO_2, actively transferring CO_2 from the gas to the liquid phase.
After the absorption, the CO_2-loaded solution is fed into a heating element, increasing the temperature of the solution. Then, the solution is sent to a stripper column to liberate gaseous CO_2. The lean solution is then cooled and recycled back to the absorber while the gaseous CO_2 is collected at the top of the stripper column.

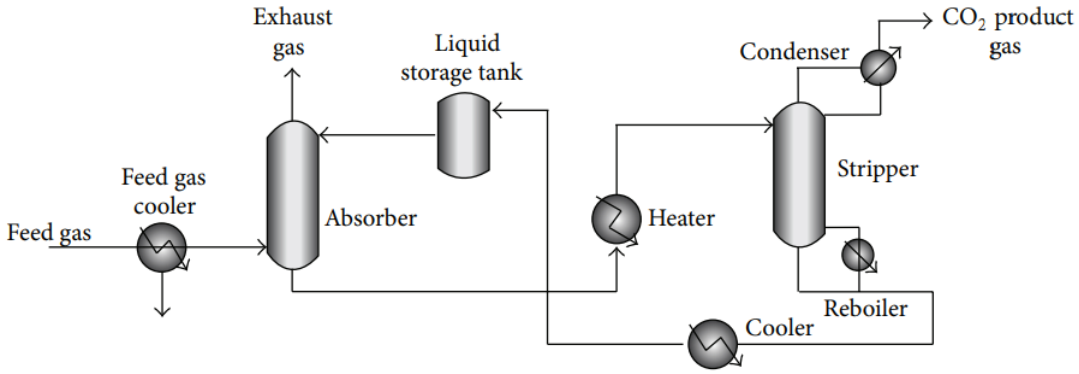

Figure 1: Schematic diagram of CO_2 absorption plant [2]

The energy consumption of such separation technique depends on the solvent used during the process. The nature of the solvent determine the amount of CO_2 that can be processed per unit mass of solvent and the energy requirement for the stripping of CO_2 at the regeneration stage. The absorbent should have a suitable capacity for CO_2 absorption with a high kinetic rate of absorption, negligible vapor pressure, and high chemical and thermal stability.
Solvents used for CO_2 absorption can be separated in two categories; the physical and chemical solvents (example and performances of different solvent for the CO_2 absorption are listed in table 2 of the document [2]).

1.2.3 Adsorption

Adsorption refers to the uptake of CO_2 molecules onto a the surface of another material. Adsorption has the advantage, compared to absorption, the regeneration energy is lower since the heat capacity of the solid sorbent is lower than the one of the liquid solvent. However, this technology suffers from some disadvantages: it is susceptible to attrition, the sorbent has often a large volume due to low volumetric adsorption capabilities, and, the thermal management of large adsorber vessel can be complex.
It exists two types of adsorption approaches; the physisorption in which the adsorption occurs via weak Van der Waals forces, and the chemisorption which uses stronger covalent bonding [4]. The major physical adsorbent suggested for CO_2 adsorption includes activated carbons and inorganic porous materials such as zeolites while chemical adsorption uses metal oxides (CaO, MgO, etc), metal salt and hydrotalcites as adsorbent material [2].

Adsorption processes are implemented with the adsorbent either used in a packed bed or fluidised bed configuration. In packed bed, the flue gases flow through the adsorbent particles, the gas makes is way up the column while the CO_2 molecules are adsorbed onto the particle surfaces. In fluidised bed, flue gases flow inside the column at velocities such that the adsorbent particles are suspended in the gas flow, while being suspended, the particles adsorb the CO_2 molecules onto their surface.

Regardless of the adsorption technology, the regeneration process is the same, either by lowering the pressure (pressure swing adsorption) or by increasing the temperature (temperature swing adsorption) to allow CO_2 molecules to escape. By carefully alternating the regeneration and adsorption between two identical reactors, the overall process can be operated continuously [4]. On the next figure are shown both different techniques of regeneration:

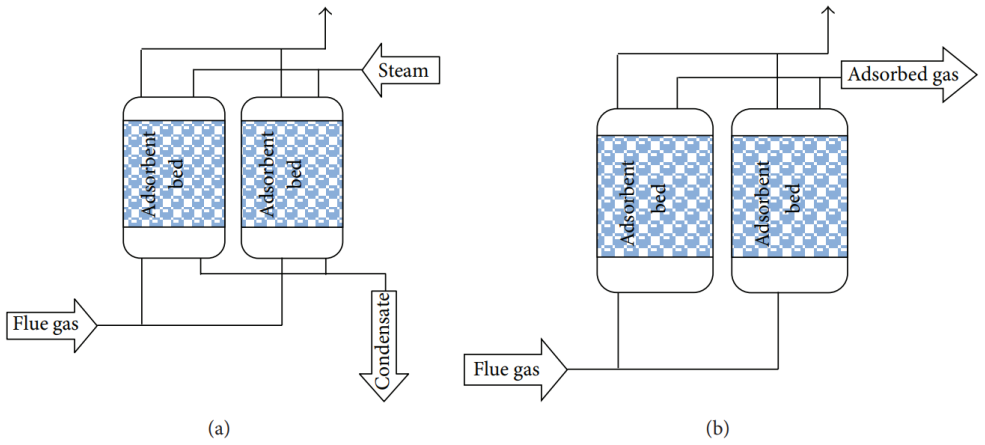

Figure 2: Schematic diagrams of the (a) TSA adsorption cycle and (b) PSA adsorption cycle [2]

1.2.4 Cryogenic separation

The cryogenic method of separation utilises low temperatures for condensation, separation and purification of CO_2 from flue gases. This process uses a series of compression, cooling and expansion steps to separate the different components of the gases. This separation process enables the direct production of liquid CO_2, with high purity, that can directly be stored or transported. Moreover, the process is relatively straight forward, involving neither solvent nor other components and is easily scalable. However, the major drawback of this technology is the amount of energy required by the different compression and cooling units (energy consumption is often in the order of the MJ/kg_{CO_2}).

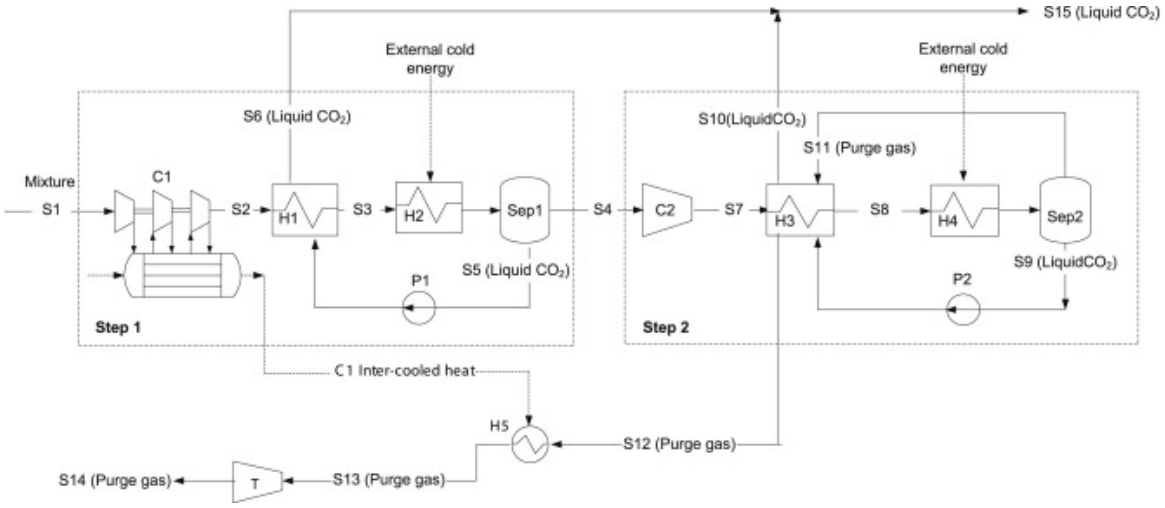

Figure 3: CO_2 cryogenic liquefaction and separation system [5]

The initial pressure and concentration of the mixture have significant effects on the system performance, the lower the initial pressure and the lower the CO_2 concentration, the more the separation process will consume energy [5]. Indeed, compressing the gas mixture to an appropriate pressure of 30 to 80 bar is necessary to maintain the CO_2 condensation temperature at a relatively high level (above 45 °C). The higher the initial pressure, the less substantial the compression work, which leads to the decrease in the energy penalty for CO_2 capture.

For this reasons, the cryogenic CO_2 capture technique is mainly used for the purification of streams that already have a high CO_2 concentration (above 50%), for example, when combined with other capture techniques.

2 Water electrolysis

2.1 Thermodynamics of the reaction

Water electrolysis is the electrochemical mechanism responsible of the water molecule splitting into hydrogen and oxygen by supplying it by electrical and thermal energy. The overall reaction can be written as follow:

$$H_2O \Rightarrow H_2 + \frac{1}{2}O_2 \tag{1}$$

The energy demand of the reaction is given by the heat of the reaction (ΔH), which can be split into the heat demand (ΔQ) and the electrical demand (expressed via the change in free Gibs energy ΔG)

$$\Delta H = \Delta Q + \Delta G \tag{2}$$

The electrolysis process is highly dependent of the temperature at which it is operated. It is either operated at low temperature (50-90°C), in this case, almost all the energy required for the reaction (ΔH) must be provided by electricity, or, it can be operated at high temperature (>650°C) where a big part of the energy for the reaction is provided by heat. Indeed, as seen in Fig.4, with the increasing electrolysis temperature, the overall energy demand ΔH decreases, up to the point of buoyancy (100°C at 1 bar) at which ΔH will start to slightly increase as the temperature of the reaction increases. The jump in energy required around 100°C is due to the latent heat of vaporisation of water, already provided if the water is in the vapour state. After this point, as the temperature of the steam increases, the overall energy demand stays almost constant while the electrical energy demand ΔG will significantly decrease balancing the increase of heat requirement of the reaction ΔQ. Therefore, over 100°C, the more heat is provided to the cell, the less electricity is required by the electrolysis reaction.

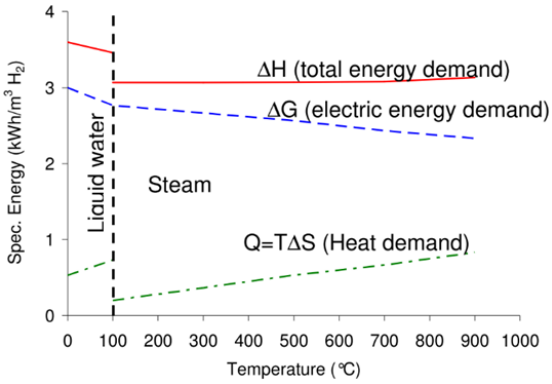

Figure 4: Energy demand of water electrolysis as a function of the temperature [6]

The minimum voltage required to proceed to the electrolysis reaction is called the reversible voltage (V_{rev}). It is defined by the following equation:

$$V_{rev} = \frac{\Delta G}{zF} \tag{3}$$

With ΔG the Gibbs free energy of the reaction, F the Faraday constant equal to 96 485 C/mol and z is the number of charges in the reaction, which in the case of a water electrolysis is 2. Accordingly with what as been explained above, this voltage decreases with temperature and lies in the range of 1.25 to 0.91V for temperature changing from 0 to 1000°C. However, this relation does not take into account the heat integration and is therefore ideal. In order to have a better representation of reality, the losses related to entropy must be added. Indeed, when water is splitting into oxygen and hydrogen, some entropy is generated. Therefore, it is more suitable to employ the enthalpy ($\Delta H = \Delta G + T\Delta S$) in place of ΔG for the electrolysis voltage calculation. The electrolysis voltage is known as the thermoneutral voltage and can be expressed as:

$$V_{th} = \frac{\Delta H}{zF} \tag{4}$$

This voltage means that all the energy required for the electrolysis is supplied electrically (including heat). In the case of a water electrolysis, V_{th} ranges from 1.47-1.48V, when operating below 100°C, to only 1.26-1.29V, for steam between 100 and 1000°C.

While thermoneutral voltage represents the standard operation voltage for high temperature electrolyser, low temperature electrolyser such as alkaline and PEM (see in section 2.2/2.3) is operated above this voltage due to internal losses or overvoltages. This extra energy supply results in heat generation by the cell which could lead to temperature increase inside the module hence degradation; an external cooling system is sometimes required. The cell voltage can be expressed as the sum of the reversible voltage for the reaction and the overvoltages caused by non-idealities:

$$V_{cell} = V_{rev} + V_{act} + V_{diff} + V_{bub} + V_{ohm} \tag{5}$$

Overpotentials are, respectively, the activation voltage, the diffusion voltage, the bubble voltage and the ohmic overpotential.

The quantity of hydrogen produced by an electrochemical process can be written using the Faraday's law where m is the mass of gas produced, Q is the total electric charge passed through the substance in Coulombs, F is the Faraday constant (in C/mol), M is the molar mass and z is the number of electrons transferred in the process:

$$m = \frac{Q}{F} \times \frac{M_{H_2}}{z} \tag{6}$$

In ideal conditions, the charge Q passing through the electrolysis cell is directly proportional to the amount of hydrogen produced, and, in case of water electrolysis, for each mole of hydrogen produced two electrons ($z = 2$) are released in the circuit. The electric charge Q can be linked to the current via the relation:

$$Q = I \times t \tag{7}$$

From those equation (eq.6/7), the theoretical hydrogen output by unit time of an electrolyser cell can directly be calculated:

$$m_{H_2} = \frac{I \times M_{H_2}}{2F} \tag{8}$$

Therefore, according to Faraday's law, in an ideal electrolysis, the current is directly proportional to the production of hydrogen. However, in a real electrolysis process, non-idealities (such as parasitic current and mass flow losses) within the cell are present. To account for these losses, the electrolysis model must be extended by the Faradaic efficiency (η_F), defined as the ratio of actual to theoretical hydrogen production rate.
The global electrolyser cell efficiency can be written based on the Higher Heating value (HHV) of hydrogen (equals to 3.54kWh/Nm^3):

$$\eta_{HHV} = \frac{\dot{m}_{H_2} \times HHV_{H_2}}{P_{el}} = \frac{\eta_F \times \frac{n_{cell} I}{2F} \times HHV_{H_2}}{n_{cell} V_{cell} I} = \frac{1.48}{V_{cell}} \times \eta_F \tag{9}$$

This efficiency is often used for the low temperature electrolyser since the higher heating value corresponds to the enthalpy of reaction, in standard conditions, from liquid water to gaseous hydrogen. The efficiency of the process can also be written based on the Lower Heating value (LHV), this efficiency value is often used to compare different industrial processes:

$$\eta_{LHV} = \frac{\dot{m}_{H_2} \times LHV_{H_2}}{P_{el}} = \left(\frac{LHV}{HHV}\right)_{H_2} \times \eta_{HHV} = \frac{1.25}{V_{cell}} \times \eta_F \tag{10}$$

In either case, the efficiency of the electrolysis process is inversely proportional to the cell voltage and sensible to several other parameters:

- It decreases with rising current density
- It increases with increasing temperature
- It decreases slightly with increasing pressure

2.2 Alkaline electrolyser

The alkaline electrolysis of water represents an industrially mature technology used since the beginning of the 20^{th} century and is currently used for large scale hydrogen production (up to a MW scale). [7]

This type of electrolyser is characterised by its two electrodes operating in a alkaline electrolyte solution of KOH or NaOH (with an electrolyte concentration 20-30%). Both electrodes are separated by a diaphragm, used for the separation of the produced gases and the transfer of the hydroxide ions OH^- from an electrode to the other. This diaphragm is also non-conductive to electrons which prevents electrical shorts between electrodes while allowing small distances between them. The cells electrodes are typically composed of a Ni-based metal given that nickel is resistant to corrosion in the alkaline media and is relatively low cost. Other metals can be used as additives to the electrodes: cobalt is used at the anode side while iron and vanadium, for example, are used on the cathode side.
At the cathode, the electric current is used to dissociate water molecules into H^+ and OH^-, the H^+ ions will go through a reduction process in the electrolyte bath and combine to form H_2 molecules in gaseous form. The hydroxyl ions (OH^-) will be transferred under the influence of the electrical circuit from the cathode to the anode through the porous diaphragm, where they will undergo a reduction forming ½ molecule of oxygen (O_2) and one molecule of water (H_2O). The O_2 recombined at the surface of electrode escapes as does hydrogen on the other electrode. The produced gas quality after drying is typically in the range of 99.5–99.9% for H_2 and 99–99.8% for O_2 [7]. The electrochemical mechanism is shown in the next figure:

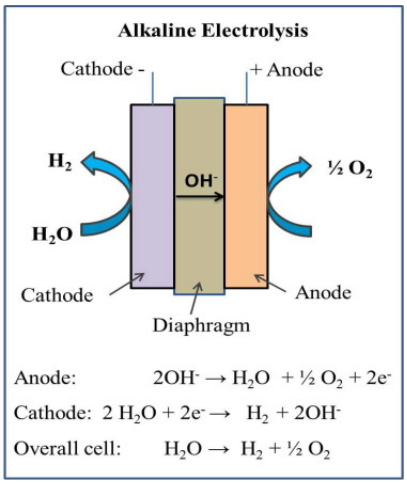

Figure 5: Schematic of an alkaline electrolysis cell [8]

Alkaline electrolysis cells are commonly operated under a voltage range of 1.8 to 2.4V and at relatively low current density of around 0.2-0.4A/cm^2. The operating temperature conditions of the cell are between 60 and 90°C while stack pressure can go as high as 30 bar.
To give an idea of what is used in the industry, an overview of the characteristic I-V curves for alkaline electrolysis from literature is shown here after (Fig.6):

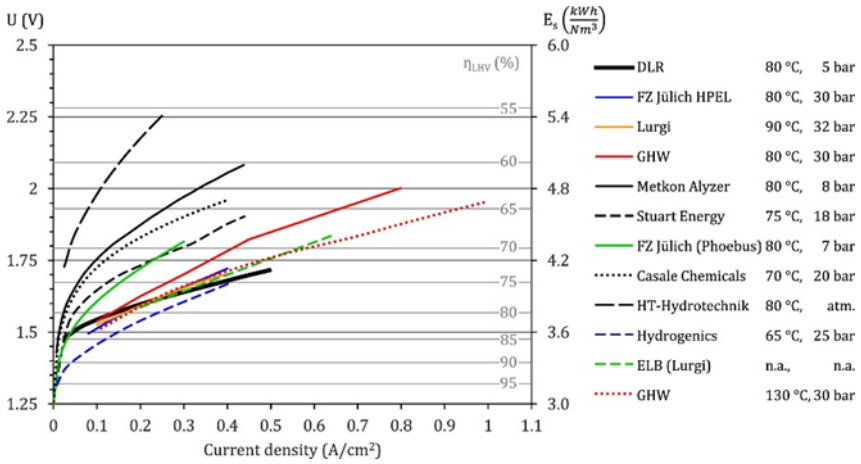

Figure 6: Overview of characteristic I-U-curves of alkaline electrolysis from literature [7]

2.3 Proton Exchange Membrane electrolysis

The Proton Exchange Membrane or Polymer Electrolyte Membrane electrolysis (PEM) was first introduced in the 1960s by General Electric with the goal to overcome the drawbacks of the alkaline electrolysis technology. The PEM electrolyser uses a solid polymer electrolyte (SPE) that is responsible for the conduction of protons, separation of produced gases, and electrical insulation of the electrodes. In PEM electrolysis, water is electrochemically split into hydrogen and oxygen at their respective electrodes (hydrogen at the cathode and oxygen at the anode). [8]

The PEM electrolysis is operated by pumping water to the anode where it is spilt into oxygen (O_2), hydrogen ions (H^+) and electrons (e^-). Hydrogen protons travel via proton conducting membrane to the cathode side. Electrons exit from the anode through the external power circuit, which provides the driving force (cell voltage) for the reaction. At the cathode side, hydrogen ions and electrons re-combine to produce hydrogen. The mechanism is shown on the next figure:

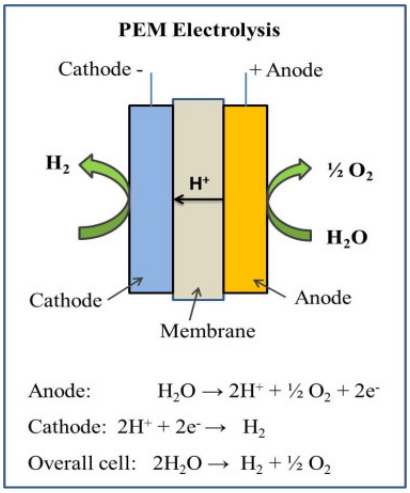

Figure 7: Schematic of an PEM elctrolysis cell [8]

The polymer electrolyte membrane is responsible for a highly pure hydrogen yield, typically greater than $99.99\%_{H_2}$ after drying. Also, due to the solid electrolyte and the high current density, the PEM electrolysis features compact design, support high pressure operations, and allow a high differential pressure between the oxygen and hydrogen side thanks to its structural properties.

The state-of-the-art electrocatalysts for PEM electrolysis uses noble metals such as Pt/Pd (at the cathode) and IrO_2/RuO_2 (at the anode), making them very expensive compared to other technologies. The membrane is made, as its name indicates, of solid polymer, one of the most used is the fluoropolymer (PFSA) Nafion [9]. Most of the PEM electrolysers operate under high current density, in the range of 0.6 to 2A/cm^2 and at a cell voltage between 1.8 to 2.2V. The cell operating temperatures are like the one of the alkaline electrolysers, around 50 to 80°C while the operating pressures depend on the use case of the electrolyser, but it can go as high 200 bar.
An overview of the characteristic curves I-U of what has been tested in the literature in shown in the figure here after (Fig.8):

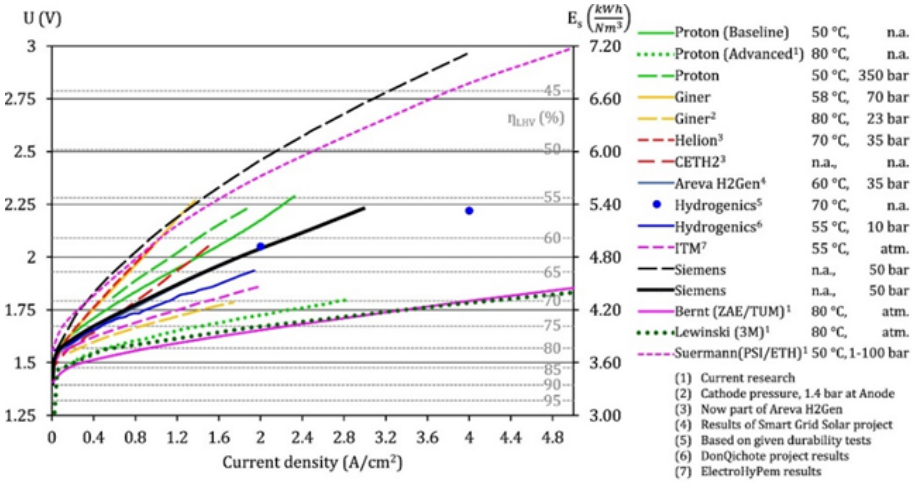

Figure 8: Overview of characteristic I-U curves of PEM electrolysis from literature [7]

2.4 Solid Oxide Electrolyte Cell

A Solid Oxide Electrolyser Cell (SOEC) is a solid oxide fuel cell running in regenerative mode to achieve the electrolysis of water. In this technology, the electrolyte is a solid material which, at high temperature (around above 600°C), starts to conduct oxide ions while remaining impermeable to the steam and the hydrogen gas. SOECs are available in a wide range of structural design (electrolyte-supported, metal-supported, ceramic electrode supported) and in different form factors (tubular, planar,). However, the general characteristics of the technologies remain the same: cells are combined in series to form stacks via metallic interconnections, providing electrical transfer, gas separation between the different cells as well as gas distribution across the cells. Then, the stacks are assembled into modules which are, in turn, combined into SOEC plants making the technology easily scalable.

The working principle of this kind of cell is the following: steam is fed into the porous cathode. When a sufficient voltage is applied between the electrodes, the steam at the cathode-electrolyte interface, is reduced to H_2 and oxygen ions (O^{2-}). the hydrogen gas diffuses back up through the cathode before being collected at its surface, while the oxygen ions are conducted through the electrolyte. The electrolyte must have sufficiently good selectivity to avoid hydrogen passing through, leading to recombination of H_2 and O_2. At the electrolyte-anode interface, the oxygen ions are oxidised to form pure oxygen gas, which is collected at the surface of the anode.

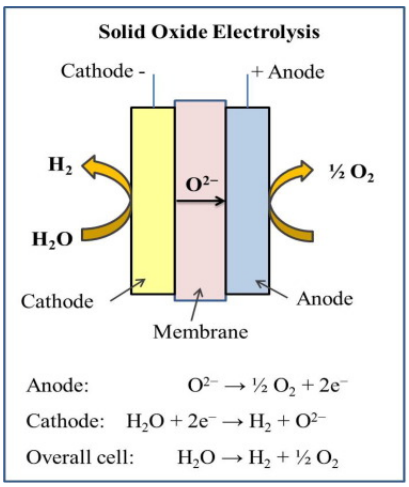

Figure 9: Schematic of a SOEC [8]

The cell operates between 650°C and 1000°C at pressure up to 20 bar. In most cell designs, the majority of the cell comprises either yttria-stabilized zirconia (YSZ) for electrolyte-supported cells, or a composite of metallic Ni and YSZ for fuel electrode (cathode) supported cells. YSZ is a solid solution of few mole-% yttria (Y_2O_3) in zirconia (ZrO_2) which are abundant material making them easily available [10]. On the other hand, the anode electrode is made of Lanthanum strontium manganate (or LSM) [11].

SOEC electrolysis is operated at high temperature, meaning that, as explained in section 2.1, this technology uses less electricity than the others. Its current density is, in average, between 0.3 and 2A/cm^2 and its operating DC voltage can vary between 0.7 and 1.5V. This technology is operated at high temperature because those conditions favour the thermodynamics and kinetics of the reaction. The thermodynamic conditions are more favourable in the sense that the molar Gibbs energy of the reaction (ΔG) drops from 1.23 eV (237 kJ/mol) at ambient temperature to 0.95eV (183kJ/mol) at 900°C, while the molar enthalpy of the reaction (ΔH) remains essentially unchanged ($\Delta H \approx$ 1.3eV or 249kJ/mol at 900°C), as seen on Fig.4.

SOEC electrolysis can be operated in three different modes:

- *Thermoneutral mode*, in which the electrical input is equal to the total energy demand, the heat demand "Q" necessary for the water splitting equals the heat released by the joule losses within the cell. The electrical to hydrogen conversion efficiency is 100%.
- *Endothermal mode*, the electricity energy supplied to the cell is below the enthalpy of the reaction, the cell voltage is below the thermoneutral one. Therefore, external heat must be supplied to the system to maintain the required temperature and pre-heat the inlet gas. Hence this mode operates at an electricity to hydrogen conversion efficiency above 100%. Also, this mode offers the lowest degradation rate of the three since it operates at the lowest current density.
- *Exothermal mode*, the opposite of the endothermal mode, where the electricity energy supply exceeds the enthalpy of the reaction, creating additional heat. This heat generated by the cell can be used in the installation for preheating inlet gas or must be handle by an external cooling system. This mode has the advantage of operating at higher current density than the other two, potentially reducing the size of the system (more current translates to higher production rates). However, this higher current could be a source of prematurely ageing of the components. The efficiency of this operation mode is below 100%.

To give an idea of what has been studied in the literature, an overview of the characteristic I-V curves for solid oxide cell electrolysis is shown here after (Fig.10):

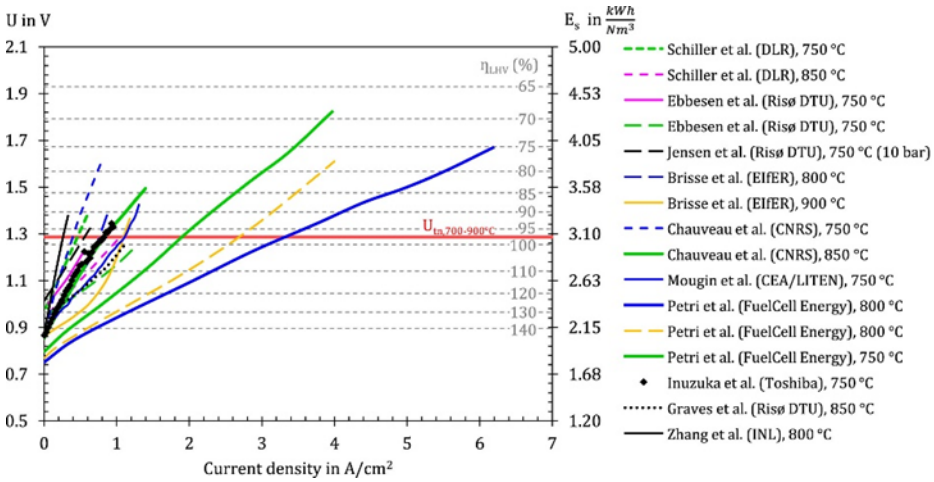

Figure 10: Overview of characteristic I-U-curves of solid oxide electrolysis from literature [7]

The graph shows that most SOEC cell are operated below 1A/cm^2. This is mainly due to degradation issues. Exceptions are made, notably by Petri et al. (Fuel Cell Energy) who reached a current density of 6A/cm^2 to show the potential of the technology to run at thermoneutral voltage and much higher current density once the degradation is reduced. However, several SOEC electrolysis have been performed below thermoneutral voltage and under current limitations due to degradation.
Regarding the cell degradation, operating the cell in a dynamic mode, meaning when the current supply is not constant (in the case of a wind/solar powered electrolyser f.e.), does not seem to impact the degradation rate of the electrolysis cell [10] [12].

2.5 Comparison of the different electrolysis technologies

The two key elements for evaluating the cell performances of the different electrolysis technologies are the operating voltage and the current density. The operating voltage defines the electrolysis electrical efficiency as seen it the first part of the electrolyser description, while the current density determines the production of hydrogen per cell area. Therefore, the more interesting cell for electrolysis will be the one with the lower voltage and the higher current density possible. When looking at a map of the different electrolysers used in literature (Fig.11), for large scale production, the PEM technology comes as the one capable of producing the more hydrogen with only little to no efficiency penalty compared to the more mature and established alkaline technology. The more efficient is, without any competition, the solid oxide electrolyte cell technology with still a relatively good current density allowing fast hydrogen production. However, this technology is still the least mature of the three and the least widespread making it more expensive to implement.

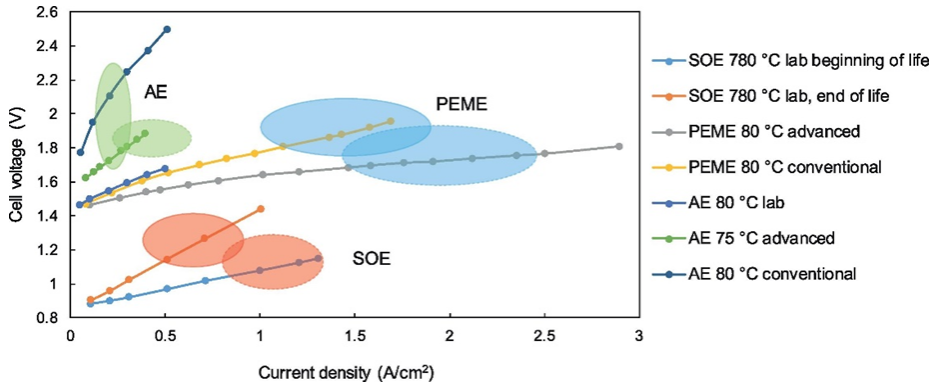

Figure 11: Comparison between the different electrolysis technologies at stack level with typical operating conditions for today (solid eclipse) and future (dashed eclipse) performances [13]

By looking at the literature, a table detailing the range of parameters of the different technologies can be made. This will simplify the comparison between the three technologies depending on the parameter of interest. The overall comparison of the performance, pros and cons of the technologies, is done in the following section.

	AEL	PEM	SOEC
Cell temperature (°C)	60-90 [14] [7]	50-80 [7] [14]	650-1000 [15]
Typical pressure (bar)	<30 [16] [7]	<200 [17] or 30-60 [17]	<15
Current density (A/cm^2)	0.1-0.45	1-2 (Can work from 0.1)	0.3-1
Voltage (V)	1.8-2.4 [14]	1.8-2.2 [14]	0.7-1.5
Cell area (m^2)	<3.6	<0.13	<0.06
H_2 Production rate per stack (Nm^3/h)	<1400 (1400 for a 6MW Siemen's stack)	<400 (400 in case of a 2MW stack)	<10
Gas purity (%)	>99.5 [17] [18]	>99.99 [17] [18]	>99.9 [15]
Load flexibility (% of nominal load)	20-100	0-100	-100/+100 (<0 in FC mode)
Cold start-up time	1-2h	5-10 mins	Hours
Warm start-up time	1-5 mins	<10 s	15 mins
Nominal stack efficiency (based on the LHV)	63-71%	60-68%	100%, when operating at thermoneutral voltage
... specific energy consumption (kWh/Nm^3)	4.2-5.9	4.2-5.5	>3
Nominal system* efficiency (based on LHV)	51-60%	46-60%	76.8-84.6%, including water evaporation
... specific energy consumption (kWh/Nm^3)	4.5-6.6	4.2-6.6	3.7-3.9
Lifetime (kh)	55-120	60-100	8-20**
Efficiency degradation (%/year)	0.25-1.5 [16]	0.5-2.5 [16]	<4.38***
Investment cost (€/kW)	800-1500	1300-2200	2000 [10] [7]
Maintenance cost (% of investment cost per year)	2-3	3-5	3-4 [15] [19]

Table 1: Comparison between the range of parameters of the different water electrolysis technologies [7]

*: Including auxiliaries and heat supply (SOEL)

**: High uncertainty due to pre-commercial status of SOEL

***calcul based on a voltage increase of 0.5%V/1000h [2, p10 line 15]: $EE = V_{rev} \times \eta_F / V$, based efficiency (100% here for the stack efficiency) after 1000h (1 year = 9000h), $V_{1year} = V \times (1.005)^9 \Rightarrow EE_{1year} = EE/(1.005)^9$ And so the efficiency loss for 1 year is $1 - EE_{1year} \Rightarrow = 4.38\%$ (in [20] they claim degradation rates of 0.11%V/1000h by the year 2019)

2.6 Conclusion on the different water electrolysis technologies

Alkaline electrolysis (AEL) represents the most mature technology (TRL of 9) having been commercially available for over a century. It has the lowest specific investment (in the range of 800-1500€/kW) and maintenance costs of the three (around 2-3% per year of the investment cost). However, with the increase in development for the other two technologies, alkaline electrolyser will become less and less relevant regarding cost, and its lower efficiency ($63 - 71\%_{LHV}$ at the stack) will not be as acceptable as it is today. Moreover, AEL were first designed for stationary application and load, resulting in slow response time (1-2h when cold) and poor capabilities of load variation (lower limit around 20-25% of the nominal load due to a risk of flammable mixture appearing due to cross contamination of the gas fluxes). This makes it not really suitable for the developing market of renewable source where high load flexibility is a requirement.

PEM electrolysis is now a mature technology (TRL of 8) which was introduced to overcome the drawbacks of the alkaline electrolysis technology, indeed, it has a better load variation range (from 0 to 100% of the nominal load), a short response time (less than 10s when at temperature and in the order of minutes when cold), operates at higher current density resulting in smaller cell for a similar production and is capable of pressurized operation (up to 200 bar versus only 30 for the AEL). However, PEM electrolyser seems to be more expensive than alkaline electrolyser (between 1300 and 2200€/kW) while operating at a lower stack efficiency (between 60 and $68\%_{LHV}$).

Solid oxide electrolyte cell (SOEC) is the youngest of the commercially available electrolysis technology, compared to the other two (alkaline and PEM) its TRL is still relatively low (around 5) meaning that there is still room for improvement in the coming years for this technology. This low TRL makes SOEC quite expensive (around 2000€/kW in 2020). This technology also suffers from limitation: the technology is limited to low operating pressure, slow start-up times (in the order of hours for the cold start-up), short lifetime compared to the other two (up to 20 000h) and low production capabilities (up to 10Nm^3/h per stack). However, SOEC remains the most efficient technology of the three with a stack efficiency up to 100%, decreasing to a maximum of 84.6%$_{LHV}$ when considering the water evaporation and 76.8%$_{LHV}$ when including the water evaporation, rectifier losses, surface heat losses and auxiliary losses.

	Alkaline electrolysis	PEM electrolysis	SOEC electrolysis
Advantages	Mature technology Long lifetime Relatively low cost Up to the MW range	High current density Fast system response High operating range ($\%_{load}$) Compact design High pressure operation	Efficiency up to 100% Non-noble catalyst
Disadvantages	Low current density Poor partial low application Low dynamics Corrosive liquid electrolyte	High cost of components Stacks below the MW range Acidic corrosive environment	Still not commercially widespeard High tendency to degradation (reduce lifetime) Limited pressurised operation Slow start-up times Cost of the infrastructure (currently)

Table 2: Summary of the advantages and disadvantages of the technologies for water electrolysis

3 Carbon dioxide (CO_2) electrolysis

In order to produce carbon monoxide, necessary for the syngas used in most of the Power-to-Fuel processes, several methods can be used. Syngas can either be synthesised using chemical processes, such as the Reverse water gas shift reaction (covered in section 5), or by using an electrochemical process, actively reducing CO_2 into CO. In this section, the second method will be covered, the CO_2 electrolysis for CO production.

3.1 Technologies for CO_2 electrolysis

Several methods to electrochemically produce CO from CO_2 has been proposed throughout the years. Unfortunately, most of them are still in an early stage of development making them unsuitable for commercial use. Only few of these technologies are of interest for large and efficient CO production with the most plausible technology, for now, being the high temperature electrolysis using SOEC electrolyser. Other technologies for CO_2 reduction exist but are still in a very early stage of development and, therefore, still have very low efficiency or are hard to implement outside of a laboratory environment. The two other techniques which will be mentioned here are the low-temperature and molten carbonate electrolysis.
Test times exceeding a year in dry CO_2 electrolysis mode suggest that SOEC is today, by far, the most mature technology for direct electrochemical conversion of CO_2 into CO [22]. Moreover, compared to CO_2 electrolysis at low temperature, high temperature SOEC CO_2 electrolysis can utilise the internal heat produced by the ohmic resistance of the electrolysis cell and heat waste from other industrial processes to reduce the electrical demand of the reaction, reducing the operational cost, making it even more favourable.

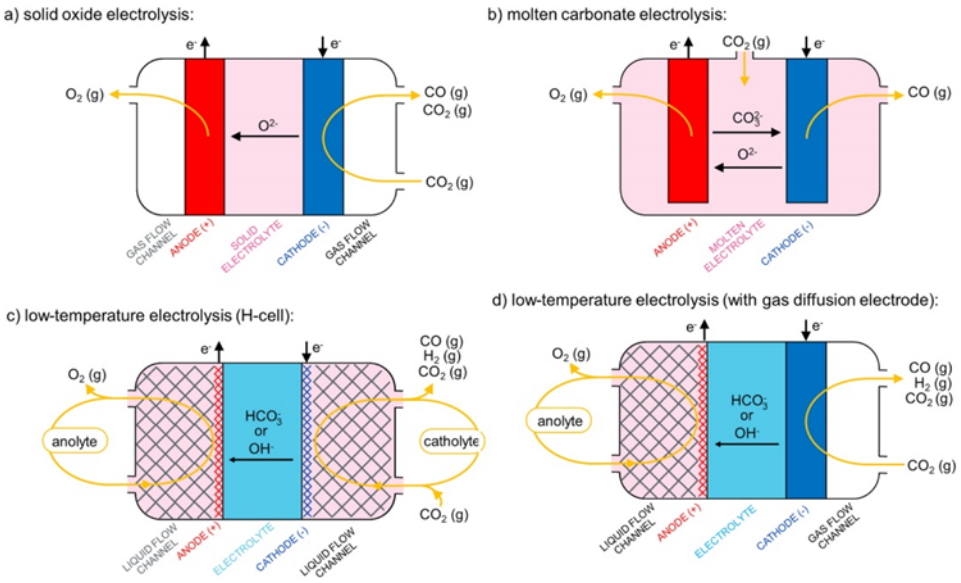

Figure 12: Schematic of different CO_2 electrolysis technology [22]

3.2 Thermodynamics of the reaction

As for the water electrolysis, the minimum energy required to process a CO_2 electrolysis is given by the thermodynamics of the reaction. The reaction of splitting the CO_2 molecule occurring inside and electrolyser cell is the following:

$$CO_2 \Rightarrow CO + \frac{1}{2}\, O_2 \tag{11}$$

The total energy demand for splitting CO_2 is given in the next figure and, as for the water electrolysis, is function of the temperature. The total energy demand ΔH is the sum of an equivalent "heat energy" ΔQ and an "electrical energy" ΔG (with ΔH the total enthalpy of formation, ΔG the variation of Gibbs free energy and $\Delta Q = T\Delta S$).

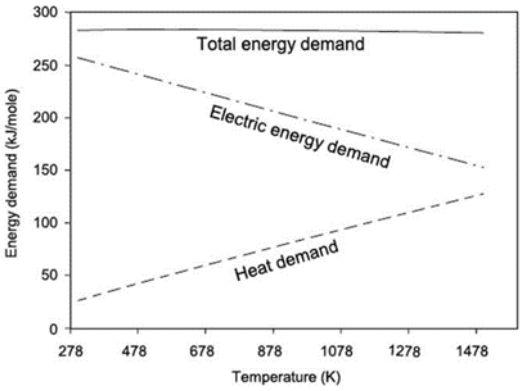

Figure 13: Energy demand for CO_2 electrolysis [21]

Similarly to water electrolysis, the higher the temperature, the lower will be the required electrical energy. Numerically, the electric energy demand (ΔG) at 25°C is around 90% (=257kJ/mol) of the total energy demand while at 800°C, it only represents 67% (=189kJ/mol) [22]. Therefore, at elevated temperature, a significant part of the energy can be provided in the form of heat, a lower quality energy than electricity, which can be provided from external sources or even joules losses within the electrolyser. This allows the high temperature electrolysis to operate at an overall greater efficiency compared to the low-temperature electrolysis.
As for the water electrolysis, the reversible cell voltage can be obtained using the Faraday's law, with z the number of electrons involved in the reaction (2 in case of direct conversion of CO_2 to CO) and F Faraday's constant (=96485.3 C/mol):

$$V_{rev} = \frac{\Delta G}{zF} \tag{12}$$

The reversible voltage is the minimum voltage required for sustaining a CO_2 splitting and, in the case of an electrolysis operated at 25°C, under 1 bar of partial pressure for the oxygen on the anode side and with an unitary CO_2/CO ratio at the cathode, this voltage is equal 1.33V. If now the electrolyser cell is heated up to 800°C, while maintaining the same condition, the reversible voltage drops to just only 0.97V [22].
The reversible voltage, however, is very sensitive to the process conditions. Indeed, as explained above, it changes with the temperature but also with regards to the partial pressure of the different gases reacting. The Nernst equation gives the relation between the partial pressure of the reactant and the reversible voltage of the cell:

$$V_{rev} = \frac{\Delta G}{zF} - \frac{RT}{zF} \ln\left(\frac{p_{CO_2}}{p_{CO}\sqrt{p_{O_2}}}\right) \tag{13}$$

Where R is the universal gas constant (= 8.314 J/molK), T the temperature (expressed in K), p_{CO_2} and p_{co} the partial pressure of CO_2 and CO on the cathode side and p_{O_2} the partial pressure of oxygen on the anode side.

3.3 High temperature CO_2 electrolysis using SOEC

As mentioned in the water electrolysis section, SOEC stands for Solid Oxide Electrolyte Cells, in this technology, the electrolyte is commonly made of ceramics, which have the capacity, at high temperature (above ~600°C), to conduct oxide ions while remaining impermeable to gaseous oxygen and electrons, avoiding shorts in the cell, even for short distances between electrodes. The ionic conductivity of the ceramic has the particularity of exponentially increasing with temperature. This improves the rate at which the electrolysis can be operated and is one of the reasons why most SOECs electrolysers operate at very high temperature (in the range of 700 to 900°C). The most commonly used materials for the electrolyte are the following: stabilised zirconias such as yttria-stabilized zirconia (YSZ) and scandia-stabilized zirconia (ScSZ), and doped cerias such as gadolinia-doped ceria (GDC) or samaria-doped ceria (SDC).
In high temperature CO_2 electrolysis using SOEC, the CO_2 is injected and reduced at the cathode (also referred as the fuel electrode), where it dissociates into CO and oxygen ions. Under the action of the external electric field, the ions are diffused to the anode through the solid ceramic electrolyte. At the anode side, oxygen ions release two electrons each and re-combinates to form gaseous oxygen molecules. The global electrolysis process is presented on Fig.14 here below:

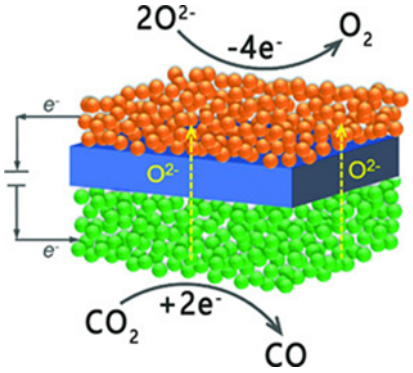

Figure 14: Schematic of the reaction of electrolysis on a SOEC [23]

In high temperature CO_2 electrolysis using SOEC, the gas velocity, the electrode permeability and the gas composition have significant effects on the cell performances.
Therefore, in order to maximise the cell performances, porous electrodes, which benefit the gas diffusion and permeation, are used for both sides.
For the fuel electrode (cathode), while the composition may vary, the most common materials used are composites of metallic such as Ni, and either CGO or YSZ. Nickel, in the electrode, acts as the electronic conductor for electrons as well as catalyst for the reactions. However, Ni has the disadvantage of being sensitive to sulphur poisoning, a tendency to coke and suffers from instabilities towards redox cycling (repetitively coupled reduction and oxidation reactions) [22].
On the anode side, common materials include doped perovskites of lanthanides and transition metals, such as LSM, LSCF, SSC and others [24].

The efficiency of the SOEC electrolyser for CO_2 can be determined in the same way as for the water electrolysis:

$$\eta = \frac{V_{rev}}{V_{rev} + V_{add}} \times \eta_F = \frac{V_{rev}}{V} \times \eta_F \tag{14}$$

This coefficient characterises the efficiency of converting an applied electrical potential into carbon monoxide, with η_F representing the faradaic losses due to non-ideal selectivity of the process and V_{add} the polarisation losses (the overpotential appearing with a specific current density). In the case of solid oxide electrolysis, the faradaic efficiency, η_F, is very close to 100% as long as the CO_2 source is pure enough; deviations from a value of 100% tend to indicate that the cells have been operated under unwanted conditions.

The faradaic efficiency is the measure of selectivity for the electrochemical process. Here, in the case of CO_2 electrolysis for CO production, this efficiency is characterised as the amount of CO produced over the theoretical amount of CO that an ideal reaction is supposed to produce. If side products are generated, the final amount of CO will not be the desired one, leading to a lower faradaic efficiency.

In the next figure, is compared the Faradaic efficiency of several electrolysers test plant found in literature for SOEC, molten carbonate, and low temperature CO_2 electrolysis as a function of the current density.

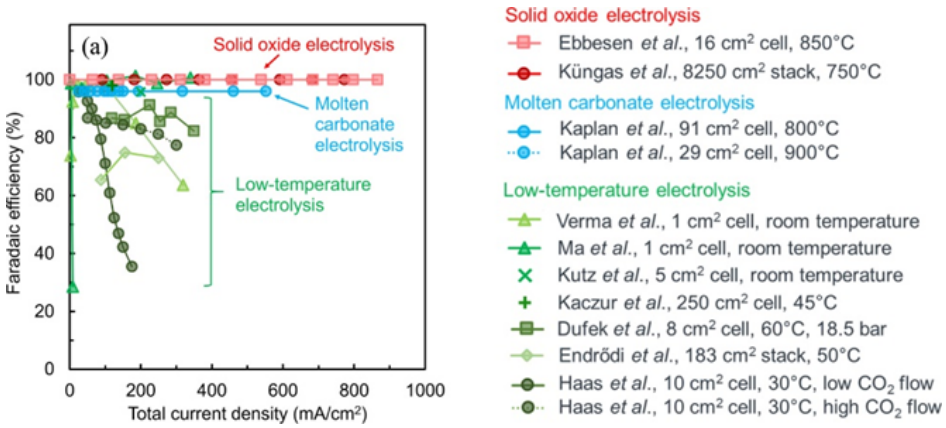

Figure 15: Faradaic comparison of state-of-the-art low-temperature, molten carbonate, and solid oxide electrolysers [22]

As seen on the figure, state-of-the-art solid oxide electrolyser stacks operates at 100% faradaic efficiency over a very large range of current density compared to other technologies which, mainly for low-temperature electrolysis, require very low current densities to be energetically competitive with the SOEC technology, resulting in smaller CO production rates. This parameter is important because high CO production rates help reduce the cost of the expenditure since less catalyst and active area is necessary for the production of a fixed amount of gas.

When considering the polarisation loss, the energetic efficiency of the electrolysis can be calculated in function of the current density applied to the cells. This energetic efficiency is shown for different test plant and technologies in the following figure:

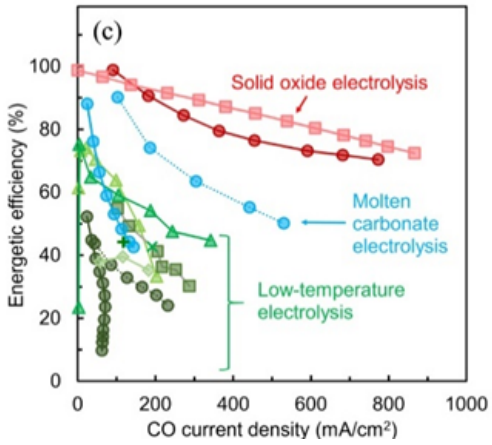

Figure 16: Efficiency comparison of state-of-the-art low-temperature, molten carbonate, and solid oxide electrolysers [22]

Note that the energetic efficiency, as plotted on Fig.16, is only considering the electrochemical processes in the electrolysis cell. The electric consumption and efficiency losses due to, for example, blowers or re-circulation pumps are not taken into account, although such losses may be substantial. These additional losses are not considered in the global technological since due to the wide variation in equipment used and their quality, the result may significantly vary from an installation to another.
The graph above (Fig.16) shows that, as the current density increases, the energetic efficiency of the cells decreases. However, the SOEC electrolyser seems to be less impacted by this efficiency loss compared to the low-temperature and molten carbonate electrolysis. Its efficiency remains high even at elevated current density (∼70% for 800-900mA/cm^2). The performance of SOEC compared to the other two technologies can be explained by the quasi-perfect faradaic efficiency of the technology and its low cell overpotential.

Another interesting value for an electrolysis installation is the electric power consumption (EPC) of the electrolyser (auxiliaries not considered) to produce 1Nm^3 of gas (in this case CO). The formula for this electric consumption is the following:

$$EPC = \frac{V \times z \times F}{\eta_F \times V_m} \qquad \text{with,} \quad V = \frac{V_{ref} \times \eta_F}{EE} \tag{15}$$

Where EE is the electrical efficiency of the cell such that $EE = V_{ref}/(V_{ref} + \text{overpotential})$, here assumed equal to 90%, which is a reasonable assumption in regard to the SOEC technology, V_m is the molar volume of CO considered as an ideal gas for the calculation (V_m = 24.4 litres at 25°C and 1 atm), z is the number of electrons involved in the reaction ($z = 2$) and F is the Faraday constant, equal to 96485.3C/mol. Theoretically, an electrochemical CO_2 reduction process with a faradaic efficiency (η_F) of 100% operating at the reversible voltage of 1.33V at 25°C will have an EPC of 3.238kWh/Nm^3, while the corresponding theoretical EPC at 800°C is 2.361kWh/Nm^3. Therefore, an electrolyser operating at 5kWh and η_F = 100% at 25°C will generate around 1.8kWh waste heat for every Nm^3 of CO produced.

3.3.1 Pressurised operation

Operating at high pressure is, in most cases, beneficial for an electrolysis process since the product being either hydrogen, carbon dioxide or a combination of the two, is usually used or stored at high pressure. Besides, compression of liquid water or CO_2 requires very little energy and CO_2 will, in most cases, already stored at high pressure to maximise its density.
Furthermore, at higher operating voltages, such as for instance, the most relevant thermoneutral voltage, the increase in pressure lowers the overpotential due to improved electrode kinetics and reduced diffusion restrictions. This means that, at a low current density, the performance is worse for high pressure (higher voltage and thus power consumption) but, at higher current density, the pressurized operation is better [21].
However, when operating at high pressure, elevated temperatures and in presence on carbon atoms, like in the case of a CO_2 or co-electrolysis, carbon formation within the cell can happen, decreasing the cell longevity by actively blocking the reaction zones onto the electrodes. This carbon deposition is favoured at high pressure.

3.3.2 Cell degradation

Solid oxide electrolyte cell, as for other electrolysis technologies is suffering from degradation over time. The main and unavoidable degradation is the natural degradation of the components, increasing the electrical resistance hence the voltage required for driving the electrochemical reaction. This degradation was a major issue in the last 15 years for the SOEC development but thanks to large improvement in the technology during last years, it has largely decreased and is now below 0.5%V/1000h [25] which translates after calculation (using 0.5 %V/1000h degradation) to around 4.4% per year. This was confirmed by Haldor Topsøe [26] in an experiment in which a degradation of 0.3-0.4%V/kh (equivalent to around 3.1%/a) was demonstrated for more than 7000h.

Another source of degradation comes from contaminants present in the electrolyser feed. The contaminant includes sulphur, silica, chlorine, phosphorus, arsenic, antimony, and selenium, for example [21], which can block the electrocatalytic active sites, causing electrodes degradation and leading to an increase of the polarization resistance. Therefore, it is beneficial for the installation lifespan to limit the impurities in the inlet stream. This can be limited by purifying the inlet stream before entering the electrolyser.

Carbon formation can also occur on the electrodes of the SOEC cells, especially when the cell operates at low temperature and at high pressure while in presence of carbon atoms. This carbon formation and deposition will actively block the reaction zone, reducing the conversion rate of the cell, and causing higher fuel electrode overpotential.

3.4 Conclusion

When comparing the different methods available for CO_2 reduction, the high temperature electrolysis stands out as being the most promising: SOEC has significantly better performance than low temperature and molten carbonates regardless of the performance metric. It has a better Faradaic efficiency, lower cell voltages (improving efficiency), lower area-specific resistance (lowering the losses) and a lower electric power consumption. It also has high conversion efficiencies, which has been verified experimentally in stack having an active area above 8000cm^2 [27].

Although CO_2 electrolysis using solid oxide electrolysis stands out as the only current option for efficient industrial CO_2 reduction, the technology is not yet completely ready for commercial use. Nowadays, the main issue with SOEC is still its high tendency to suffer from cell degradation in presence of impurities in the feed flow. This degradation leads to higher resistances in the process. Therefore, higher voltage are required to drive the reaction resulting in a lower cell efficiency.
Besides, due to its low TRL, the technology is currently still very expensive, even if, in the years to come, improvement will be made as the research and development continue to make the initial investment cost decrease. The main challenge in research and development for the coming years to reach commercialisation of CO_2 electrolyser using SOEC can be summarised as such [46]:

- Further fundamental understanding of the electrochemical reactions that occurs in SOECs
- Further fundamental understanding of degradation mechanism and materials behaviours in the CO_2 electrolysis process
- More extensive research studies and developments on materials of SOECs are necessary
- Improvement of economic and technological feasibility for the SOEC technology

Typical parameters and their range for the SOEC cell used for the CO_2 electrolysis are listed in Table 3

Parameters	Values
Operating voltage (V)	0.98 – 1.4 [22] [26]
Current density (mA/cm²)	>750 [22] (Polarization curves and area-specific resistance)
Temperature (°C)	700 – 900 [22]
Pressure (bar)	Low pressure (depending on the operating conditions)
Fuel electrode	Ni, CGO, YSZ
Oxygen electrode	doped perovskites of lanthanides, LSM, LSCF, SSC...
Electrolyte	yttria-stabilized zirconia (YSZ) scandia-stabilized zirconia (ScSZ) gadolinia-doped ceria (GDC) samaria-doped ceria (SDC)
Electric efficiency (%)	70 – 100 (operating at thermoneutral voltage) [22]
Efficiency loss (%/year)	<4.38*
CO Production rate per stack (Nm^3/h)	2.67 [26]
specific energy consumption on stack level (kWh/Nm^3 CO)	<3.4 [26]
Installation cost (€/kW)	>2000€/kW currently [25] Based on SOEC for water electolysis
Lifetime (h)	Highly depending on the inlet stream purity and the tolerable efficiency decrease over time

Table 3: Summary of the operational range of the SOEC elctrolyser for CO_2 electrolysis

*calcul based on a voltage increase of 0.5%V/1000h [22]: $EE = V_{rev} \times \eta_F / V$, based efficiency (100% here for the stack efficiency) after 1000h (1 year = 9000h), $V_{1year} = V \times (1.005)^9 \Rightarrow EE_{1year} = EE/(1.005)^9$ And so the efficiency loss for 1 year is $1 - EE_{1year} \Rightarrow = 4.38\%$ (in [28] they claim degradation rates of 0.11%V/1000h by the year 2019)

4 Water and CO_2 co-electrolysis

The co-electrolysis of water and CO_2 is looking to be one of the most promising way of producing syngas in the coming years, combining both the efficiency of the high temperature electrolysis and its capability of working at high mass flow rate. Water and CO_2 co-electrolysis constitutes one of the corner points of Power-to-Fuel strategies, for CO_2 recovery and carbon neutral fuel production.

4.1 SOEC technology for co-electrolysis

Today, the best way to operate simultaneously a water and a CO_2 electrolysis is by using a Solid oxide Electrolyte Cell (SOEC) in a co-electrolysis process. This technology is attractive due to unrivalled conversion efficiencies and is now suitable for large scale application thanks to the tremendous developments and improvements made during the last 10 to 15 years. Moreover, SOEC technology is easily scalable since SOECs cells are gathered and connected in series to form stack; these stacks are then built into modules and assembled in systems to reach the desired gas production rate.

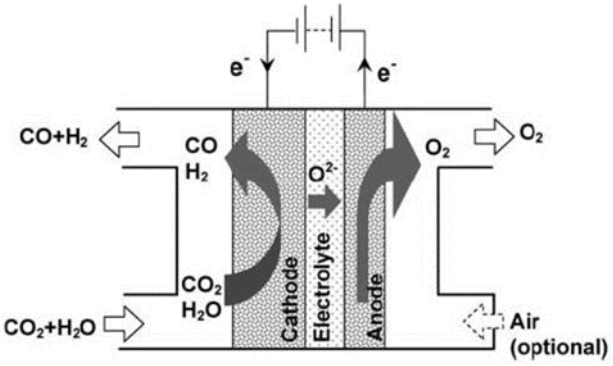

Figure 17: Schematic of a SOEC electrolyser cell [29]

SOECs are made of one electrolyte and two electrodes and are available in a wide range of structural designs (electrolyte-supported, metal-supported, ceramic fuel supported). However, the cell's main components remain the same; two electrodes separated by a solid electrolyte. The electrolyte is made of a solid material which, at high temperature (around above 600°C), starts to conduct oxide ions while remaining impermeable to the steam and other gases. Most SOECs operate at high temperature (between 600 and 1000°C). This gives to the SOEC technology two advantages compared to competing electrolyser types (alkaline and PEM): faster kinetics and more favourable thermodynamics leading to a better electrical efficiency of the process. The electrolyte material commonly used are YSZ and GDC (Gadolinia-doped Ceria) because they provide both good thermal and chemical stability and have good conductivity for O^{2-} ions. Electrodes, on the other hand, are commonly composed of Ni/YSZ or Ni/GDC for the cathode (also called fuel electrode) and LSM/YSZ for the anode (sometimes called oxygen electrode). Other materials for the cell components are detailed in the document written by Nechache and Hody [30], with further explanation on the pros and cons of each.

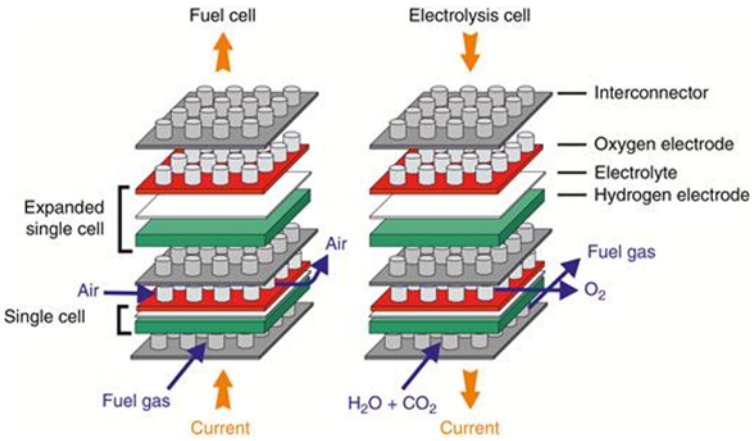

Figure 18: Schematic of a SOEC stack [31]

The operating principle of such electrolyser is the following: when a sufficient DC voltage is applied to the electrodes, carbon dioxide and water molecules are electrochemically reduced to carbon monoxide and hydrogen respectively. Oxygen ions are formed during this process, thanks to high temperatures, they are pumped through the permeable electrolyte on the anode side where they are oxidized into oxygen molecules while giving 2 electrons to the electrode. The global reaction of the co-electrolysis process is the following:

$$2H_2O + CO_2 \Rightarrow 2H_2 + CO + \frac{3}{2}O_2 \tag{16}$$

However, the electrochemical reactions of splitting CO_2 and H_2O are not the only reactions taking place in the cells. Indeed, due to the high operating temperatures, two other competing reactions react within the cell. The most important of the two is the one participating to the syngas production, the Reverse Water Gas Shift (RWGS) reaction (eq.17) while the second, detrimental, is the methanation reaction (eq.18), catalysed by the Nickel-based electrode.
Compared to electrolysis of only CO_2 or water, the intervention of the RWGS in the co-electrolysis process makes it very complicated to analyse. This is due to the sensitivity of the Water Gas Shift process regarding the process conditions and setup which impose to be precise on the exact conditions employed when disusing and comparing experimental results.

$$CO_2 + H_2 \Leftrightarrow CO + H_2O \tag{17}$$

$$CO_2 + 4H_2 \Leftrightarrow CH_4 + 2H_2O \tag{18}$$

4.1.1 Thermodynamics of the reaction

The required energy for steam and CO_2 electrolysis (not considering the side reaction) is given by the value ΔH, the total energy for the co-electrolysis reaction. This energy can be split in two other energies via the formula:

$$\Delta H = \Delta G + \Delta Q = \Delta G + T\Delta S \tag{19}$$

Where ΔG is the variation of free Gibbs's energy which accounts for the minimal electrical energy required to drive the electrolysis and ΔQ is the heat demand of the reaction, equal to the temperature at which the electrolysis is done, multiplied by the entropy variation. The Gibbs energy decreases with increasing temperature, meaning that the electricity demand of the syngas production is getting lower the higher the operating temperature. However, as the temperature increases, the total energy requirement of the reaction (ΔH) increases slightly, meaning that the reduction in electricity energy requirement should be counterbalanced by the heat provided to the reaction. Heat being a lower quality energy form, it is cheaper to provide. The decrease in ΔG, or electricity demand, is around 25% between low (100°C) and high temperature (800°C) electrolysis (3.1 $kWh/Nm^3_{H_2}$ versus 4.1$kWh/Nm^3_{H_2}$ for low temperature electrolysis) [32].

This relatively low electricity consumption made possible by the high temperatures allows the SOEC electrolysis to be impressively efficient. SOECs, used for co-electrolysis can reach theoretical efficiencies up to 100% (based on HHV) at the stack when operating under thermoneutral voltage, meaning when the heat demand necessary for the water splitting equals the heat released by the joule losses within the cell. However, when the converter efficiency and the practical energy losses are considered, the overall conversion efficiency drops around 87 to 93%$_{HHV}$ [32] which translates to an LHV-based efficiency of 73.5 to 78.6%$_{LHV}$.

For pure water electrolysis or pure CO_2 electrolysis, the thermoneutral voltage is given by the following relation:

$$V_{th} = \frac{\Delta H}{2F} \tag{20}$$

From this equation and the operating temperature of the cell (ΔH increases slightly with temperature), the minimum voltage required to start the reaction can be obtained: $V_{th,H_20} = 1.29$ V and $V_{th,CO_2} = 1.46$ V, for a cell temperature of 800°C. In case of a co-electrolysis, the thermoneutral voltage will range between the two values of pure-component electrolysis depending on the inlet composition, oxygen utilisation, and temperature (via the equilibrium constant K_{eq}); The thermoneutral voltage of the cell will be closer to the one of pure-steam if the inlet composition of the mixture is mainly composed of steam and conversely if the composition is dominated by CO_2.
At an operating temperature of 800°C with a syngas composition of around $H_2O/CO = 2$, a typical value of V_{th} will be ≈1.34 V [33].

4.1.2 Pressurised operation

Operating at high pressure is, in most cases, beneficial for the installation since the product of an electrolysis being either hydrogen, carbon dioxide or syngas is usually used or stored at high pressure. Besides, compression of liquid water or CO_2 requires very little energy and CO_2 will, in most cases, already stored at high pressure to maximise its density.
Furthermore, at higher operating voltages, such as for instance the most relevant thermoneutral voltage, the increase in pressure lowers the overpotential due to improved electrode kinetics and reduced diffusion restrictions. This means that at a low current density the performance is worse at high pressure (higher voltage and thus power consumption) but at higher current density the pressurised operation is better [34].
However, due to the presence of both carbon atoms and hydrogen atoms, the co-electrolysis process will optimally operate at low pressure. Indeed, at higher pressure, the production of methane will be favoured as well as the potential carbon deposition onto the electrodes by the Boudouard reaction. This is a difference with the simple water electrolysis using SOEC which, due to the non-presence of carbon atoms, can go as high as 15-20 bar. The production of methane in a co-electrolysis process using a SOEC cell can be limited by running the electrolyser at low pressure, high temperature and low current densities, then the methane production becomes negligible [35] (Fig.19 vs Fig.20).

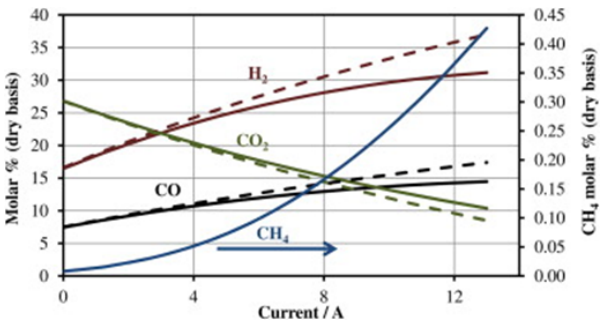

Figure 19: SOEC co-electrolysis model with (solid) and without (dashed) accounting for the methanation reaction at 800°C and 20 bar [36]

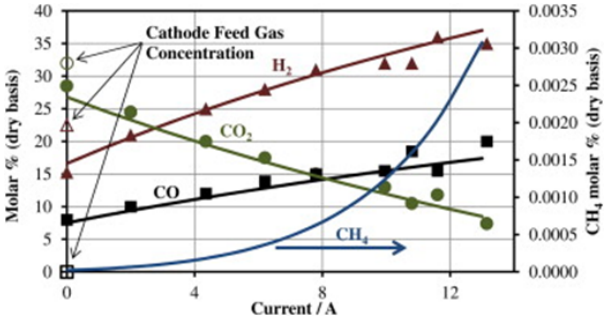

Figure 20: SOEC co-electrolysis model (lines) and experimental data (symbols) from Stoots and al. [33] at 800°C and atmospheric pressure (1 bar) [36]

Du et al. [37] estimated, by a simulation, that the best operating pressure under which both RWGS reaction and electrolysis are maximised is approximately 3 atm. In the same paper, the research team proposed to use a counter-current flow (between hydrogen flow and air flow) to increase the heat exchange and avoid important temperature loss due to the absorption by the RWGS that occurs at the cathode.

4.1.3 Cell Durability and Robustness

The durability of the cell used for the co-electrolysis (SOEC) is subject to two types of degradations.
Firstly, is the natural degradation of the component, increasing the current resistance hence the voltage required for driving the electrochemical reaction. The degradation rate of the cells was a major issue in the last 15 years for the SOEC development but thanks to large improvement in the technology in the last years, the degradation has largely decreased and is now below 0.5%V/1000h which translates after calculation (using 0.5%V/1000h degradation) to around 4.4% per year [32].
Secondly, is the degradation of the cells due to impurities in the inlet stream. The fuel electrode is the most impacted by this kind of contamination (which is expected since it is the one where the gas are introduced). The contaminant includes sulphur-containing impurities and silica-containing impurities, for example, which can block the electrocatalytically active sites, causing electrodes degradation and leading to an increase of the polarisation resistance. Therefore, it is beneficial for the installation lifespan to limit the impurities in the inlet stream, this can be limited by purifying the inlet stream before entering the electrolyser. Another alternative for limiting the impurities will be to make the syngas produced re-circulate inside the cell [38] or even to switch periodically the cell to a fuel cell mode [38]. The benefit of the syngas recirculation is observed on the cathode because, in state-of-the-art solid oxide co-electrolysis cell system, the cathode is typically, in part, composed of nickel which is an easily oxidable material. When oxidise, Ni loses its electrical and catalytic properties which is detrimental for the cell performance. Consequently, reducing gases such as the one produced by the electrolysis (H_2 and CO) fed together with the reactant (CO_2 and H_2O) will maintain a reducing atmosphere at the cathode, slowing down the cell degradation [39].
Finally, is the degradation of the cell caused by unwanted carbon deposition onto the reaction sites which actively blocks the reaction zones, reducing the conversion rate of the cell, and causing higher fuel electrode overpotential. This last type of degradation appears when the cell is running in unwanted conditions of temperature and pressure. To alleviate this problem, the operating temperature of the cell can be reduced (La Faro et al. [40] have found a compromise to maximise the cells life span by reducing the operating temperature at 525-700°C while maintaining a good electrical efficiency) or, as proposed earlier, pure hydrogen can be injected at the inlet to reduce the phenomenon.

After the durability concerns for the SOEC electrolyser, it is good practice to mention the robustness characteristics of this technology. Robustness characterises the capability of the electrolyser to turn ON and OFF repetitively. Historically, SOEC technology had quite bad performances towards thermal cycles (cool-down/heat-up),

but in recent years, with improvements in cell technology, this has changed. Stacks based on ceramic-supported cells can now sustain up to around 150 thermal cycles [41] while stacks based on metal-supported cells can withstand more than 2500 cycles [42]. In a study, an 8-cell stack was operated for 1200 hours and was powered by a wind turbine in which the load was modified every 5 minutes. The electrolyser stack did not show any additional degradation meaning that small variation in power (not complete shut-down cycles) does not impact the durability of SOEC. [31]

4.1.4 Selectivity of the process

The presence of both hydrogen atoms and carbon atoms inside the electrolysis cell enable the production of methane in the process which is detrimental for the installation, increases the work of compression between the different units and uses resources necessary for the process. Therefore, its production must be limited as much as possible.
Fortunately, in a SOEC electrolysis, methane production is limited because the reaction is operated at high temperature (non-favourable to the methanation since this reaction is exothermic) and, even more limited if the cell is restricted to low pressure operations (see impact of pressure on methane production in Fig.19 and Fig.20). Therefore, when those conditions are met, the methane production can be neglected.
G. Cinti et al. [43] tested different inlet feed compositions with variable ratios between CO_2, H_2O and H_2. The H_2 concentration is set to 10% in the different cases, it is used to guarantee a reducing atmosphere in the cell, avoiding the oxidation of the nickel-based electrode. The ratio experimented during the experiment are the following:

	S1		S2		S3	
	20:70:10		30:60:10		40:50:10	
	mol/h	*% mol*	*mol/h*	*% mol*	*mol/h*	*% mol*
Cathode						
CO_2	1.71	20	2.56	30	3.41	40
H_2O	5.97	70	5.12	60	4.26	50
H_2	0.85	10	0.85	10	0.85	10
TOT	8.53		8.53		8.53	
Anode						
Air	8.92		8.92		8.92	

Figure 21: Test flow and composition [43]

The electrolysis conditions used in the experiment were the following: the electrolyser stack is made of 4 cells composed of Ni/8YSZ cathode, LSM/8YSZ anode, 8YSZ electrolyte with an active area of 80cm² per cell. The inlet gases enter the cells at 650°C and the stack is operating at 750°C. The current applied to the cells was increased by step of 12.5 mA/cm² each minute up to a maximum limit of 1.4V.
The dry gas composition of the gas mixture leaving the stack is shown in the following graphs:

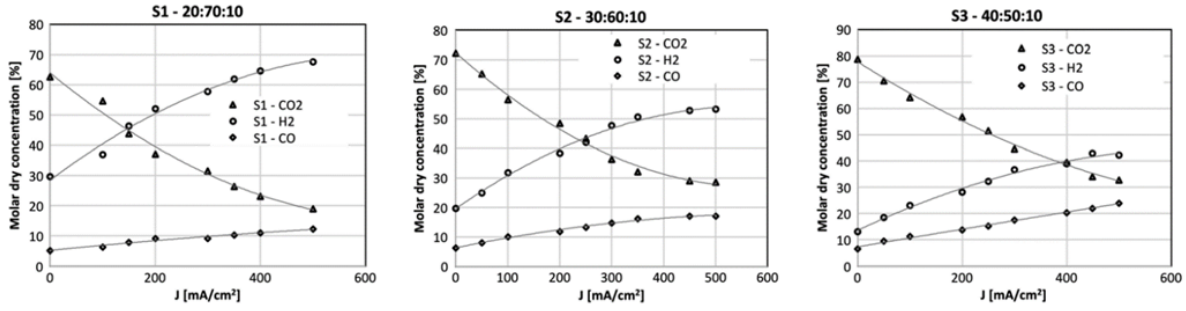

Figure 22: Dry gas composition for inlet feed composition S1, S2 and S3 [43]

The Ratio of H_2/CO in the exit gas composition is almost constant and seems independent of the current applied to the stack. Its value is the following, depending on the inlet feed composition:

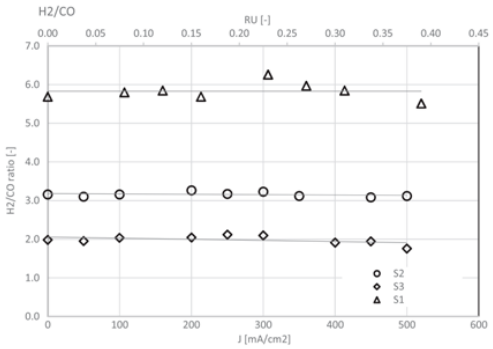

Figure 23: H_2/CO ratio as produced syngas. RU is the reactant utilisation. [43]

4.1.5 Efficiency

The SOEC electrolysis technology used for co-electrolysis can reach a theoretical efficiency up to 100% (based on HHV) at the stack when operating at thermoneutral voltage, meaning when the heat demand necessary for the water splitting equals the heat released by the joule losses within the cell. However, when the converter efficiency and the practical energy losses are considered, the overall conversion efficiency drops to around 87 to 93%$_{HHV}$ or 73.5 to 78.6%$_{LHV}$.

The electrolyser, during its lifetime, will suffer from natural degradations. These degradations have largely decreased in the last years of development and is now below 0.5%V/1000h which translates after calculation to 4.4% degradation per year. Additional degradation can occur, such as carbon deposition or oxidation on the electrodes and cell poisoning by contaminant present in the gas feed, however their impacts on the efficiency are not easily calculable.

4.1.6 Methane assisted electrolysis

In 2015, Wang and al. [39] proposed to assist the co-electrolysis of H_2O and water with methane at the oxygen electrode. The goal of this will be to produce syngas on both sides of the SOEC cell, hence increasing the productivity and electric efficiency while using undesirable product extracted from a parallel process, a Fischer-Tropcsh reactor for example (see on section 1).
In 2017, Wang proved the concept by maintaining cells for more than 70h and showed that this process can provide syngas at both electrodes with a ratio H_2/CO of 2 [44]. The drawback of such recycling technology is the impact on the cell lifespan, high degradation rate is expected due to the carbon deposition occurring in presence of CH_4 and the elevated temperatures.

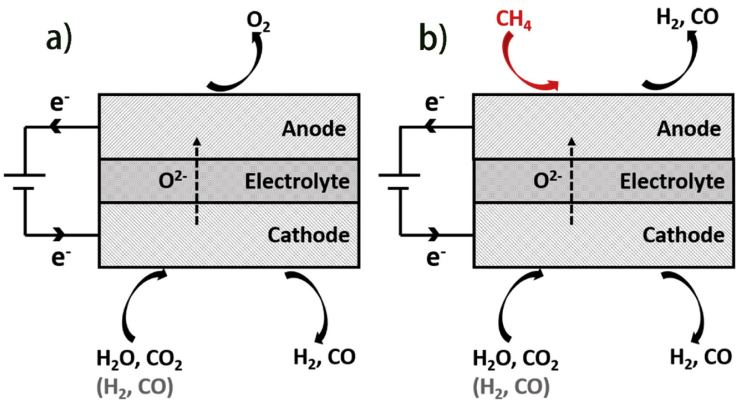

Figure 24: Schematic of a non-assisted (a) and methane assisted (b) co-electrolysis in a SOEC [39]

For every mole of water and CO_2 introduced at the cathode, 2 moles of CH_4 must be introduced at the anode to trigger the methane assisted reaction. When operating in methane assisted co-electrolysis, the cell can achieve a production of 5 moles of H_2 and 3 moles of CO, which is a clear improvement compared to a simple co-electrolysis, capable of only 1 of each. This better conversion is realised while maintaining a lower overall energy consumption (470 kJ/mol) due to a relative increase of the total heat demand, which was yet compensated by the decrease of the electric energy consumption.

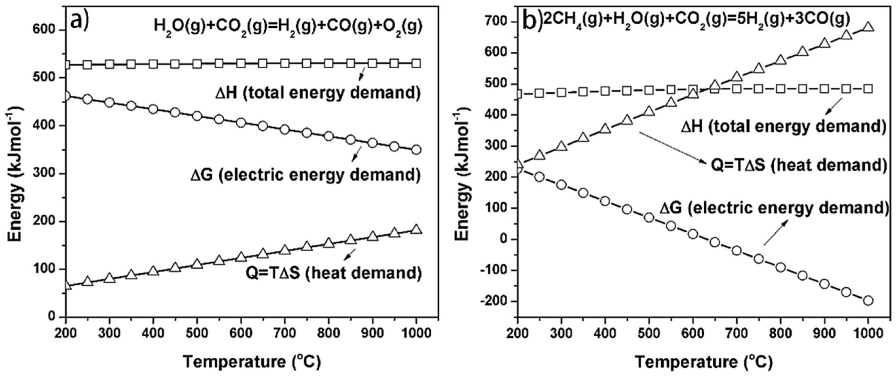

Figure 25: Energy demand for the non-assisted co-electrolysis reaction (left); Energy required by the CH4 assisted co-electrolysis (right) [39]

However, this technology, though promising, is still at a relatively low stage of research and development, and still has improvement to make regarding the degradation of the cells. Indeed, introducing hydrocarbons into the cells can result in large carbon deposition on the electrodes due to cracking, further increasing the degradation rate of the cells already caused by the impurities present in the CO_2 feedstock.

4.1.7 Cost estimation

The cost estimation to produce syngas by a SOEC co-electrolysis process is a challenging task because high temperature co-electrolysis is still under development and no or only few large-scale units for long term operation have been implemented. However, according to literature estimates, in 2020, a 5MW SOEC system has a CAPEX value of around 2000€/kW whereas this cost is projected to decrease, approaching the 1000€/kW by 2030 and the 530€/kW by 2050, based solely on the cost reductions due to economics of scale [45]

4.2 Conclusion

The co-electrolysis represents a very appealing option for direct syngas production from water and CO_2. Even if the technology is still relatively new, it has seen a real improvement in development during the last decade, making it closer in terms of TRL compared to the other syngas production technologies and increasing its viability in the electrolyser market in terms of production capabilities.
Currently, the main issue with SOEC is still its high tendency to cell degradation in presence of impurities in the feed flow. This degradation leads to higher resistances in the process. Therefore, higher voltages are required to drive the reaction resulting in a lower cell efficiency. Furthermore, due to the low TRL, the technology is nowadays still very expensive compared to other syngas production methods. Even if, in the coming years, improvement will be made as the research and development continue making the initial investment cost decrease. The typical parameters and their range for the SOEC cell used for the co-electrolysis are listed in the following table:

	Operating range
Temperature (°C)	525-800 [40] [29]
Pressure (bar)	<3 [37] (maximised RWGS and electrolysis ∼3)
Stack voltage (V)	1.343 V at 800°C [33]
Current density (A/cm²)	0.4-1 [47]
Conversion (CO_2 + H_2O to CO + H_2) (%)	76.6 for H_2O [36] 76.9 for CO_2 [36]
Efficiency (based on LHV) (%)	76.8 – 84.6 [48]
Voltage degradation rate (V%/kh)	<1 [32] [49]
Efficiency degradation rate (%)	<4.4
Load flexibility (%)	0 - 100
Electricity consumption (kWh/Nm^3)	3.1 (H_2O/CO_2 = 2 at the input) [32]
Cost (€/kW)	>2000 [45]
Maintenance cost ($\%_{Capex}$/a)	4 [29]
Production capability per stack ($Nm^3_{H_2}$/h)	No large-scale plant in operation (but tested at 0.85$Nm^3_{H_2}$/h [46])

Table 4: Summary of the operational range of the SOEC elctrolyser for co-electrolysis

5 Reverse Water Gas Shift

5.1 Operating principle

The Reverse Water-Gas Shift Reaction (RWGS reaction) was discovered in the 19^{th} century as a method of producing water from carbon dioxide and hydrogen, with carbon monoxide as a side product. In the use case of syngas production, CO is no longer a side product but the main product wanted by the reaction. The complete reaction is the following:

$$CO_2 + H_2 \Rightarrow CO + H_2O \quad \Delta H = 42 \text{ kJ/mol} \tag{21}$$

Due to the presence of both carbons and hydrogens atoms, this reaction is always accompanied by additional side reactions: the methanation reaction and the Sabatier reaction, detrimental to the syngas production process. These two side reactions are favoured at lower temperatures, while the main reaction of RWGS is not. Therefore, to avoid the production of methane and prevent the use of hydrogen and carbon monoxide in other reaction than the RWGS one, the reactor must operate at the highest possible temperature as shown in the following graph:

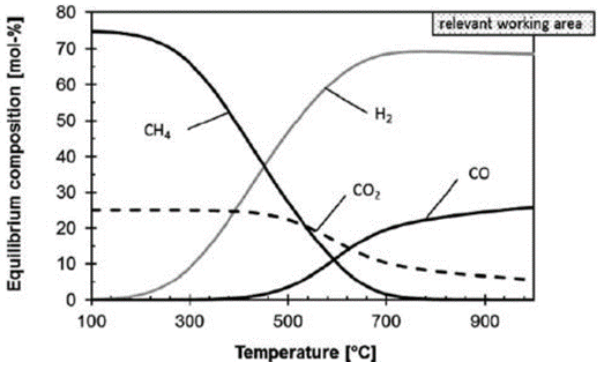

Figure 26: Impact of the temperature on the thermodynamic equilibrium, at 1 bar and $H_2/CO_2 = 3$ [50]

Therefore, the production of CO in a reactor containing both H_2 and CO_2 by the RWGS reaction is favoured at high temperature (800-1000°C), but not the side reactions.

The overall process (the combination in the reactor of the RWGS, methanation and Sabatier reaction), when no temperature control is implemented, can be considered as self-stabilizing (temperature wise). This behaviour implies that the reactor in which the reactions occur can be designed without any internal cooling system. This characteristic can be explained by looking at the competing reaction inside the RWGS reactor:

- The primary reaction: $CO_2 + H_2 \Rightarrow CO + H_2O \qquad \Delta H = 42$ kJ/mol
- The side reaction of methanation: $CO_2 + 3\ H_2 \Rightarrow CH_4 + H_2O \qquad \Delta H = -206.5$ kJ/mol
- The side reaction of Sabatier: $CO_2 + 4\ H_2 \Rightarrow CH_4 + 2\ H_2O \qquad \Delta H = -165$ kJ/mol

The combination of the heat brought by the two side reactions, highly exothermic, and the heat consumption by the endothermic primary reaction will lead to a stabilisation of the reactor temperature. The side reactions are favoured at low temperature (as seen in Fig.27), releasing a large quantity of heat, leading to an increase of temperature, favouring the endothermic RWGS reaction, reducing the temperature, decreasing the equilibrium yield of the RWGS reaction while favouring the side reactions, etc... The reaction is self-limited.

However, in order to maximise the CO yield inside the reactor, it is mandatory to keep the temperature above 700°C for both, high kinetics, and avoidance of methanation/Sabatier reaction, therefore limiting the methane production. Moreover, the reactor should have a high thermal stability to avoid temperature decrease locally, leading to methane production.

Beside temperature, other factors are impacting the selectivity of the process inside a RWGS reactor:

- The H_2/CO_2 ratio: the feed ratio of H_2/CO_2 has an impact on the CO_2 conversion; the higher the ratio the higher the conversion (up to a point, as seen on Fig.27). Increasing the CO_2 conversion leads to a greater yield of CO by the RWGS reaction but also increases the methane yield because the equilibrium of the methanation and Sabatier reaction will be shifted towards the products.

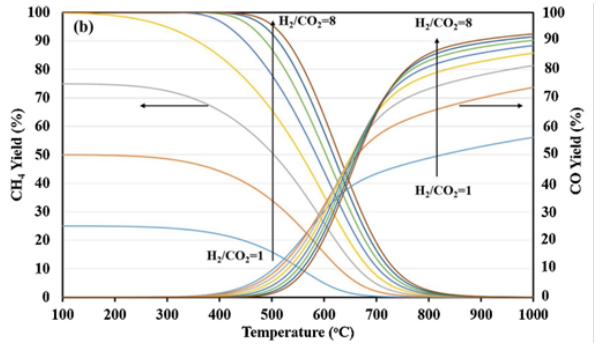

Figure 27: Effect of temperature and H_2/CO_2 ratio on CO and CH_4 yields at 100kPa [51]

For a given H_2/CO_2 ratio, as the temperature increases, CO_2 conversion first declines and then rises to higher values because of the competition between the Sabatier and the RWGS reaction. At lower temperature, the highly exothermic Sabatier reaction is favoured, increasing the temperature within the reactor, and reducing the amount of CO_2 available. Progressively, as the temperature increases, the RWGS reaction will start to dominate, thermodynamically reversing the situation.

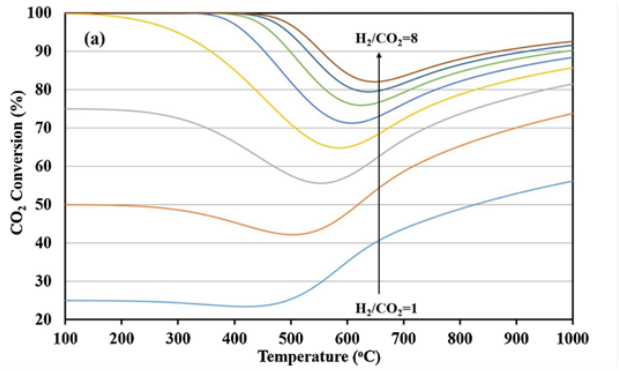

Figure 28: Effect of temperature and H_2/CO_2 ratio on CO_2 conversion at 100kPa [51]

- The pressure: even if pressure only has a limited (negligible) impact on the RWGS reaction, it has a negative impact on the CO yield, especially at lower temperature. The opposite is true for the yield of the side reactions, increasing production of CH_4 at higher pressure and lower temperature.

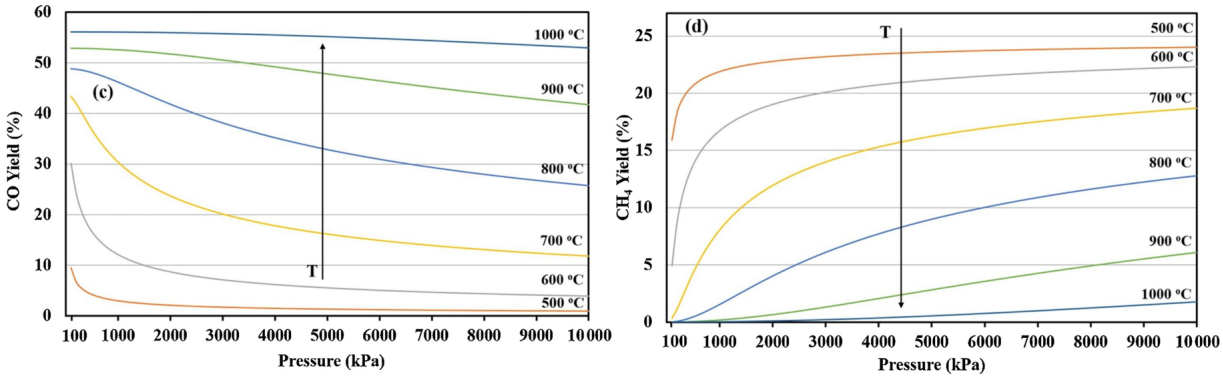

Figure 29: Effect of pressure and temperature on CO (left)/CH_4 (right) yield for H_2/CO_2 of 1 [51]

- Presence of water in the inlet stream: the presence in water molecules in the inlet stream will result in a lesser CO_2 conversion inside the reaction because, when looking at the RWGS reaction, adding water will result in an equilibrium shift of the reaction towards the reactant. Therefore, it is important to dry the inlet gas stream coming from the electrolyser since the presence of water vapor in the RWGS reactor would lead to less CO_2 conversion (up to 10% less) hence a lower overall CO yield.

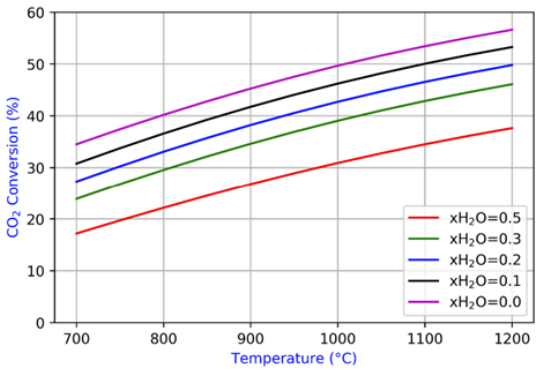

Figure 30: Effect of temperature and H_2O concentration on CO_2 conversion [52]

In theory, it seems that temperature between 800-1000°C and pressures up to 3 bar [53] may be appropriate process conditions to operate a RWGS reactor while minimising the effect of the side reactions hence minimising the amount of methane produced.

In practice, the RWGS reaction is often operated at much lower temperature, typically between 500 and 600°C via the presence of a catalyst used to lower the reaction temperature of the process hence its cost [54].

5.2 Reactor technologies for the RWGS process

Reactor used for the reverse water gas shift reaction is achievable without any temperature management since, as said in the previous section, the process is self-stabilising thanks to the side reaction occurring aside from the main RWGS reaction. However, the reactor needs a heating system, in order to launch the reaction when coming from rest and to maintain a high enough temperature for good kinetics and low methane production.

5.2.1 Adiabatic packed bed reactor

An adiabatic packed bed reactor is composed of a column in which a catalyst bed is placed. The reactants flow through the column while contacting the catalyst, the reaction is happening at its surface and products come out at the other end on the column.
This technology has a simple design but has the disadvantage of requiring a stop of the production to change the catalyst when it will eventually be deactivated.

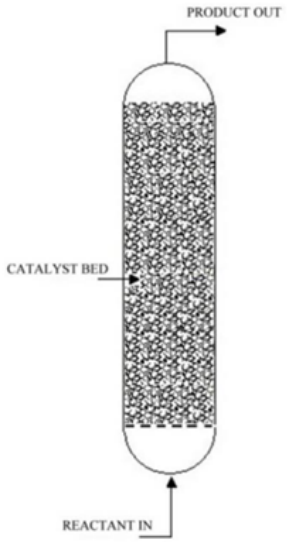

Figure 31: Adiabatic packed bed/fixed bed reactor [55]

Catalyst deactivation can occur for several reasons. One of these reasons is the carbon deposition onto the catalyst due to unwanted reactions inside the reactor. This carbon deposition will obstruct the catalyst pores resulting in a smaller contact/reaction area with the reactant. The more the catalyst is covered, the less efficient and the longer is the process. Depending on the type of carbon formed and its expansion on the catalyst, it will be more or less difficult to remove it by the catalyst regeneration process. The catalyst regeneration requires high temperature (therefore energy) and a stop of the reaction process (in the case of a fixed bed reactor). It is the best interest to avoid as much as possible the condition for carbon deposition.
The second phenomena leading to catalyst deactivation is the sintering or coalescence of the crystallites of the active phase of the catalyst. This phenomenon is strongly activated by the temperature of the process as well as the nature of the adsorbed species. The effect is more or less strong depending on the nature of the crystallites and the material on which they are deposited in the case of supported catalyst [54].

5.2.2 Adsorptive reactor

The adsorptive **fixed bed** reactor (Fig.32) is in a way similar in design to the adiabatic reactor; a cylinder in which a catalyst bed is placed but, here, the catalyst is not the only material present; it is mixed with an adsorbent material.

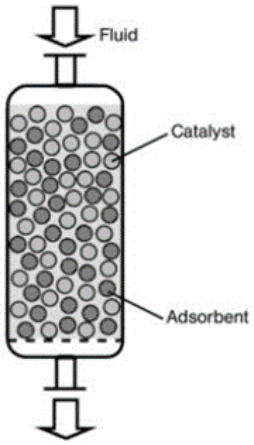

Figure 32: Adsorptive fixed bed reactor [56]

This reactor is based on the "Le Chatelier" principle. The water vapor formed during the RWGS reaction will be adsorbed by the adsorbent material resulting in an equilibrium shift towards the desired products of the RWGS reaction (CO). Beside the increased yield in CO, the water vapor adsorption is accompanied with the release of adsorption heat. The heat released is in the same order of amplitude as the enthalpy required for the RWGS reaction. Therefore, the adsorption of water during the process allows a better yield to CO conversion as well as a reduction in external heat consumption for the reactor.
The catalyst used to initiate the RWGS reaction is usually Cu/ZnO for industrial reactor scale while the adsorbent used are often Zeolite 3A. However, after a certain time, the adsorbent will start to saturate and will not be able to adsorb water anymore. To elevate this, the reactor must undergo a regeneration process. There are two types of regeneration possible for the adsorbent: the temperature swing adsorption (TSA) or the pressure swing adsorption (PSA). TSA is the most common regeneration technique of the two. It consists in heating up the adsorbent to a temperature above 270°C to empty it of its water content. However, this regeneration technique has the issue that, at such temperature, the Zeolites could be damaged [57]. PSA, on the other hand, uses pressurised inert gas such as nitrogen for purging the adsorbent from its water through several cycles of pressurisation and depressurisation. This method, although efficient and non-destructive for the zeolite, has the drawback of being costly compared to TSA due to the electricity demand on the pump for the pressurisation of the fixed bed reactor. Nevertheless, both these purging techniques have an issue. They require to stop the RWGS process inside the reactor, leading to loss of time and transient temperature behaviour. A way to alleviate this problem is with an absorptive moving/fluidised bed reactor (Fig.33).

A **moving/fluidised bed** reactor uses the same working principle as the fixed bed one, but, here, the regeneration of the adsorbent is totally decoupled from the RWGS reactor. In this configuration, the reaction process can go on continuously with, in parallel, the mix of catalyst/adsorbent flowing down the reactor to be regenerated before sent back in.
The main advantages of this technology over fixed bed reactor are that the process is continuous, meaning steady-state operation, therefore, no need of switching ON and OFF the reactor leading to thermal stress and transient behaviour. Moreover, compared to a fixed-bed reactor, the regeneration of the adsorbent being totally decoupled from the reactor, this operation can be processed in a unit designed and optimised for that purpose, increasing the overall efficiency of the regeneration process.

The disadvantage of moving-bed reactors is the necessary handling of solids and the abrasion/corrosion which comes with these moving solids.

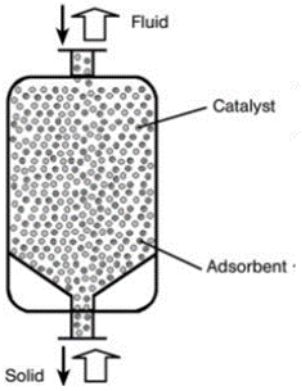

Figure 33: Adsorptive fluidised bed reactor in counter-current configuration [56]

Additionally, in moving bed reactor, it seems that the non-adiabatic case showed an advantage over the adiabatic case (which is not true in the case of a fixed bed reactor). This improvement in performances can be related to the supplementary degree of freedom that non-adiabatic reaction brings, allowing the reactions inside the reactor to self-stabilize. Moreover, in a non-adiabatic process, increasing the length of the reactor as a positive impact on the performances whereas for increasing solid velocities inside this reactor, the performances benefits decrease. This can be explained by the residential time of the catalyst inside the reactor, with increasing lengths and lower velocities, in a non-adiabatic reactor, the temperature control (possible because non-adiabatic) starts to have an impact on the reaction. Therefore, longer residential time in the reactor leads to better control so better performances and inversely. [58]

5.2.3 Membrane packed bed reactor

The membrane reactor technology for reverse water gas shift synthesis is another technology that has proven its effectiveness for overcoming the thermodynamic equilibrium limitation of the RWGS process. It allows to reach CO_2 conversion greater than equilibrium limits at temperature below 300°C.

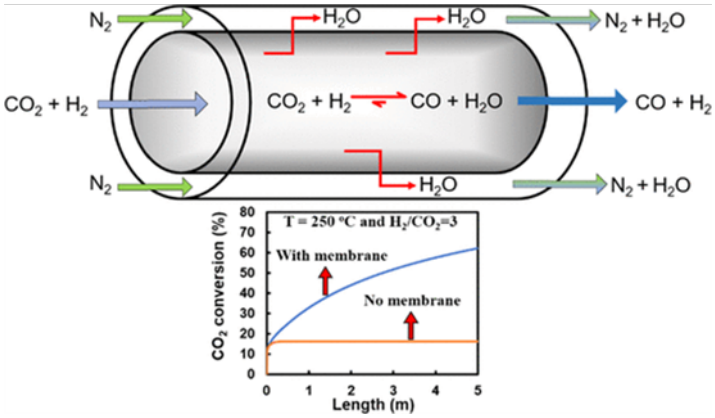

Figure 34: Membrane packed bed reactor [59]

This reactor is made of two concentric tubes. The inner tube acts as a packed bed reactor filled with catalyst and it is where the RWGS reaction takes place. The walls of this inner tube are made of a water-permeable material, letting the water molecule out of the tube (example includes zeolite membrane: MOR, ZSM-5/MFI, FAU, and H-SOD [59]). The second and outer tube is used to purge the water molecules produced during

the RWGS reaction. This purging is done via a sweep gas flowing through, for example nitrogen gas (N_2), responsible of carrying water outside of the reactor. As for the adsorptive reactor technologies, removing water from the reaction has effect of greatly enhancing the RWGS reaction equilibrium resulting in lower temperature required by the reaction as well as increasing its conversion rate. Moreover, an insulation layer can be added on the outside of the sweep tube to ensure that no heat loss can occur between the reactor and the environment, guaranteeing adiabatic operation. The longer the membrane reactor tube, the higher will be the single pass CO_2 conversion, as seen on the graph in Fig.34.
A downside of this technology, brought by its relatively low operating temperature, is the reduced choice of catalyst and the favoured production of methane. Indeed, because the reactor operates at lower temperature, the side reactions will more likely compete with the principal RWGS reaction, the catalyst choice must be made accordingly. Only catalyst, with higher selectivity towards CO conversion and limiting CH_4 formation are suitable for such application. An example of possible catalyst is $CuO/ZnO/Al_2O_3$ [59].

5.2.4 Microchannel reactor

The microchannel technology can be considered as a low TRL alternative for the RWGS process. This reactor as a similar operational principle as the fixed bed technology but has a more complex design. The reactor is made of thin alternating plates, on which a catalyst has been deposited. The unit is compact and the plate arrangement allows a very efficient thermal management, so, enabling isothermal behaviour for the reactor which, in presence of the right catalyst, allows to achieve a maximum equilibrium CO_2 conversion. However, despites all the advantages, this technology still suffers the same difficulties as the more typical fixed bed reactor when it comes to the catalyst replacement. Moreover, due to the very thin design of the metal plates and the high operating temperature, metals could have a tendency to melt, increasing the leak risks.

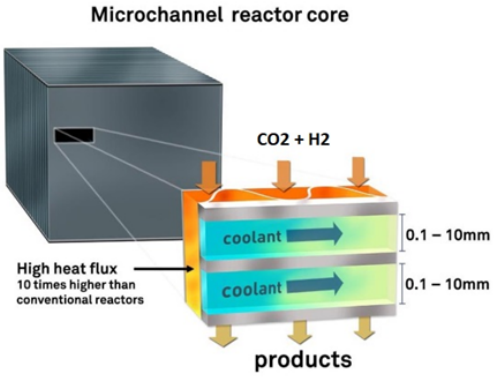

Figure 35: Microchannel structure for RWGS reaction, inspired by [60]

comparison of the reactor technologies

	Adiabatic packed bed	Adsorptive fixed bed	Adsorptive moving bed	Membrane	Microchannel
Temperature (°C)	<1000	<260	<260	200 – 300 [59]	<1000 but depending on the melting characteristic of the metal composing the reactor
Temperature control	Adiabatic operation, reactor insulated	Limited due to gaseous phase	Limited due to gaseous phase	Adiabatic operation, reactor insulated	Excellent temperature control due to high surface to volume ratio, isothermal operation
Pressure (bar)	No limitation in the range of RWG reaction	No limitation in the range of RWGS reaction	No limitation in the range of RWGS reaction	5 [59] [61]	No limitation in the range of RWGS reaction
Pressure drops (bar)	High in large scale reactor	High in large scale reactor	Very high due to cross flow between the gases and the adsorbent/catalyst mixture	Low because of the gas removal and non-presence of adsorbent	Low because catalyst coated to the walls
Productivity capabilities	High	High	High	Low	Low
TRL	High	High	High	Low	Very Low
Scalability	Very High	High	High	Average	Low
Catalyst removal	Offline	Offline	Online	Offline	Offline (even impossible if the catalyst is coated to the walls)
Adsorbent regeneration	/	Offline Require TSA or PSA and can damage the catalyst	Online The adsorbent regeneration is done in a separated unit therefore it is more efficient	/	/

Table 5: Comparision between the different RWGS reactor technology

5.3 Catalyst types for the RWGS process

Catalysts play an essential role in the RWGS process. They allow to radically reduce the temperature necessary for the reaction (compared to the equilibrium temperature of the reaction) and, therefore, the costs associated with these high temperatures. Most of the RWGS studies are focusing on two types of catalyst: oxides catalysts and supported metal catalysts, primarily, Cu, Pt, and Rh.

5.3.1 Supported metal catalyst

- Cu-based catalyst:
  Good performance at low temperature (∼165°C) and little to no production of methane as side products. Require high H_2/CO_2 ratio in order to achieve high CO_2 conversion. To enhance the catalyst activity, Cu can be dispersed on supporting material such as SiO_2, which allows better CO_2 conversion. Promoters can also be added to such catalyst arrangement to increase the catalyst efficiency; adding potassium for increasing the surface-active sites hence leading to better catalytic activity or iron promoters to prevent Cu nanoparticules sintering increasing the catalyst stability while improving its activity [50].

- Pt-based catalyst:
  Platinum allows, like copper, to operate the RWGS reaction at relatively low temperatures without producing methane but this material is very expensive and can be poisoned by CO, reducing its activity [62]. Moreover, Pt must be supported (usually over CeO_2) to increase its mechanical stability and to increase its number of active sites.

- Rh-based catalyst:
  Rhodium catalysts are mainly used for CO_2 hydrogenation in amine solution at relatively low temperatures (100-300°C). The low temperature operation causes high methane selectivity (the CH_4 selectivity can reach more than 80% for a H_2/CO_2 feed ratio of 3) [50]. Matsubu et al. [62] determined that the selectivity towards CO increases on Rh/TiO_4 for low Rh loadings at 200°C and low H_2/CO_2 feed ratios. For Li/RhY, the selectivity towards CO increases with the amount of Li promoter, the selectivity improves

from 0.3% at no Li, to 86.6% at an atomic ratio Li/Rh = 10. However, the CO_2 conversion decreases to half with the Li addition [50].

- Other transition metals and bimetallic particles or systems:
  Tests at low temperature (around 150°C) were performed on other transition metals such as M/La-ZrO_2 with "M" representing either Pt, Pd, Ni, Fe or Cu. These tests showed that the CO_2 conversion was practically the same for Ni, Fe and Cu supported La-ZrO_2, but the selectivity towards CO was improved (to 100%) on Fe and Cu whereas on Ni, it slightly decreased (96.5%) [63].
  Lu et al. [64] observed that, at low NiO loadings (<3%) on CeO_2, the selectivity towards CO was of 100% between 400 and 750°C while, at higher loading, the selectivity decreases due to higher aggression. Similar results were observed by Sun et al. on Ni/Ce-ZrO_2 for which, when the Ni loading increases, the selectivity towards CO and the CO_2 conversion decreases. This leads to the conclusion that Zr appears to lower the CO selectivity and the CO_2 conversion.
  Wang et al. [65] [66] studied different methods of supporting Ni on CeO_2 and found that the highest RWGS activity was observed on catalyst synthesized by impregnation since Ni is deposited as NiO, favouring the CO formation. 1% Ni/CeO2-impregnation catalyst achieved 45% conversion and 100% selectivity towards CO in a $H_2/CO_2 = 1$ flow at 750°C. Other studies found that increasing the Ni loading result in a increased catalyst activity: 2% Ni/CeO_2 achieved 35% CO yield at 600°C with $H_2/CO_2 = 1$ and 45% yield at 750°C, 3% Ni/(Ce-Zr)O_2 achieved 50% CO_2 conversion and 100% CO selectivity at 750°C and $H_2/CO_2 = 1$. Supporting Ni on SBA-15 does not have a significant impact on the catalyst activity but the incorporation of Cu in a Cu-Ni/SBA-15 both improves the CO selectivity and CO_2 conversion.
  Kharaji et al. [67] tested the supported bimetallic Mo-Fe/-Al_2O_3 system and found that it increases the CO formation rates, the CO_2 conversion and the CO selectivity compared to the monometallic version of the catalyst. This can be explained by the iron improving the CO_2 conversion and the Mo enhancing the stability of iron, thus the catalytic activity of the system.

5.3.2 Oxides catalyst

Oxide catalysts are studied because of their ability to work at high temperatures (above 700°C). There are many options for oxide catalyst available for the RWGS application. Some examples include perovskites for CO_2 hydrogenation with 97% CO selectivity and a CO_2 conversion of 40%, iron oxides catalysts like Fe_3O_4 offering high selectivity towards CO (around 99%) at 500°C (with no further information in the CO_2 conversion) or In_2O_3 and CeO_2. In_2O_3 being inactive alone, suppressing RWGS reaction (due to weak adsorption on the catalyst surface) and inhibiting the CO production. But, when coupled to CeO_2, it forms an active catalyst with high CO_2 conversion rates at temperature of 500°C and H_2/CO_2 ratios of 1/1. [50]
A summary of the tested catalysts and their characteristics (conversion, selectivity, optimal H_2/CO_2 ratio, and temperature) can be found in table 2 of the document by Yolanda A. and John N. Kuhn [50]

5.4 Energetic efficiency of the process

The energetic efficiency of the RWGS based on the Higher Heating Value (HHV) of the reactants entering and products leaving the process has been estimated at around 88% while the efficiency based on the LHV values is at 100% (endothermic process with heat provided to it so by the energy conservation principle and by neglecting heat loss, the LHV efficiency is 100%). This is calculated when considering a reactor with recirculation and a CO_2 conversion of 55% [50], with a catalyst choice an operating condition allowing a selectivity towards CO close to 100% (the side products of the reaction were not considered in the computation of the process efficiency). The calculations are available in appendix 56.

Part II

Syngas conversion to hydrocarbons

1 Fischer-Tropsch Synthesis

1.1 Operating principle

The Fischer-Tropsch (FT) process is a collection of reactions converting a synthetic gas feed into useable hydrocarbons such as light olefins, liquid fuels, waxes or chemicals. The nature of the product and its chain length will depend on the syngas composition (CO/H_2 ratio), the operating conditions inside the FT reactor (temperature and pressure), the type of reactor and the type of catalyst used in this reactor. The process was first developed by Franz Fischer and Hans Tropsch in Germany in the 1920s.

The FT synthesis can be summarised in a few stoichiometric equations. In the catalytic FT, one mole of carbon monoxide reacts with two moles of hydrogen to form mainly straight-chain 1-alkenes C_nH_{2n} together with n-alkanes, some internal alkenes and minor amount of branched hydrocarbons and primary alcohols (n representing the carbon chain length).
The reactions occurring in a Fischer-Tropsch reactor are the following:

- Main reactions:
  - The reaction to produce alkanes/paraffins:

    $$nCO + (2n+1)H_2 \Rightarrow C_nH_{2n+2} + nH_2O \qquad \Delta H = -(146 \times n)\text{kJ/mol} \quad (22)$$

  - The reaction to produce alkenes/olefins:

    $$nCO + (2n)H_2 \Rightarrow C_nH_{2n} + nH_2O \quad (23)$$

- Side reactions:
  - Water Gas Shift reaction (if Fe-based catalyst used):

    $$CO + H_2O \Leftrightarrow CO_2 + H_2 \qquad \Delta H = 42\text{kJ/mol} \quad (24)$$

  - The reaction to produce alcohols:

    $$nCO + (2n)H_2 \Rightarrow C_nH_{2n+1}OH + (n-1)H_2O \quad (25)$$

  - Boudouard reaction:

    $$2CO \Rightarrow C + CO_2 \qquad \Delta H = -254\text{kJ/mol} \quad (26)$$

  - Sabatier reaction:

    $$CO_2 + 4H_2 \Rightarrow CH_4 + 2H_2O \qquad \Delta H = -165\text{kJ/mol} \quad (27)$$

  - Hydrogenation of carbon monoxide to methane:

    $$CO + 3H_2 \Rightarrow CH_4 + H_2O \qquad \Delta H = -206\text{kJ/mol} \quad (28)$$
    $$2CO + 2H_2 \Rightarrow CH_4 + CO_2 \qquad \Delta H = -254\text{kJ/mol} \quad (29)$$

– Catalyst oxidation/reduction:

$$M_xO_y + yH_2 \Leftrightarrow yH_2O + xM \tag{30}$$
$$M_xO_y + yCO \Leftrightarrow yCO_2 + xM \tag{31}$$

Theses reactions are, for the most part, highly exothermic. Therefore, the heat released by the reaction must be extracted to avoid temperature increases inside the reactor which could lead to unwanted product generation and damages to the reactor and catalyst.

1.1.1 Chain termination

Assuming that the chain growth probability is independent of the chain length, the polymerisation is described by the Anderson-Schulz-Flory (ASF) equation:

$$P_n = (1-\alpha) \times \alpha^{n-1} \tag{32}$$

With P_n the mole fraction of a hydrocarbon with a chain length n (probability of forming a hydrocarbon of length n). The distribution depends on a single parameter: α, the probability a chain will grow rather than desorb from the catalyst, α, is independent of n. The chain growth probability (α) for a CH_2 monomer into a hydrocarbon chain is defined as the ratio of the propagation rate k_p and the sum of the propagation and termination rates ($k_p + k_t$):

$$\alpha = \frac{k_p}{k_p + k_t} \tag{33}$$

This α can be tuned by the temperature, syngas composition, pressure, catalyst choice, and presence of promoters. A high value of α implies that there will be a high production of heavy hydrocarbon whereas a low value of α will result in a greater production of lighter hydrocarbons. The range of α depends on the reaction conditions and catalyst type.
The expected chain length for a reaction with given conditions and catalyst can be written as:

$$< n >= \sum n \times P_n = \frac{1}{1-\alpha} \tag{34}$$

Such that the weight function is:

$$W_n = P_n \times \frac{n}{< n >} \tag{35}$$
$$= \alpha^{n-1}(1-\alpha)^2 n \tag{36}$$

And the plot of this weight function depending on the number of carbon in the chain is:

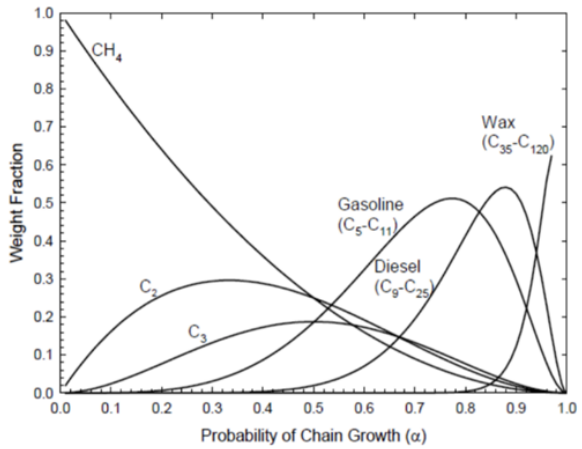

Figure 36: product distribution of the FT synthesis depending on the α parameter of the reactor [69]

The maximum probability of forming the n-length hydrocarbon with respect to α (obtained by doing the derivative $dPn(\alpha)/d\alpha = 0$) is obtained for a chain growth probability α:

$$\alpha = \frac{n-1}{n+1} \tag{37}$$

and is given by:

$$P_n = \frac{2}{n+1} \times \left(\frac{n-1}{n+1}\right)^{n-1} \tag{38}$$

The chain growth probability (α) can be tuned by modifying the operating temperature and pressure, the syngas composition, the type of catalyst and presence of promoters or not:

- Temperature is one of the primary process parameters that can control the selectivity of the FT process; for example, high reaction temperature leads to fast hydrogenation (more CH_4 yield and so less CH_2 formation) leading towards lower carbon number species, for either cobalt-based or iron-based catalyst. Besides, high temperature (above ∼300°C) favours the Boudouard reaction (2 CO ⇒ CO_2 + C), creating carbon deposition onto the catalyst surface which will accelerate its deactivation. [70]

- The composition of the inlet syngas has also an important impact of the Fischer-Tropsch synthesis (FTS) selectivity. Higher CO partial pressure will result in an increased surface coverage of the catalyst hence increasing the probability of chain growth. On the other hand, by increasing H_2/CO ratio, lighter hydrocarbons are favoured. The presence of water is another parameter affecting the selectivity, indeed, during the FTS, water is created as a side product of the main reaction but an excessive amount of water in the reactor will lead to undesired effect on the rate of reaction and the selectivity of the products. Besides, in the case of iron-based catalyst, presence of water and CO_2 can lead to re-oxidisation of iron, detrimental for the catalyst.

- Pressure seems to have only a moderate impact on the FTS. According to the literature, the process selectivity leans towards heavier products and more oxygenates one as the total pressure increases. Also, increasing the pressure has a slight but moderate impact on the CO conversion and the selectivity of the C_{5+} chains. However, as the pressure increases, the coke formation within the reactor will become significant, this is detrimental for the catalyst activity since coke will deposit on the catalyst surface, blocking its active sites.

- Space velocity inside the reactor has also an influence on the products selectivity, indeed, the lower the space velocity of the gas inside the reactor hence the higher the residence time and the lower the selectivity towards methane. This parameter also seems to influence the selectivity towards olefins (high space velocity for decreasing olefins selectivity) while having no effect on paraffins selectivity. [71]

The process dependency can be summarised in a table, where ↑ represents an increase in process selectivity, ↓ a decrease in process selectivity and * a complex relation. In every case, the parameters of the reaction are increasing:

Parameter	Chain length	Olefin selectivity	Alcohol selectivity	Carbon deposition	Methane selectivity
Temperature	↓	*	↓	↑	↑
Pressure	↑	*	↑	*	↓
H_2/CO	↓	↓	↓	↓	↑
Space velocity	*	↓	↓	*	↑

Table 6: Reaction condition impact on the products [72]

1.2 Different methods of Fischer-Tropsch synthesis (FTS)

Fischer-Tropsch processes are often divided according to their respective operating temperatures: High temperature reactor (HTFT) which typically operates between 300 and 350°C and the low temperature reactor (LTFT), around 190-260°C. Cobalt catalysts are principally used in low LTFT synthesis (T = 220–240 °C) whereas Fe-based catalyst can be used either in low temperature process as well as in higher temperature ones. The main effect of the temperature level difference between these two processes is a shift in average chain length on the product side.

Other catalysts than Co and Fe are available for the Fischer-Tropsch synthesis, notably Nickel and Ruthenium. However, Ni is not used in industry due to its high selectivity towards methane while Ru has high activity for CO hydrogenation and can work at low temperatures (<150 °C) to produce long chain hydrocarbons, but is expensive, and reserves are low. Therefore, cobalt and iron-based catalysts are the only two types used in industry due to their relatively low cost and abundance.

1.2.1 High temperature FTS using Fe-based catalysts

In high temperature Fischer-Tropsch or HTFT, hydrocarbons are synthesised at temperatures averaging 340°C and high pressure of around 25 bar. This FTS methods is more suitable for the production of lighter products such as gases and gasoline (short hydrocarbon chains) with an high content of unsaturated hydrocarbons and alcohols.
Because of the high operating temperature and the higher risk of coke formation, this FTS is realized with only iron-based catalysts. Iron is the most common industrially used metal for Fischer-Tropsch catalysts because it has the advantage of being effective and cheap. However, its activity and selectivity are poor compared to other metals. To alleviate this problem, iron-based catalyst can be enhanced by adding special additive called promoters (such as Alkali metals, ruthenium and platinoids) to the catalyst or by changing the physical format of the catalyst particles. Moreover, iron-based catalysts have the advantage of having a good mechanical integrity, allowing them to have a better resistance to the abrasive environment inside, for example, a circulating reactor bed.

Fe-based catalysts also have the advantages of being Water Gas Shift (WGS) active materials, meaning that when water is formed inside the FT reactor, in the presence of CO, the WGS reaction will occur, depending on the equilibrium inside the reaction. If the FT reaction requires a larger H_2/CO ratio, the CO will be converted thanks to the WGS reaction to H_2, increasing the ratio. Therefore, in the case of a Fe-HTFT, the inlet syngas stream does not need to have a precise H_2/CO ratio, it can slightly change without impacting too much the FT process.

1.2.2 Low temperature FTS using Fe-based catalysts

Low Temperature Fischer-Tropsch or LTFT is a synthesis of hydrocarbons at relatively low temperature averaging 230 °C and high pressure of around 25 bar. This pathway is ideal to produce, mainly, saturated hydrocarbons with low alcohols content and with a good selectivity towards long hydrocarbon chains and jet fuel. This type of FT reaction is generally carried out in slurry-phase reactor or fixed bed reactor because of the low resistance of cobalt to abrasion, which takes place in a circulating bed reactor, for example.

Cobalt possesses very low intrinsic WGS activity and, thus, is more useful for high and constant H_2/CO ratio of around 2 or 2.1. Also, cobalt being highly expensive, it is typically supported on other material to increase the fraction of exposed cobalt surface. The support materials are, for example, Al_2O_3, SiO_2 or TiO_2 [73].

1.2.3 Comparison between the two FTS methods (Co-LTFT and Fe-HTFT)

Depending on the targeted products, the preferred FT technology may vary; in the case of a FTS using Fe-based catalyst, short olefins are mostly produced whereas in FT synthesis with Co-based catalyst, long paraffin chains are the main products [74]. For example, in the case of a company wanted to synthesise e-kerosene in a FT reactor in order to produce aviation fuel, kerosene consisting mainly in paraffins (at around 85% composition) of length from 8 to 16 carbons [75], low temperature, cobalt-based catalyst will be more appropriate from a product selectivity point of view. However, the cost of Fe-based catalyst compared to Co-based ones is significantly lower. This may become an advantage for the use of iron catalyst in reactors, this one having to be followed by and hydrogeneration reactor to produce paraffins from the olefins produced by the FT process. [76]

Another difference between low and high temperature FTS is the state of the products (liquid, solid, gas) at the exit of the reactor. In HTFT synthesis, product is a two-phase gas-solid mixture, while in LTFT the product is a three-phase mixture (gas-liquid-solid). In general, Co-LTFT tends to produce more methane than Fe-HTFT catalyst. Besides, Co-based catalysts are more sensitive to pressure variation than Fe-based ones, its alpha-value tends to increase with pressure [77].

Inside the reactor, the syngas space velocity also has an impact on the product selectivity depending on the catalyst type used. In the case of a Co-based catalyst, the selectivity towards methane increases with space velocity whereas for Fe-based catalyst, this selectivity decreases with space velocity. Also, when operating under pressure, the productivity of iron-based catalyst increases while the one of cobalt catalyst decreases [72].

Co-based catalyst has the advantage compared to Fe-based catalyst that water and CO_2 do not have an inhibiting effect on the rate of the FTS. On the other hand, water and CO_2 (water, coming from the FTS and CO_2 coming from the WGS reaction) have both an inhibiting effect on the kinetics of iron-based catalysts. This implies that in the case of a Fe-based catalyst, the rate of the reaction will decrease as the reaction progresses, on one hand, due to the consumption of the reactant and, on the other hand, due to the formation of inhibiting products (H_2O and CO_2) [77].

One of the big differences between the use of cobalt or iron catalyst is the syngas composition required for proper Fischer-Tropsch. Fe-based catalysts are WGS active materials, meaning that they can perform the WGS reaction if the conditions are favourable. During the process, if the ratio H_2/CO is not perfectly right, the equilibrium will be such that the WGS reaction will happen, consuming CO to produce H_2, increasing the ratio. This mechanism provides a stabilising effect of the syngas composition (H_2/CO ratio), allowing to the inlet stream some tolerances regarding this ratio. Unlike HTFT where iron catalyst is used, the low temperature technology based on cobalt catalyst is more sensitive to a fixed ratio, considering that no WGS reaction occurs in the synthesis to moderate the ratio. As a result, in case of Co-LTFT, a ratio of H_2/CO fixed around 2 must be guaranteed.

It is important to mention that it is not necessary a good thing for the industrial process to highly rely on the WGS reaction since it would generate large amounts of CO_2 in the FT gas loop, increasing the processing cost (compression work increase and separation necessary) ([72],p61).

	Fe-based catalyst	Co-based catalyst
Operating temperature	200-240°C and 320-350°C	200-240°C
Operation pressure	20-40 bar	20-30 bar
H_2/CO ratio	1.8-2.2	2
Selectivity	Higher yield of oxygenates and other undesired products	Lower yield of oxygenated and olefins
Productivity	Higher productivity at high pressure and space velocity	Low productivity at high pressure and space velocity
Catalyst activity	Low	High
Catalyst stability	Low	High
Cost	Low	High

Table 7: Comparison between iron and cobalt catalyst for FT synthesis

The major impact of the choice of the catalyst material concerns the share of the syncrude compound classes, which are primarily represented by paraffins (alkanes), olefins (alkenes), aromatics, and oxygenates. Regarding longer-chain hydrocarbons, cobalt-based catalysts lead almost exclusively to the formation of paraffins, whereas, with iron-based catalysts, both olefins and oxygenates are formed in notable proportions. The formation of aromatics is only promoted in the case of Fe-HTFT for certain chain length ranges [78].
These differences can be observed in the following table extracted from the book "Greener Fisher-Tropsch Processes for Fuels and Feedstock" [72] in which both FT processes are compared regarding the generic compositions of the main industrially produced FT syncrude types:

Product fraction	Carbon range	Compound class	Syncrude Composition (mass%) *	
			Fe-HTFT	Co-LTFT
Tail-gas	C_1	Alkane	12.7	5.6
	C_2	Alkene	5.6	0.1
		Alkane	4.5	1.0
LPG	$C_3 - C_4$	Alkene	21.2	3.4
		Alkane	3.0	1.8
Naphtha	$C_5 - C_{10}$	Alkene	25.8	7.8
		Alkane	4.3	12.0
		Aromatic	1.7	0
		Oxygenate	1.6	0.2
Distillates	$C_{11} - C_{12}$	Alkene	4.8	1.1
		Alkane	0.9	20.8
		Aromatic	0.8	0
		Oxygenate	0.5	0
Residue/Wax	$>C_{22}$	Alkene	1.6	0
		Alkane	0.4	44.6
		Aromatic	0.7	0
		Oxygenate	0.2	0
Aqueous Product	$C_1 - C_5$	Alcohol	4.5	1.4
		Carbonyl	3.9	0
		Carboxylic acid	1.3	0.2

Table 8: Comparison between the generic product of Fe-HTFT and Co-LTFT; *:The syncrude composition is based on the total mass of product from FT synthesis, excluding inert gases (N_2 and Ar) and water-gas shift products (H_2O, CO, CO_2 and H_2). Zero indicates low concentration and not necessary the total absence of such compounds [72],p83.

These compositions are not fully representative of any specific technology, and within each syncrude type, considerable variation can be found. For example, the Shell middle distillate synthesis [79] uses a CO-based LTFT synthesis to produce a heavy paraffinic syncrude with a composition close to the one in the previous table while, in contrast, the original German normal pressure process [80] produced a more olefinic syncrude containing less than 10% wax and around 20% alkenes.
Besides, the difference in syncrude composition between different processes, the composition of a particular synthesis will change over time as the catalyst inside the reactor is aging and progressively deactivating (with a catalyst aging depending on several factors, explained in a following section).

1.3 Catalyst deactivation

In the case of Co-based catalyst, the main causes of degradations leading to catalyst deactivations are poisoning, re-oxidation of active sites, carbon species deposition, carbidisation, surface reconstruction, sintering of cobalt crystallites, metal-support solid state reactions and attrition [81].
Poisoning is caused, in part, by alkali metals which decreases the activity of the catalytic material, however,they

also have the positive effect of increasing the chain growth probability (α), so important in the FTS [82]. Sulphur is another catalyst poison, it causes a geometric blockage of the catalyst active sites, inhibiting the CO adsorption. Its impact depends on the nature of the sulphur species. Carbon deposition can occur due to high operating pressures, wanted for longer chain formation and increased conversion rate in LTFT. However, if the pressure is too high, catalyst deactivation can occur due to coke formation [82].

Fe-based catalysts are impacted by the same causes of deactivation as the cobalt based synthesis. However, the oxidation of the active iron by water is much more pronounced in this case. Also, carbon deposition is particularly more important for HTFT because the Boudouard reaction (2 CO $\Rightarrow$ C + CO_2) is favoured at higher temperature (>270°C). The carbon produced will be deposited onto the catalyst surface, limiting the access to the active sites where the FT reaction can take place.
In general, supported cobalt catalysts have a much longer lifetime than iron catalysts because of the greater resistance to re-oxidation of cobalt compared to iron [77].

1.4 Reactor types for Fischer-Tropsch

1.4.1 Fixed bed reactor [72]

This reactor technology was one of the oldest installed at commercial scale. Its mechanical structure is basic, and its operating principle is simple. This design is robust and dominant in the industry for low temperature Fischer-Tropsch synthesis. The reactor design is like a shell-and-tube type heat exchanger, composed of tubes filled with catalyst. At industrial scale, tubes have a diameter of around 5cm and their number can go as high as 5000 tubes per reactor. These tubes are immersed in a boiling water which removes the heat released during the FTS occurring in the tubes. To regulate the temperature inside the shell, a pressure valve is responsible of adjusting the steam pressure in the shell side.

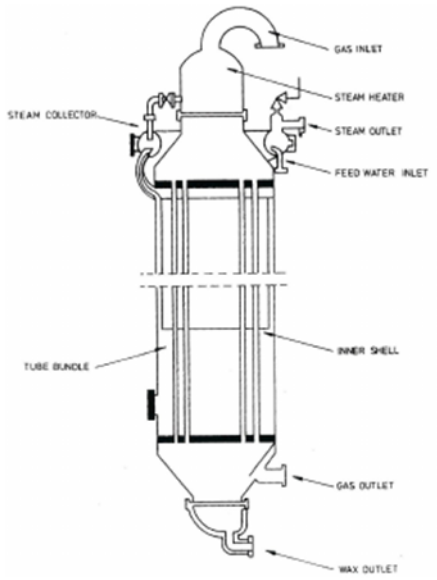

Figure 37: Fixed bed reactor ([72], chap3.5)

The inlet stream (syngas) enters at the top of the reactor and goes down inside the tubes, through the catalyst bed, where the reaction occurs. At the bottom of the tubes, the products (mainly long hydrocarbons chains and waxy products in case of an LTFT) exit and are then separated depending on their state (gaseous stream leaves the reactor at the gas outlet while waxy products leave the reactor at its bottom). The catalytic bed inside the tube remains fixed during the reactor operation.

The wax products recovered at the bottom of the reactor can either be extracted to be used as such or be reduced into lighter hydrocarbons or they can either be recycled inside the same reactor in order to greatly improve the heat transfer inside the tubes, allowing a better temperature hence reaction control. However, this recirculation will result in higher energy consumption because of the use of more and bigger pumps. The reactor is called in this case a trickle bed reactor.
The advantage of this reactor technology is that the catalyst bed is fixed, therefore, in case of contamination by a catalytic poison, only the top part of the bed will suffer from deactivation, making the technology more robust and the catalyst longer lasting in case of non-pure syngas.
The drawbacks of this technology are the followings: The catalyst replacement is complex, and its utilisation is low. Also, due to the geometry of the tubes and the catalytic bed inside, a high-pressure drop is present between both ends of the reactor. Then a poor heat transfer due to gaseous state of the reactant and cooling steam can result in poor heat management and, ultimately to a high frequency of catalysts replacement due to coking.

1.4.2 Slurry bed reactors [72]

The slurry bed reactor also called slurry bubble column reactor was introduced by Sasol in 1933 to replace the mutitubular fixed bed. This technology is considered as one of the most efficient technologies suitable for LTFT, considering that it was designed to overcome both fixed and fluidised bed reactors problematics. Moreover, this technology can be easily scaled up to meet the demand of a specific installation.
In this reactor, the inlet syngas is introduced at the bottom of the reactor then, a gas distributor will make sure that the syngas is well spread over the whole area of the reactor column. The distributed syngas enters the slurry phase in which the catalyst is supported. It is in this slurry phase that the FT reaction occurs, the light products, in gaseous form, leave the slurry bed and then pass through a mist separator before leaving the reactor. The heavy products (waxy products), on the other hand, do not leave the catalytic bed but are collected on the side wall of the reactor where they are separated from the catalyst micro particle, catalyst particle which are recycle inside the reactor to keep a controlled catalyst concentration inside the slurry phase.

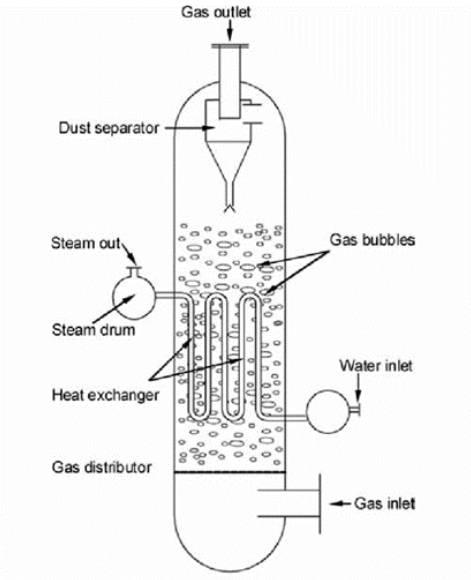

Figure 38: Slurry bed reactor ([72], chap3.5)

The heat management inside the reactor is handled by a heat exchanger composed of cooling tube in which steam is circulating. The temperature control inside this slurry bed reactor is better than in a fixed bed reactor since the heat exchanger is immersed in the slurry phase, which has a way better heat transfer coefficient compared to gas compounds.

This technology has many advantages for LTFT synthesis; The heat management hence the reaction control is easy thanks to the good heat transfer inside the reactor provided by the liquid phase of the catalyst bed, the product selectivity is high, the catalyst removal is simple, the pressure drop between the inlet and outlet is relatively low and the catalyst utilisation is high (mostly compared to the fixed bed technology) since the liquid phase allows a good blend.
However, this technology has some drawbacks; On one hand, there is the complex separation of the catalyst from the waxes which can result in catalysts attrition, and, on the other hand, this technology will be very sensitive to syngas purity since every contaminant present in the inlet stream will spread instantly inside the catalyst bed, causing a rapid poisoning and a premature catalyst deactivation.

Note that this technology is also called fluidised bed reactor in the case where the reactor contains solid catalyst particles but is not liquid supported. Both reactors are similar in operation; a distributed gas passes through a reactor containing solid catalyst particles suspended in a fluid. However, in slurries reactor, the catalyst is suspended in a liquid, whereas in fluidised beds, the suspending fluid is the reacting gas itself.

1.4.3 Circulating fluidised bed reactor [72]

The circulating fluidised bed (CFB) reactor technology is based on a moving catalyst bed between the reactor enclosure and an external cooling unit. This continuously moving catalyst enhance the thermal transfer, allowing more precise operation hence better selectivity towards the desired products. Also, it limits the formation of coke inside the reactor. This technology is well suited for HTFT application (and not for LTFT) because the synthesis only occurs in gas phase.
The working principle of CFB is the following: the hot syngas entering the reactor are mixed with the catalyst particle coming down the standpipe with a mass flow controlled by a valve. The reaction starts as soon as the mixing is done. Then, the syngas/catalyst mixture enters the transportation reactor where the heat released by FTS is extracted thanks to a heat exchanger. High quality steam is produced during the process and the process temperature inside the reactor is controlled by varying the steam pressure. After reaction, the reacting gaseous mixture is passed through a catalyst separation cyclone, separating the catalyst and the FT products, the catalyst is then sent back into the loop and the produced hydrocarbons leave the reactor.

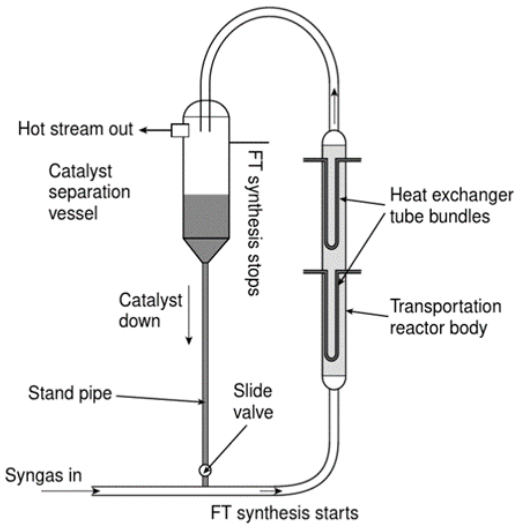

Figure 39: circulating fluidised-bed reactor ([72], chap3.5)

CFB technology has several advantages. It has a high gas throughput which allows a high production capacity, the heat management inside the reactor is efficient allowing good control over the reaction condition hence the selectivity of FTS and the catalyst can easily be replaced, without stopping the process.
However, CFB also has its number of drawbacks; Its high gas flow rates and large catalyst recycling cause excessive catalyst-attrition and erosion. The technology has a low catalyst efficiency due to unreacted catalyst inside the reactor system and, the technology is rather complex and expensive to operate and install compared to other FT reactor type.

1.4.4 Microchannel reactor

Microchannel reactor is the latest technology in the reactor field. It is becoming more and more easy to manufacture thanks to the progress in 3D printing technologies. Its development was pushed to specially overcome the problematic linked to the heat management for highly exothermic reactions. With their characteristic dimensions in the micro or millimetres range, this class of reactors has a very high surface-to-volume ratio compared to other reactor technologies (of at least two order of magnitude) allowing them to offer unmatched heat and mass transfer for multi-phase reaction. Therefore, microchannel reactors are well suited for highly exothermic reactions such as the FTS since the heat released by the reaction can effectively be extracted, allowing a quasi-isothermal process, a high catalyst activity and a long catalyst lifetime (no active site blockage by cocking). Moreover, thanks to its ability of maintain a uniform temperature during the reactions, the selectivity of the FT process can precisely be controlled and tuned depending on the wanted product while reducing the probability of hotspot and coke production/deposition inside the reactor, increasing its lifetime.
Besides, since the scale-up of such reactors is intended to happen by parallelization (stacking of reactor in parallel to each other), the properties of the reactors should be conserved, even at larger scale with no additional drawbacks.
The major drawback of this technology is managing the catalyst. Catalyst materials must be coated on the inner wall of the microchannel, allowing high space velocity and low pressure drop. However, this catalyst deposition technique only provides low productivity due to the limited amount of gas/catalyst contacts. Moreover, the major inconvenient of the catalyst coating is that the micro-structured reactor must be thrown away if the catalytic material would come to deactivate. Other techniques for catalyst insertion in microchannels are experimented (such as catalytic power for example), however, these technologies also come with their challenges. Despite the advantages, the microchannel technology is still not at a sufficient TRL for industrial or commercical application but remains limited to small scale use such as in pharmaceuticals applications.

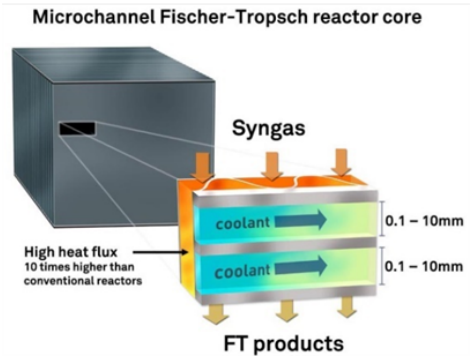

Figure 40: Schematic of a microchannel reactor for FT synthesis [69]

Reactor technologies comparison

	Fixed bed [82]	Slurry bed [82]	fluidised bed [82]	Circulating fluidised bed [82]	Microchannel [83] [84]
Operating temperature (°C)	220-240 To avoid catalyst swelling hence tube blocking (in the case of tube filled reactor)	220-240 Higher temperatures lead to hydrocracking of the waxes	320-350 To avoid agglomeration of catalysts by heavy waxes	320-350 To avoid agglomeration of catalysts by heavy waxes	200-240 300-350 Depending on the type of catalyst used hence the type of synthesis performed
Temperature control	Limited due to gaseous phase	Excellent temperature control for well mixed bed, almost isothermal	Excellent temperature control however, below slurry bed due to better heat capacity of liquid compared to powders	Excellent temperature control thanks to turbulent flows, almost isothermal	Excellent temperature control due to high surface to volume ratio, isothermal operation
Operating pressure (bar)	20-30	20-30	Up to 40	20-40	10-40
Pressure drops	High in large scale reactor (~4 bar)	Low, up to 4 times lower than in fixed bed (probably due to the nature of the catalyst bed, liquid vs solid) (~1 bar)	Lower than in Circulating fluidised bed since the velocities are lower	High, gas + catalyst mixture circulating in tubes and separated by a filter introducing pressure loss	Very low if coated catalyst Low if catalyst powder, High space velocity
Catalyst	Fe/Co-based	Fe/Co-based	Fe-based	Fe-based	Co-based if used in LTFT Fe-based if used in HTFT
Catalyst loading	Only the first cm of the catalytic bed is affected by the poisoning	Catalyst loading 4 times lower than in fixed bed because of smaller particles but high sensibility to poisoning	Less carbon deposition than CFB than higher catalyst loading and lower replacement rate	Carbon deposition results in lower catalyst loading hence lower conversion	Light catalyst loading if coated on the channel wall (only few contacts area with the gas)
Catalyst removal	Offline	Online	Online (less replacement necessary than CFB)	Online	Impossible, must change the entire reactor
Selectivity	High carbon number products	High carbon number products	Mainly low carbon number products (80%<C10)	Mainly low carbon number products (80%<C10)	High selectivity towards high carbon number products
Conversion	~60% per pass (when wax recycling is used)	~60% per pass	>85%	~85%	60-70%
Upscaling	Easy by adding tubes in larger shell, Upscaling possible up to 3000-4500 barrel/d	Easy, Upscaling possible up to 3000-20000 barrel/d	/	/	Easy by adding micro channel in reactor parallel, But very low production rate per reactor
Installation cost	High construction cost	Lower than fixed bed (up to 25%) due to use of smaller catalyst particles	Lower than CFB (up to 40%) and similar to slurry bed	High	High due to the low TRL
Operational cost	Average	Low	Low	High, maintenance required	High for now due to the low TRL

Table 9: Comparison between the different technologies of FT reactor

1.5 Criteria for selecting the right reactor and catalyst

The choice, optimisation and operational conditions of reactor design play a crucial role in the products selectivity of the FT synthesis. The FT process being highly exothermic, heat management inside the reactor is one of the main concerns of its design. If the heat produced by the reaction is not managed properly, the temperature rise inside the reactor will result in an increased methane yield and greater carbon deposition onto the catalyst, accelerating its deactivation. The most popular reactors for FTS currently used in the industry can be classified in four groups: slurry phase reactors, fixed bed reactors, fluidised bed reactors, and circulating fluidised bed reactors. Another reactor type can be added to this list; the Milli-structured reactors which may not be as widespread as the other four but show significant advantages in certain area compared to other technologies.

The choice of a FT reactor technology can have a huge impact on the industrial installation up and downstream of the FT reactor. To properly choose the type of FT reactors suitable to an installation, there is several criteria to consider:

1.5.1 Syngas composition and purity

The syngas composition has a significant impact on the reaction occurring inside the reactor, in which the ratio H_2/CO is the most important parameter. Depending on the type of catalyst used inside the reactor, its value must be carefully chosen or not, either the catalyst is WGS active or not. When the catalyst is not WGS active (f.e. cobalot catalyst), the H_2O and CO_2 molecules present in the inlet flow or produced in the FTS will be considered as "inert" in the reactor. Therefore, the H_2/CO ratio will decrease through the reactor depending on the usage ratio of the FT technology. In the case of such catalyst, it is necessary to provide directly the

right H_2/CO ratio required by the FT technology at the inlet of the reactor. However, when the catalyst used is WGS active (f.e. iron catalyst), the overall composition of the gas mixture is not as important for the FT process, because; under the action of the WGS reaction, the H_2/CO ratio will change progressing through the reactor. In this case, the operating conditions will impact the equilibration rate of the WGS reaction whereas the local H_2/CO ratio will be determined by the reactor type and the reaction kinetics [72].

The syngas purity, on the other hand, is representing the quality of the inlet flow and the amount/concentration of contaminant it contains. Contaminants are molecules which deactivate the catalyst inside the reactor, decreasing its efficiency and lifetime. Depending on the type of FT reactor technology, syngas purity must be very strict or not. For example, in the case of fixed bed reactor, the contamination will start by the top of the catalyst bed, where the inlet gas are introduced, then as the reactor operates, the catalyst poisoning will progress through the bed in a front, making it easy to deal with and inexpensive since only a part of catalyst must be replaced at a time. In this case, the syngas purity is not too important, and its quality will depend on the trade-off between the catalyst replacement cost and the syngas purifying cost.
However, for other FT reactor technologies such as slurry bed or fluidised bed, the catalyst circulation inside the reactor will allow the catalyst poison to spread over the whole bed, significantly decreasing the catalyst lifetime. In this case, syngas purity and cleaning are much more important than in reactor technologies with fixed bed since in case of contamination, the whole catalyst will have to be replaced.

1.5.2 Catalyst deactivation, lifetime, and replacement

The reactor type choice will determine if it is possible to replace catalyst online or if a complete stop of the operations is required. But this replacement is firstly determined by the type of catalyst used and its resistance against deactivation. All catalysts deactivate over time, but the nature of the FT technology (the operating conditions inside the reactor) will determine the rate of this deactivation and its impact on the process selectivity. Usually, catalyst deactivation is accompanied with an increase in methane selectivity, detrimental to the installation since it increases the compression cost while decreasing the productivity towards targeted products. The catalyst replacement cost is affected by both the rate at which it is necessary to replace and its actual cost. Cobalt catalysts are more expensive than iron-based catalysts but balance that with their longer lifetime and/or their better yield [72].

Concerning the catalyst replacement, the reactor type will be the determining factor if it is possible to remove and replace catalyst online or if the operation will have to be stopped. The online replacement of catalyst is possible with slurry bed and fluidised bed reactor, the FT technology can even, in principle, be operated at an equilibrium catalyst composition resulting in a stable activity and selectivity profile for the reactions. Although this seems advantageous from an operational perspective, the constant change in catalyst composition implies that old and fresh catalysts will be blend while some "very old" catalyst may be stuck inside the reactor and never replaced, leading to a smaller catalytic activity at best and to a selectivity shift towards unwanted products at worst. The online catalyst replacement is not possible in the case of fixed bed reactor and may be very labour intensive in the case of a multitubular fixed bed reactor. Therefore, the catalyst lifespan will be considered more critical in the case of a fixed bed technology than in moving bed [72].

1.5.3 Turndown ratio

The turndown ratio represents the ability of the facility to operate at lower syngas feed than it was design to. The turndown ratio is calculated as the ratio of actual feed rate to design feed rate. The ability of the facility to operate at lower syngas feed may or may not be important depending on the application but is dependent on the robustness of the facility. Fixed bed reactors are better suited to low turndown ratio than slurry or

fluidised bed reactors in which a minimum slurring or fluidisation velocity must be maintained in order to operate properly [72].

1.5.4 Steam quality

The FT synthesis being a very exothermic process, the heat released by the reaction can be used for power generation using high-pressure steam or pre-heating of different stream within the facility. The steam quality highly depends on the operating conditions of the FT technology, the higher the operating temperature of the FT process, the higher the steam quality. Therefore, fluidised bed reactors have an advantage compared to slurry and fixed bed reactors when it comes to the production of high-quality steam [72].

1.5.5 Fischer-Tropsch products composition and quality requirement

There are significant differences in composition between the syncrude produced by the LTFT and the HTFT. The syncrude composition affects the ability to refine the products towards the targeted hydrocarbons. The technology used for the FT synthesis as well as its precise operating conditions are other factors modifying the carbon chain length distribution and the relative concentration of the various compound classes hence its ability to be effectively refine towards the wanted products.

The syncrude quality is a measure of the number of impurities present in the outlet mixture. It will determine if an additional separation step is required downstream of the FT unit or not. In the case of slurry bed and fluidised bed reactor, a catalyst/syncrude separation step is required since the liquid FT products are either mixed with slurry phase or small catalyst particles. Depending on the efficiency of the catalyst separation unit, catalyst particles produced by attrition in the FT reactor may find their way into the products. Therefore, the downstream equipment must be designed to account for these impurities, or the efficiency and lifetime of theses equipment may decrease due to plugging and fouling. [72]

1.6 Fischer-Tropsch product upgrading to e-fuel

The processes used for upgrading the products from the FT synthesis reactor to gasoline and diesel blending stock are like the one used for conventional crude refining, only having some operating parameters differing. Main units used for the FT product refining are the following: distillation, hydrogen production, wax (C_{20+}) hydrocracking, naphta (C_5-C_{10}) and middle distillate (C_{11}-C_{19}) hydrotreating, C_5/C_6 isomerisation, and catalytic reforming (for the chain with carbon length of C_7-C_{10}) [85].

Gases exiting the FT reactor are cooled by heat exchange before being depressurised in a flash drum, allowing the unreacted syngas, light fuel gases (or LFG), and inert gases to evaporate and separate from the heavier hydrocarbons (C_{5+}). This allows to feed the hydrogen recovery subsystem with a pressurised, hydrogen rich stream (this stream can eventually be passed through a WGS reactor to further increase its H_2 partial pressure) [85]. The other products of the FT synthesis are sent to a distillation tower in which they will be fractionated into naptha, middle distillates, waxes, and LFG. The working principle of such column is based on the difference in boiling point of the different hydrocarbons and uses high temperature ($\sim$400°C) at atmospheric pressure to evaporate the gases while the heaviest hydrocarbons stay liquid [85]. As the gaseous products are rising in the column and cooling down, they pass in perforated trays, in which the lower boiling point molecules are condensed and trapped, effectively separating the products.

The separated naptha and middle distillate fractions are then sent to a specific hydrotreating plant. In this unit, the hydrocarbons are fed with hydrogen to a metal-oxide catalytic reactor operating at around 350°C.

In this reactor, olefins are hydrogenated to paraffins (via saturation) to increase the heating value and octane rating of the gas stream [85]. An example of the saturation reaction occurring in such unit is given here below:

$$C_8H_{66} + H_2 \Leftrightarrow 2C_{16}H_{34} \tag{39}$$

Then the products of chain length C_5/C_6 from the naptha hydrotreater and wax hydrocracking are gathered and sent to a reactor for catalytic isomerisation. This process re-arranges the molecular structure of the normal, straight chain molecules of pentane and hexane to iso-pentane and iso-hexane which are branched molecules. These new molecules have the advantage of an increased octane number compared to the straight chain equivalents, making them more suited for the gasoline and diesel applications. The reactor used for this process operates at around 200°C and under a pressure of 20 bar [85].
The products having a chain length C_7/C_8 extracted from the naptha hydrotreater and wax hydrocracking are also sent to a similar process of isomerization in order to increase their octane rating. This main reforming reaction is endothermic and the feed gas is heated to a temperature of around 480°C before entering the reactor, operating at a pressure of 40 bar. The product from this process is called reformate and has the highest octane rating, it represents most of the gasoline blending stock (this process can achieve octane rating of 87 to 88) [85].

1.7 Efficiency of the FT process

The calculation of the energetic efficiency of the Fischer-Tropsch process can be difficult due to the non-deterministic and highly conditions dependant nature of the reactions taking places. However, several studies have effectively estimated and calculated this efficiency.

Fu et al. [86] calculated a syngas to Fischer-Tropsch Liquid (FTL) conversion efficiency of $71\%_{LHV}$, with the detail of the calculation being the following: The conversion from syngas to FT product in the reactor is 95%, only 80% of the energy in the gas is retained in the paraffin FT products, the remainder being released as reaction heat. The selectivity of the FT process to C_{5+} products is 95% and the heavier part of these products can be converted to fuel using hydrocracking with a 98% efficiency. The energy contained in the FT off gas (light hydrocarbons) can be used to generated heat or electricity. Therefore, the overall efficiency of the conversion from syngas to FTL is 71% (0.95×0.80×0.95×0.98). However, this study considers a relatively generous syngas conversion to FT product, making the estimation a bit high.

Another study, based on detailed process modelling made by Becker et al. [85] has obtained similar efficiencies in the different units, the only difference being for the conversion of syngas to FT product and the FTL upgrading efficiency. In this study, the syngas conversion chosen as the baseline for their study is based on a high-end Fischer-Tropsch slurry bubble reactor using a cobalt-based catalyst in a LTFT process. The efficiency of the syngas-to-FTL is detailed as such: syngas conversion of 80%, efficiency of 84% for the reaction heat, 94.1% of selectivity towards C_{5+} (with an alpha value of 0.9), and a 90.4% FTL upgrading efficiency. This result in an overall process efficiency of $57.16\%_{LHV}$.

2 Methanol synthesis

Methanol is good alternative fuel due to potential H_2 carrier and higher energy content of 726.3kJ/mol. Its can also be used as a base product for other processes, notably, the methanol-to-gasoline process, with the goal of increasing its energy content and its usability as a transportation fuel for cars, planes, etc.
Methanol is also interesting as an energy storage solution (instead of H_2) since it is liquid at room temperature, therefore is easily transportable and safe, compared to hydrogen.

The commercial production of methanol first started in the 1920's by a society called BASF. At this time, methanol was synthetized from syngas using a zinc/chromia based catalyst under a pressure of 300 bar and temperatures above 300°C. The thermodynamic limitations associated with the synthesis led to investigation for other synthesis technique, the high-pressure limitation was mitigated by the introduction in 1960 of a new catalyst, Cu/ZnO, by a company called ICI (now Johnson Matthey). This process is still the one used nowadays, with pressure in the range of 50 to 100 bar and temperature between 200 and 300°C.
The temperature range is determined by the catalyst used by the process, the lower bound is determined by the copper catalyst activity while the upper band represents its limit of thermal stability and increase in catalyst deactivation rate.

Methanol can be synthetised either by using carbon monoxide (CO) as carbon source or by using carbon dioxide (CO_2). In both cases, the reaction converting CO_2/CO and H_2 to methanol (CH_3OH) is called hydrogenation. This process consists in combining one mole of CO_2/CO and 3/2 moles of H_2 to produce methanol in an exothermic process:

$$CO_2 + 3H_2 \Leftrightarrow CH_3OH + H_2O \qquad \Delta H = -49.5\text{kJ/mol} \tag{40}$$

$$CO + 2H_2 \Rightarrow CH_3OH \qquad \Delta H = -90.6\text{kJ/mol} \tag{41}$$

Both reactions are exothermic and molecularly reduced. Therefore, the reactions are thermodynamically favourable at low temperature and high pressures (with optimal pressure depending on the catalyst used, from 50 bar for $Cu/ZnO/Al_2O_3$ to 300 bar for $Ni(CO)_4$ for example [87]).

2.1 Difference between the CO and CO_2 feed

The main difference between the CO and CO_2 hydrogenation is the greater amount of heat released in the case of a CO-based feed flow. Indeed, compared to the CO_2 hydrogenation process, almost two times as much heat is released by the CO hydrogenation reaction. This impacts the choice of reactor technology used for the synthesis since, in the case of a synthesis using a CO-based feed flow, the heat exchanger design will required to be very efficient in order to avoid hotspot and carbon deposition onto the catalyst. However, in the case of a CO_2-based feed, a simple cooling solution inside the reactor is sufficient to control the temperature of the process, lowering the cost and increasing the efficiency (less heat loss at the cold source).
Another difference between the two processes appears when looking at the maximum conversion determined by the chemical equilibrium (plotted in Fig.41). The equilibrium limited methanol yield for the CO_2-based feed gas (18-58% at 200-250°C and 50-100 bar) is substantially lower than the CO-based one at 55 to 89% of conversion.

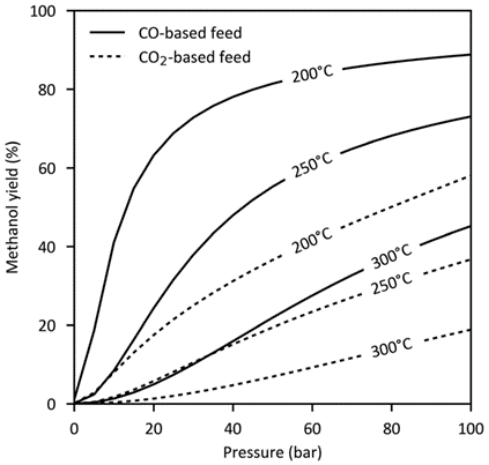

Figure 41: Equilibrium conversion of CO- or CO_2-based feed gas to methanol [88]

This gap can be explained by the difference in activation energy of the two molecules; the carbon monoxide molecule (CO) has a relatively low activation energy compared to the CO_2 molecule which has a high thermal stability and chemical inertness. Therefore, more heat is needed to "launch" the CO_2 hydrogenation reaction compared to the CO-based one. This results in higher temperatures required for the CO_2-based synthesis (e.g., higher temperature than 240°C) which could bring undesirable by-product in the process such as hydrocarbons and higher alcohol [89]. However, it seems, by looking at the composition of several commercial methanol synthesis [88], that the formation of other by-products is lower in the case of CO_2-based feed, below 0.05wt% in crude methanol compared to 0.1-0.6wt% for CO-based feed. The higher selectivity of CO_2 can partially be explained by the lower temperature peak in reactors during CO_2 hydrogenation, less exothermic than its CO counterparts. This will tend to produce less unwanted products as a result of better temperature stability.

A difference between the two processes can also be observed in the amount of water produced during the synthesis, indeed, the reaction of hydrogenation of CO_2 to methanol produces water as side product (which is not the case to produce methanol from CO), so, for each mole of methanol produced, a mole of water is produced. Moreover, in the case of a CO_2-based synthesis, the relatively high temperature, coupled with the presence of both CO_2 and H_2, will promote the reaction of Reverse Water Gas Shift (RWGS) in parallel to the CO_2 hydrogenation. These results will not directly be detrimental to the methanol production since by producing CO, the hydrogenation will still be possible:

$$CO_2 + 3H_2 \Leftrightarrow CH_3OH + H_2O \qquad \Delta H = -49.5\text{kJ/mol} \tag{42}$$

$$CO + 2H_2 \Rightarrow CH_3OH \qquad \Delta H = -90.6\text{kJ/mol} \tag{43}$$

In the case of a CO-based feed, the RWGS reaction is theoretically not possible but, in practice, a small CO_2 fraction will always make is way into the process, promoting the RWGS reaction. Typical compositions of crude methanol produced from CO_2 has a water content of 30-40% compared to less than 10-15% for syngas [88]. The water content in the reactor is problematic regarding the catalyst longevity since water being a strong oxidant at elevated temperature, it will participate in the prematurely catalyst deactivation by oxidation of the metal catalyst (f.e. Cu + H_2O ⇒ CuO + H_2). Therefore, water removal during the reaction seems to be the best solution to elevate this problem. However, no significant solution has been yet presented.

The keys to overcome limitations of the methanol synthesis from CO_2 and CO reside in the choice of catalyst and reactor combination which will allow better conversion and methanol selectivity. Catalyst with larger surface area and more active sites will be favoured to improve the conversion of CO_2 to methanol at low temperature while a proper choice of reactor is essential to improve the methanol selectivity and catalyst longevity by providing good heat exchange hence temperature control in the case of CO-based synthesis.

2.2 Catalyst for the methanol synthesis

CO_2/CO hydrogenation to produce methanol can be operated via several pathways. The synthesis can be made in a simple reactor using classical heterogeneous catalyst, $Cu/ZnO/Al_2O_3$ being the most common for the methanol production, but other catalytic conversion are currently in research and development for the methanol synthesis. These CO_2/CO reduction routes are the homogeneous catalysis, the enzymatic catalysis, the photocatalysis and the electrocatalysis. However, none of this catalysis technology is at TRL high enough to be commercially viable compared to the already efficient heterogeneous catalysis [90]. Example of catalyst used in this method are presented here below:

- Copper-based catalyst: these catalysts have been investigated for a long time and are considered as some of the most or even the most active catalyst for the methanol synthesis by carbon mono/dioxide hydrogenation [89].
  - Cu/ZnO is the most used of the copper catalyst for the synthesis of methanol. This system is generally operated at temperature above 250°C and pressure above 50 bar. The addition of ZnO to copper increases the surface area of the catalyst and improves the dispersion of Cu resulting in enhanced activity and selectivity [89]. This catalyst can be improved by adding Ga_2O_3 as promoter, it results in a better catalyst performance towards methanol production.
  - $Cu/ZnO/Al_2O_3$ is the most studied catalyst for methanol production from CO_2 hydrogenation. This catalyst has reported greater activity, selectivity, and stability than Cu/ZnO. Moreover, this catalyst also benefits from a longer lifetime since, zinc oxide in alumina-based catalyst mitigates the poisoning behaviour of Cu by chlorides and sulphides impurities in the feed gas. It also attenuates the agglomeration of active metal particles, increasing the overall stability of the catalyst and its long-term operation. Finally, ZnO being a basic oxide, it neutralises the acidic characteristic of alumina, inhibiting the conversion of methanol to dimethyl ether [89]. One disadvantage of this catalyst is its poor performance and limited effectiveness for the conversion towards methanol [89].
  - Cu/ZrO_2 also has a higher methanol selectivity and catalytic activity compared to Cu/ZnO. The ZrO_2, as the ZnO, improves the dispersion of copper resulting in a better catalyst activity. However, in this case, the addition of Ga_2O_3 does not improve the performance. If zinc oxide (ZnO) is added to Cu/ZrO_2 to form $Cu/ZrO_2/ZnO$, the catalyst activity is largely improved. In this catalyst, ZrO_2 is responsible for the greater selectivity towards methanol while both ZnO and ZrO_2 increase the activity of the catalyst by stabilizing Cu^+ in the Cu-based system [89]. For example, B. Anicic et al. [91] used a ZrO_2 dopped Cu/ZnO catalyst for methanol synthesis from a CO_2 feedstock, the catalyst reached a selectivity towards methanol above 99% without considering the carbon monoxide. The total conversion using this catalyst was 21%, and the selectivity of methanol and carbon monoxide is 68% and 31% respectively.
- Silver-based catalyst: this type of catalyst has not so much been investigated because of its lesser activity for methanol synthesis compared to copper-based catalyst. However, Koppel et al. [92] reported that the catalyst Ag/ZrO_2 has a greater selectivity towards methanol than Cu/ZrO_2 at low temperature (<227°C). Silver, as a material, can be used to dop Cu/ZrO_2 catalyst in order to increase its selectivity towards methanol. Bell and Rhodes (2005) claim selectivity up to 100% for the dopped Cu/ZrO_2 compared to a selectivity of only 75-90% in presence of Cu/ZrO_2 in the same reaction conditions.The catalyst Ag/ZrO_2 managed to solve the activity problem of silver-based catalyst at the cost of a lower selectivity for the process (compared to Ag/ZnO catalyst). As for the Cu-based catalysts, both the selectivity and the activity increase when the Silver based catalyst is mixed with zinc oxide (ZnO) and Zirconium dioxide (ZrO_2) to form $Ag/ZnO/ZrO_2$ [89].
  Unfortunately, all Ag-base catalysts, even if they show better selectivity towards methanol will always be less active than Cu catalyst [89].

- Palladium-based catalyst: for Pd-based catalyst, selectivity towards methanol up to 90% has been recorded using a Pd/La_2O_3 catalyst in a reactor operating at 100 bar and 350°C. Pd-based catalyst is characterised by a good catalyst activity, for example, 70% higher methanol synthesis rate for PdIn compared to a $Cu/ZnO/ZrO_2$ catalyst [89].
  If supported on an acidic support, Palladium catalyst will yield to methane (CH_4) instead of methanol (CH_3OH). However, compared to Cu-based catalyst, palladium, when combined with zinc oxide (Pd/ZnO) was found less active towards methanol synthesis from CO_2 hydrogenation. Similarly, palladium-based catalyst shows higher selectivity towards methane implying a lower methanol selectivity [89].

2.3 Catalyst deactivation

Catalyst deactivation is a common drawback of catalyst-based industrial process. It is the main point for determining the catalyst lifetime and many factors contribute to its evolution. These influencing factors are, in the case of methanol synthesis, the catalyst poisoning and the catalyst thermal sintering.
Poisoning occurs when impurities make their way into the inlet feed of the reactor. Major poisons for copper catalyst (the most used catalyst for methanol production in the industry) are sulphur compounds, responsible of blocking active sites on the catalyst surface and chlorides, responsible of an acceleration of the catalyst sintering. Note that, in the case of a Cu/ZnO catalyst, the tolerance over sulphur poisoning is higher than for other catalyst since the zinc oxide component is a sulfur scavenger by forming Zn sulfide and sulfate [93]. Other poisons include arsenic [88] and carbonyls [93] the last possibly present in the case of stainless-steel reactor resulting in a blocking of the catalyst active sites and a decrease of selectivity towards methanol in favour of the promotion of Fischer-Tropsch reactions due to the presence of iron deposition [93]. The limit of catalyst poisoning can be set to 0.5 ppm of sulphur and chloride and only few ppb of metal carbonyls [93].
Besides the catalyst deactivation by poisons, the catalyst lifetime will be reducing due to a thermal sintering of the catalyst. This thermal degradation is important in the case of the methanol synthesis since the reaction is carried out at elevated temperature and is exothermic. Therefore, in order to limit the catalyst deactivation by sintering, the heat generated by the reaction has to be extracted from the reactor. Moreover, Wu et al. [94] reported an acceleration of the crystallisation of Cu and ZnO due to the water produced in the process, leading to faster catalyst deactivation. However, it seems that small amount of silica added to the catalyst can greatly improve its stability by suppressing the crystallisation of Cu and ZnO.

2.4 Reactor types for the methanol synthesis

The reactor choice for methanol production from CO/CO_2 hydrogenation is very important for the process. Indeed, if not design correctly, a reactor could force the reaction to not operate in its best conditions, leading to low methanol selectivity and premature catalyst deactivation. The crucial parameter for a reactor, in case of methanol production, is its capability to manage the heat released by the reaction. In the case of methanol production from CO_2, the heat released from the reaction is around 2 times smaller than if methanol was mainly produced from CO. Therefore, the heat exchanger, in this case, does not have to be as big as in the case where CO is supplied.
There are two major families of reactors for the industrial scale methanol synthesis: the fixed bed reactors and the slurry bed reactors. Other concept reactors have been investigated such as membrane reactors and fluidised bed reactors, but, those still present some issues for the methanol synthesis: Membrane reactors still remain at the research and development stage and suffer from low conversion, durability issue and high cost. Fluidised bed reactors, on the other hand, have problems with attrition of the catalyst leading to reduced lifetime. [88]

2.4.1 Fixed bed reactors

In fixed bed reactor, a solid catalyst, in the form of pellet, for example, is placed in tubes and these tubes are surrounded by cooling water. The feed gas flows in an axial direction through the tubes filled with catalyst, at the other end of the tube, exit unreacted gas and products. The heat released by the reactions occurring inside the catalyst bed is extracted from the process by the surrounding boiling water (see Fig.42a).
Variation in the reactor configuration may occur depending on the design, but the principle remains the same. Several fixed-bed reactor designs have been extracted from the document [88], their characteristics and advantages are listed here below.

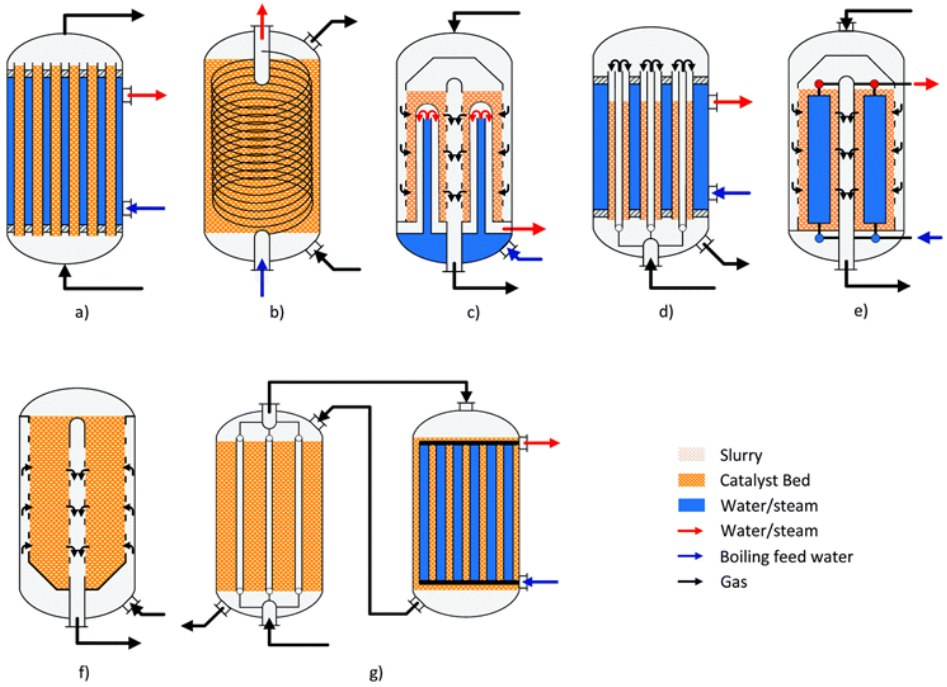

Figure 42: Schematic of different methanol reactors design; (a) Lurgi tubular reactor, (b) Linde Variobar, (c) Toyo MRF, (d) Mitsubishi Superconverter, (e) Methanol casale IMC, (f) Haldor Topsøe adiabatic reactor, (g) Lurgi MegaMethanol [88]

On Fig.42b is schematised the type of reactor used in the Linde Variobar process. The cooling is operated by a coil-wound heat exchanger in which boiling water is circulating. Linde claims that this design allows the highest catalyst per reactor volume ratio in the case of isothermal reactors as well as high heat transfer coefficient due to the crossflow design of the reactor [101].
Fig.42c is representing a multi-stage radial flow reactor, developed by the Toyo Engineering Corporation and Mitsui Toatso Chemicals. This reactor is characterised by a radial flow of syngas across the catalyst bed loaded in the shell-side. This bed is cooled using bayonet boiler tubes. Advantages of this technology are that the radial design results in very low pressure drop across the reactor (>0.5 bar) and that simple scale up is possible by vertical extension of the reactor (with single-train capacities of 5000t/d) [102].
On Fig.42d is schematised the reactor design developed by Mitsubishi Gas Chemical and Mitsubishi Heavy Industries. This complex reactor design combines the features of a tubes cooled reactor and a steam-raising tubular reactor by using double/triple-pipe tubes in a boiling water vessel. The feed gases first flow upwards through the inner tubes where they are pre-heated before passing downwards through the outer tubes which are filled with catalyst. [103]
Fig.42e schematises the Isothermal Methanol Converter reactor from Casale. This reactor is able to independently control the temperature of the different parts of the reactor by adjusting the cooling flow at different heights. This thermal control allows a quasi-isothermal temperature profile and is used to reach a maximum methanol conversion rate inside the reactor. [104]

Fig.42f represents a multi-stage adiabatic fixed bed reactor with inter-cooling. These types of reactors are especially suited for large capacities of production (up to 10 000t/d in a single line). They are proposed by Haldor Topsøe and Kellogg (now part of KBR). [88]
Fig.42g shows the schematic of a dual stage reactor concept from Lurgi. In the first stage (steam-raising reactor), the syngas is partially converted to methanol, then the product is transferred to the second stage (tubular reactor) in which it is further converted to methanol. The cooling of the second stage is realised using the cold feed gases for the first reactor, actively pre-heating them. [105]
For capacities up to 2000 tons per day, axial flow of the process gas is preferred whereas for larger capacities in a single converter (up to 7000–10 000t/d), axial-radial flow configuration is used due to the lower pressure drop [88].

2.4.2 Slurry bed reactors

In slurry reactors, the catalyst material is in suspension inside an inert liquid acting as the heat transfer medium between the reaction site and the reactor heat exchanger. Thanks to this liquid medium, conduction and convection effect occur in the reactor. Therefore, the heat removal via the internal heat exchanger is very efficient and results in an almost isothermal operation of the reactor which is ideal for maximising the selectivity of the process towards methanol. In this reactor, the inlet gas mixture is introduced at the bottom where a gas distributor will make sure that the syngas is well spread over the whole reactor area. Then, the distributed syngas will enter the slurry phase in which the catalyst is supported. It is in this slurry phase that the hydrogenation occurs. The products, if gaseous, are collected at the top of the reactor, or, in the case of liquid products, they must be separated from the slurry phase, this is one of the drawbacks of this technology. In the next figure is shown the schematic of a slurry bed reactor (or slurry bubble column reactor) in the case of gaseous inlet feed:

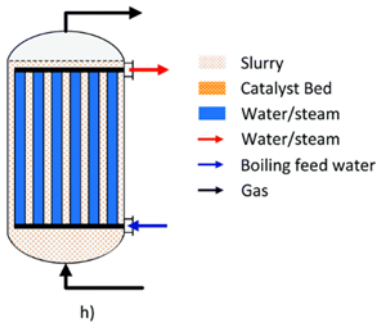

Figure 43: Schematic of a slurry bed reactor for methanol synthesis, (h) Air Products LPMEOH [88]

This technology for methanol synthesis as already been tested at industrial scale by Air Products and Chemicals in their Liquid Phase Methanol process, from 1997-2002 with a production of 235 tons per day using a CO-rich inlet feed (with a ratio H_2/CO of 2). They used mineral oil as catalyst support in the reactor, this resulted in a very efficient heat transfer but also in a relatively poor reactor volume utilisation due to the limited catalyst loading of the slurry bed (the slurry concentration was only of 20-25%) [89] [106] [88].

2.4.3 Comparison between the two technologies

Fixed bed reactor is simpler in operation than slurry-bed reactor because it does not suffer from any diffusion of reactant gases. It also has the advantage of requiring no catalyst separation on the product side since the catalyst in solid phase. The solid catalyst being static inside the reactor prevents the poisoning of the whole bed if impurities make their way into the inlet feed; this is in opposition with the slurry reactor in which the catalyst is blend with the reactant making it very susceptible to poisoning (gas purification unit may be

necessary depending on the inlet feed purity). Moreover, fixed bed reactor benefits from higher volumetric loading of catalyst compared to slurry bed reactor which are limited by a maximal catalyst concentration in the slurry reaction depending on the particle size, temperature, type of liquid medium, etc. [89]

However, when it comes to thermal management, the slurry technology is far superior to the fixed bed technology, allowing better temperature control throughout the process and the reactor thanks to convection effect inside the liquid, favouriting mixing and heat homogenisation. This could result in longer catalyst lifetime compared to fixed bed since the mixing of the catalyst slurry bed prevents hotspots hence the catalyst deactivation at elevated temperature which is not the case for solid catalyst pellet in the fixed bed technology.
Moreover, the better control of temperature in slurry bed allows to better control the selectivity of the process in order to maximise the methanol production. It was found by Kim et al. [96] that the slurry reactor is preferable to the fixed bed reactor, both in terms of productivity and selectivity for the CO_2 hydrogenation.

	Fixed bed reactor	Slurry bed reactor*
Operating temperature (°C)	240 - 300	215
Operating pressure (bar)	50 - 150	30 - 50
Pressure loss (bar)	3 – 7.5 (295t per d)	3 – 4.8 (235t per d)
Per pass conversion	36 - 60 for SRC, 55 - 80 for GCC combine to SRC**	20 - 50
Temperature management	Conduction between the catalyst pellet and gases, stationary bed ⇒ possible hot stop	Conduction and convection, better heat transfer/management in liquid phase
Catalyst replacement	Offline (simple in case of fixed-bed, complex in case of tube filled with catalyst)	Online
Products extraction	no catalyst separation from the required	Catalyst separation required
Catalyst loading	higher volumetric loading of catalyst	average catalytic loading
production capacity (t/d)	Up to 10 000	Low (compared to fixed bed)

Table 10: Summary of the operational range of the reactor for the methanol synthesis; values based on existing plants, data extracted from Table 8 of [88]

*Only few information for slurry bed reactor

**SRC = steam raising convertor, GCC = gas-cooled convertor

2.5 Effect of reaction parameters on the methanol synthesis

2.5.1 Impact of pressure

From a thermodynamic point of view, CO_2/CO hydrogenation to methanol is favourable at high pressure since the reaction is molecularly reduced. Moreover, both the RWGS reaction and the methanol decomposition reaction (eq.45) are molecularly increasing (there is more molecules on the products side than on the reactant side) meaning that their equilibrium will be shifted towards the reactant side as the pressure increase (which is good because less methanol will be decomposed and less CO_2 used to produce CO in the case of a CO_2-based feed).

However, increased pressure accelerates the oxygenate formation resulting in a higher selectivity of the process towards dimethyl ether (DME) instead of methanol [95]. The DME formation reaction is the following:

$$2CH_3OH \Rightarrow CH_3OCH_3 + H_2O \tag{44}$$

Note that with increasing pressure comes increasing cost for the compression of the inlet gas, the robustness of the storage tanks, the pipes, ...

2.5.2 Impact of the feed gas composition

Based on the equilibrium consideration of the reactions, in case of a CO-based feed, the highest methanol yield by hydrogenation will result from a gas composition with a stoichiometric ratio H_2/CO of 2 in absence of CO_2 in the gas mixture while when a CO_2-based feed is considered, the optimal H_2/CO_2 ratio resulting in a maximum methanol yield is $H_2/CO_2 = 3$.
In practice, in absence of CO_2, a slight excess of hydrogen in the inlet stream (H_2/CO ratio of 2.02-2.1) is used since it improves the space time yield of the catalyst while avoiding by-product formation by a deficiency in hydrogen [88]. In the case of a CO_2-based feed, studies [96] [97] show that as the ratio of hydrogen to carbon dioxide increases, the conversions rates of CO_2 hydrogenation increases. This could be justified that as increase in H_2/CO_2 ratio actually increases the hydrogen content in the reactor, increasing its concentration in the mixture, actively promoting the process of hydrogenation resulting in both enhance CO_2 conversion and methanol synthesis.

2.5.3 Impact of temperature

Higher reaction temperature has several impacts on the process; It improves the kinetics of molecules resulting in an increase in the rate of the reaction. Also, due to the high activation energy required to break the CO_2 energy barrier, high temperatures are required, meaning that the rate of CO_2 hydrogenation increases with increasing temperatures as CO_2 is more incline to react. However, this is only true up to a certain point: due to the exothermic property of the CO_2 hydrogenation, as the temperature increases, the equilibrium will be shifted towards the reactants, diminishing the conversion rate of CO_2 towards methanol. The reaction is not suitable at very high temperature.
Moreover, in the reactor, CO_2 hydrogenation is not the only reaction occurring, the RWGS reaction is one of the side reactions and, being endothermic, will be favoured at high temperature. Therefore, at high temperature, the favoured RWGS reaction will actively convert CO_2 into CO, resulting in a CO-based methanol synthesis, more exothermic than the one converting CO_2 to methanol, further favouring the RWGS reaction and decreasing the yield towards methanol. Moreover, at elevated temperature, the endothermic reaction of methanol decomposition (eq.45) is favoured, further decreasing the overall methanol production of the process.

$$CH_3OH \Rightarrow CO + 2H_2 \qquad \Delta H = 90.6\text{kJ/mol} \tag{45}$$

Research shows that an optimal temperature for a maximum yield of methanol exists:
Qi and al. [98] found a maximum selectivity towards methanol at 240°C for a synthesis occurring in a microreactor, pressurised at 30 bar, on a $Cu/\gamma\text{-}Al_2O_3$ catalyst and with a feed ratio of $H_2/CO = 3$.
Ahouri and al. [99] recorded a maximum methanol yield at 250°C in a fixed bed reactor operating under 30 bar, on a $Cu/ZnO/Al_2O_3$ catalyst and with a feed ratio H_2/CO of 3.
Finally, Xin and al. [100] tested a temperature range from 210 to 270°C in a slurry bed reactor operating at a constant pressure of 50 bar over a Cu/Zn/Al/Zr catalyst and found a maximum methanol yield of 17.9% at 250°C with a drop in selectivity for higher temperature.

2.6 Efficiency of the methanol synthesis

The energetic efficiency of the methanol synthesis depends on the composition of the feed flow. If the inlet feed is a syngas (only composed of CO and H_2), the only reaction occurring (aside from the side reactions not considered here) is the following:

$$CO + 2H_2 \Leftrightarrow CH_3OH \qquad \Delta H = -90.6\text{kJ/mol} \tag{46}$$

Therefore, when considering a reactor with recirculation and an overall conversion of CO of 94% (when considering the recirculation) and a selectivity towards methanol of 99% (over a Cu/ZnO catalyst), the efficiency of such process is calculated to be up to 93.45%, based on the HHV, and around 92.56% based on the LHV. The calculations are available in appendix 57

When the methanol synthesis is operated using a CO_2-based feed, both the conversion of CO_2 and CO to methanol occur in the reactor. This happens because the catalysts conversion of CO_2 has both a selectivity towards methanol (around 68% when using a ZrO2 dopped Cu/ZnO catalyst) and a selectivity towards CO by the RWGS reaction (around 31% with the last percent of selectivity for unwanted side products). Therefore, the reactions occurring in the reactor are the following:

$$CO_2 + H_2 \Leftrightarrow CO + H_2O \qquad \Delta H = 42\text{kJ/mol} \tag{47}$$

$$CO + 2H_2 \Leftrightarrow CH_3OH \qquad \Delta H = -90.6\text{kJ/mol} \tag{48}$$

$$CO_2 + 3H_2 \Leftrightarrow CH_3OH + H_2O \qquad \Delta H = -49.5\text{kJ/mol} \tag{49}$$

Therefore, when considering a reactor using recirculation to obtain an overall conversion of 94% for both CO_2 and CO, the efficiency of the methanol synthesis based on HHV when using a CO_2-based feed is around 91.88% while the efficiency based on the LHV is around 95.74%. The calculations are available in appendix 58.

3 Methanol to gasoline process

Hydrocarbons are organic compounds composed exclusively of carbon and hydrogen atoms. There are four major classes of hydrocarbons: the paraffins, the olefins, the naphthenes and the aromatics. The differences between these classes are in the arrangement of the carbon atoms inside the molecules and the ratio of carbon to hydrogen atoms.
In paraffins molecules, all carbon atoms are joined by a simple, single bonds. Their general formula is C_nH_{2n+2}. Sub-classes of paraffins are composed of N-paraffins in which carbon atoms are bonded in chainlike structures, and iso-paraffins in which small branches emanate from the main carbon chain, resulting in different physical and chemical properties as N-paraffins.
Olefins are similar to paraffins but have, at least, one double bound between two carbon atoms, resulting in fewer hydrogen atoms. Their formula is C_nH_{2n}. As for paraffins, when the molecule is composed of four carbons at least, it can form structural isomers.
Naphthenes characterise hydrocarbon's chain with a cyclic structure in which all the carbon-to-carbon bonds are single. Aromatics too have a ring/cyclic structure but carbon atoms inside the molecule are joined by aromatic bonds instead of single bonds.

Several methods exist to produce synthetic fuel (hydrocarbons chains) from methanol. The first developed was the methanol-to-gasoline (MTG) processed by ExxonMobil, then came the process called Topsoe integrated gasoline synthesis (TIGAS) developed by Harold Topsoe allowing the gasoline synthesis into a single loop. Both those techniques are currently commercially available (TRL 9) and used to produce gasoline as the main gasoline product. In order to have a better selectivity towards other products than gasoline, ExxonMobil developed a new pathway for hydrocarbon production from methanol. This path uses in combination a methanol-to-olefins and a Mobil's olefins to gasoline and distillates (MOGD) reactor to produce a blend of gasoline, kerosene, and diesel. Being more recent than MTG and TIGAS, the MTO-MOGD has a lower TRL value at around 8 [107].

3.1 MTG process

The methanol to hydrocarbons (MTH) process, also called methanol to gasoline (MTG) process was accidentally discovered in the early 1970s by the Mobil Central Research laboratories [108] by workers trying to develop a new process for making high-octane gasoline from methanol and isobutane. They used a newly developed zeolite catalyst, ZSM-5, and found that none of the isobutane was consumed and that the same products were obtained with methanol. The process of converting methanol to gasoline can be summarised by the succession of the following reactions inside two reactors:

The first part of the process is the exothermic dehydration of methanol to dimethyl ether (DME). This reaction uses an alumina catalyst inside a reactor operating in a temperature range of 250-400°C and under a pressure varying between 1 and 30 bar. The combination is depending on the process used, some examples are listed in table 14 of the document by Dieterich et al. [109]. At the exit of this reactor, the mixture is an equilibrium of methanol, dimethyl ether (DME), and water [108].

$$2\ CH_3OH \Leftrightarrow CH_3OCH_3 + H_2O \tag{50}$$

The products of the DME reactor are introduced into the MTG reactor, in which the methanol and DME are completely dehydrated over a ZSM catalyst at around 400-420°C, forming light olefins and water [108].

$$CH_3OH,\ CH_3OCH_3 \Rightarrow \text{Light olefins } + H_2O \tag{51}$$

In the MTG reactor, the conditions are such that the light olefins molecules oligomerise into higher olefins (or oligomers) which then combine through various reactions into paraffins, naphthenes and aromatics. The shape

selective catalyst limits the hydrocarbon chain length to C_{11} [108].

$$\text{Light olefins} \Rightarrow C_{5+} \text{ olefins} \tag{52}$$

$$C_{5+} \text{ Olefins} \Rightarrow \text{Paraffins/Naphtenes/Aromatics (= gasoline)} \tag{53}$$

At the exit of this reactor, the unconverted olefins are separated from the oligomers produced and recycled upstream of the oligomerisation reactor. In these recycling operations, inert impurities present with the olefin monomers, often C_2-C_4 short paraffins, tend to accumulate. These short paraffins come from:

- The degradation of the catalyst which induces a hydrogen transfer between the monomer olefins that transform them to paraffins.
- Small quantities of hydrogen which are often introduced into the reactor to improve the selectivity of the process, generate the hydrogenation of the olefin monomers and paraffins.

These paraffins are inert to oligomerisation: they accumulate during the recycle operations. This depletes the reaction medium of reactants and decreases the yield of the process.

The oligomerisation of the olefins is the main factor responsible of the selectivity of the overall MTG process. The degree of oligomerization, to achieve specific products, can be controlled by selecting the right temperature and pressure conditions, the nature of the olefin monomers and the type of catalyst.

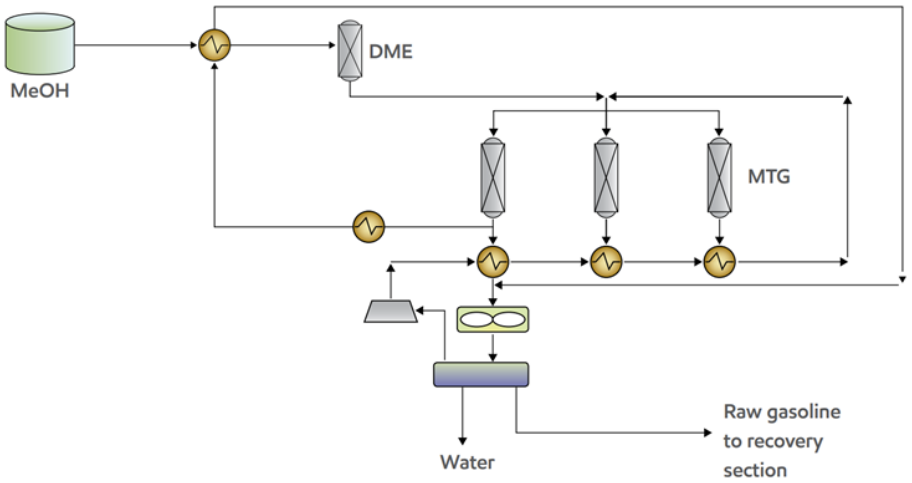

Figure 44: MTG reactor section process flow, from ExxonMobil [108]

This process results in a virtually complete conversion of methanol towards mixture of synthesis hydrocarbons and water with only a limited amount of C_2-gases. The liquid product is equivalent to conventional gasoline with virtually no sulphur and low benzene, which can be sold as is or blended with ethanol or methanol or with petroleum refinery feedstocks [108].

3.1.1 Process energetic efficiency

The energetic efficiency of the MTG process can be estimated based on the product fraction of a plant reported in the document by Zaretskij [110]. Table 11 reports the mass balance of the different products entering/leaving the MTG plant based on an inlet feed of methanol of 3000kg/h. From this table and the heating value of the different elements, an energy balance of the plant can be calculated and the HHV-based and LHV-based efficiencies of the process can be estimated. The energetic efficiency of the MTG unit is approximately of $89\%_{HHV}$ and $96\%_{LHV}$. The calculations are available in appendix 59.

Fraction	Stream type	Mass Flow (kg/h)	Hydrocarbon Yield (wt%)	Mass fraction on the product side (wt%)
Methanol	Inlet	3000	-	-
Hydrogen		7.36	-	-
Water	Outlet	1684.12	-	56
Gasoline		1057.27	79.9	35.15
Isobutane		113.8	8.6	3.79
Propane		72.78	5.5	2.42
n-butane		43.67	3.3	1.45
Light gas		18.52	1.4	0.62
Butenes		14.55	1.1	0.48
Propene		2.64	0.2	0.09
Total			100	100

Table 11: Display of the different products of the MTG [110]

3.2 MTO – MOGD process

The MTO-MOGD process is interesting compared to the MTG process because it allows the production of diesel, kerosene, and gasoline, which can then be used in transport fuel or upgraded to jet fuel thanks to is kerosene content. The full methanol-to-jet fuel is a combination of the methanol-to-olefins (MTO) reactor and the Mobil's olefins to gasoline and distillate (MOGD) process. This principle of methanol conversion into transport hydrocarbons by combining the two processes is illustrated by the following flow diagram. The process detailed in the next subsections is based on literature references [107] [111] [112].

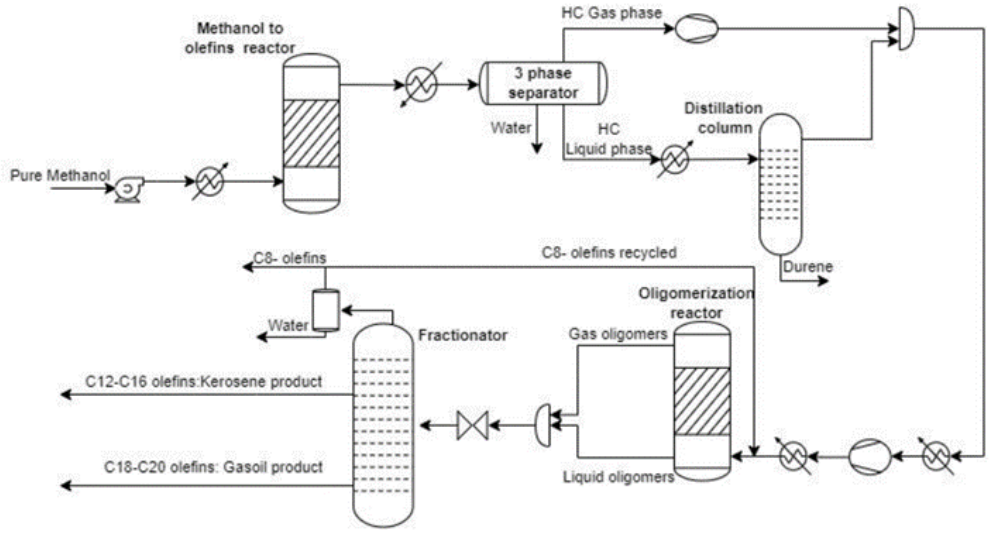

Figure 45: MTO-MOGD general reactor flow schematic

3.2.1 Methanol to olefins reactor (MTO)

Methanol is assumed to enter the process under atmospheric conditions. It is pumped and heated to the MTO reactor conditions of 2 bar and 450 °C. Inside the reactor, methanol is converted to olefins by the following reaction chain over a ZSM-5 catalyst:

$$2\ CH_3OH \Leftrightarrow CH_3OCH_3 + H_2O \tag{54}$$

$$n\ CH_3OCH_3 \Rightarrow 2n\ CH_2 + n\ H_2O \tag{55}$$

$$2n\ CH_2 \Rightarrow C_{2n}H_{4n} \tag{56}$$

In the reactor, methanol is first converted to DME and water, and further to light olefins and more water. The heat released by the exothermic reactions is extracted by the reactor's heat exchanger, allowing the reaction to operate isothermally. At the exit, the products are cooled down and water, gases and liquid hydrocarbons are separated using a three-phase separator. The non-condensable light hydrocarbons gases separated from the light olefins are burnt for heat generation. Liquid hydrocarbons are sent to a distillation column where durene (also called 1,2,4,5-tetramethylbenzene) is separated from the rest of the light olefins products and sent to a dedicated heavy gasoline treatment [107]. Durene is separated from the rest because, even if the aromatic compound "durene" has a melting point of 79°C, its isomers, isodurene (1,2,3,5-tetramethylbenzene) and prehnitene (1,2,3-tetramethylbenzene), have melting points respectively at -24°C and -7°C. Therefore, high durene content in gasoline could lead to engine issues, especially in cold climates since part of the gasoline inside the tank could freeze [107].

3.2.2 MOGD reactor and product distillation

The first of the MOGD reactors uses oligomerisation reactions to convert light olefins (C_2-C_6) into heavier olefins (C_5-C_{20}). This reactor operates under a pressure of 40 bar and a temperature of 200°C. The reactor is running in a quasi-isothermal state thanks to a low-pressure steam generation heat exchanger. The heavier olefins produced by the reactor are sent to a two-step distillation process to fraction them into C_8-olefins, water, C_{12}-C_{16} olefins and C_{18}-C_{20} olefins. The C_8-olefins are recycled to the oligomerisation reactor. The distillate blend formed by olefinic kerosene and diesel compounds is hydrotreated to saturate the C=C double bounds. This process is operated at 40 bar and 300°C in an isothermal reactor where the heat released by the reaction is used to produce high pressure steam. The paraffinic distillate product is separated from the excess hydrogen gas and sent to another distillation column in which kerosene and diesel fuels will be separated. The separated hydrogen is recycled back to the reactor feed [107].

The aromatic gasoline fraction, rich in durene, is treated by hydroisomerisation in a heavy gasoline treatment unit. The isomerisation is operated in presence of hydrogen and takes place in an isothermal reactor running at 345°C, under a pressure of 16 bar, on a Ni/ZSM-5/Al_2O_3 catalyst, heated by high-temperature heat (>500°C). The durene content of the aromatic fraction is reduced by 57mol% during the reaction. The resulting hydrocarbon–hydrogen mixture is separated and the aromatics are blended with the gasoline fraction. Then, 99.7mol% of hydrogen are recovered at a purity of 99.4mol% in the separation stage and recycled back to the reactor feed [107].
The heat supplied to the reactor comes from the combustion of the light, non-condensable olefins gases extracted from the MTO process.
The simulations performed in the document by Ruokonen et al. [107] was realised using a methanol feed of 3000kg/h corresponding to a pilot-scale production plant. Their simulation results for the process production are presented in Table 12.

Fraction	Stream type	Mass Flow (kg/h)	Calculated Hydrocarbon Yield (wt%)	Reference Hydrocarbon Yield (wt%)
Methanol	Inlet	3000	-	-
Hydrogen		7.36	-	-
Gasoline	Outlet	224	17	15
Diesel		591	45	57
Kerosene		356	27	25
Fuel Gas		98.1	7.4	1
LPG		59.1	4.5	2
Purges		1.47	-	-
Water		1679	-	-
Total			100	100

Table 12: display of the different products from the MTO-MOGD process [107]

The design of the process is based on heat integration within the model, indeed, the heating requirement in the reactor pre-heater and distillation reboiler can be covered by the internal steam and heat production of the process. Steam (HP and LP) is produced by the cooling of the exothermic reaction, and used for heat generation. The surplus of steam released by the process can be used for electricity generation within a small turbine.

3.2.3 Energetic efficiency of the MTO-MOGD process

As for the MTG process, the efficiency of the MTO-MOGD can be calculated based on the energy balance of the reactants and products through the system. The hydrocarbons fraction in the products were found in the document by Ruokonen et al. [107] and the input and output of this process are summarised in Table 12. Based on this table and the heating value of reactant/products, the efficiency of the MTO-MOGD can be estimated at around $91.4\%_{HHV}$ and $97.6\%_{LHV}$. The calculations are available in appendix 59.

Part III

Theoretical application of a CCU/Power-to-Fuel chain

Example and comparison of CCU chains for Power-to-Fuel application regarding their efficiency, selectivity and operability

With the different technologies mentioned in the previous sections for syngas production and upgrading towards e-fuels, several combinations for full Power-to-Fuel chains are thinkable. In this section, 5 examples of these chains will be presented and compared in regard to their efficiency, selectivity and operability.
In every scenario that will be made, water is supposed to be demineralized (pure H_2O) and carbon dioxide is supposed to be pure, whether it is by using a CO_2 extraction unit, or by buying it (CO_2 purification up to sufficient value may be costly).

Water electrolysis - RWGS - FT

As explained in the introduction, if the initial feedstock is set to be made of water, previously demineralised, and carbon dioxide, one way to produce syngas is by combining a water electrolysis for hydrogen generation and a reverse water gas shift reactor for the conversion of CO_2 to CO. Once the syngas produced, several options for hydrocarbons generation are available. The one choosen in this pathway uses a Fischer-Tropsch (FT) reactor for alkanes and alkenes chains synthesis. This route for Power-to-Fuel is represented by the following schematic:

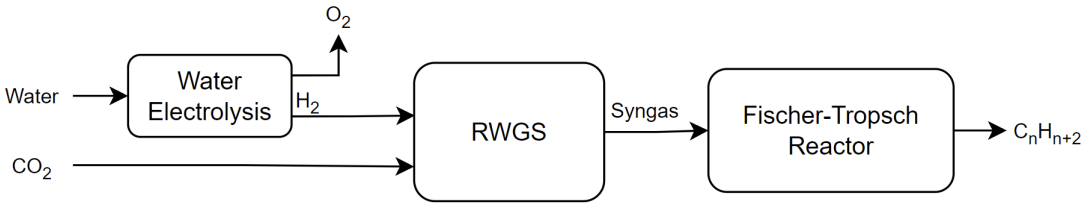

This production pathway has the advantage of being quite flexible, indeed, the water electrolysis can be operated using a either a PEM, an alkaline or SOEC electrolysis, while the products, at the end of the chain, can cover a large range of hydrocarbons chain length, and types, depending on the type of FT synthesis implemented (LTFT, HTFT).

Water electrolysis - CO_2 electrolysis - FT

As a second example of Power-to-Fuel route is another pathway utilising a water electrolysis. In this case, the syngas is not obtained from a RWGS reaction but by operating two electrolysis in parallel, the first one being the water electrolysis for H_2 generation and the second being a CO_2 for CO production. The resulting syngas obtained by mixing the electrolyser products is then sent to a FT reactor for syncrude synthesis. The schematic of this route is available in the next figure:

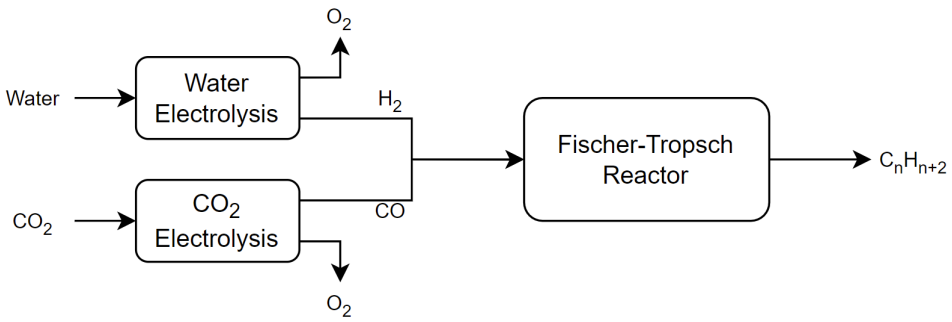

This hydrocarbons production route although relatively simple in theory is in practice hard to operate. Indeed, the CO_2 electrolysis is still, currently, at a relatively low state of development and still suffers from high degradation rate due to easy cell contamination by impurities in the based feedstock. Besides, having two electrolysers working in parallel could be a challenge regarding the electricity supply (especially in the case of renewable energy source) even if it could have benefits in terms of efficiency and flexibility.

Co-electrolysis - FT

For now, the syngas production using both a hydrogen production process and a carbon monoxide production process have been looked at. However, the direct production of syngas by a single process is possible. This process is the co-electrolysis; it uses as feedstock a mixture of high temperature steam and carbon dioxide and produces a syngas with a composition (ratio of H_2 to CO) depending on the initial mixture. The co-electrolyser allows to combine the first two steps of the previous pathways, actively increasing the global efficiency, the FT synthesis remains the same as in the two first Power-to-Fuel routes.

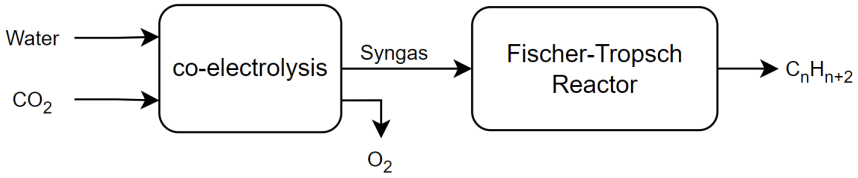

Co-electrolysis - Methanol from syngas - MtG

Another way to use syngas produced by the co-electrolysis would be in a methanol synthesis. This highly exothermic process takes syngas with a H_2/CO ratio of 2 as inlet mixture to produce methanol. Methanol is convenient since it can be used for many applications, such as energy storage, fuel and, in our case, base product for the synthesis of other fuels (dimethylether, gasoline,...). In this route, the produced methanol from the methanol synthesis will be used in a methanol-to-gasoline unit for further gasoline production, as shown in the next schematic:

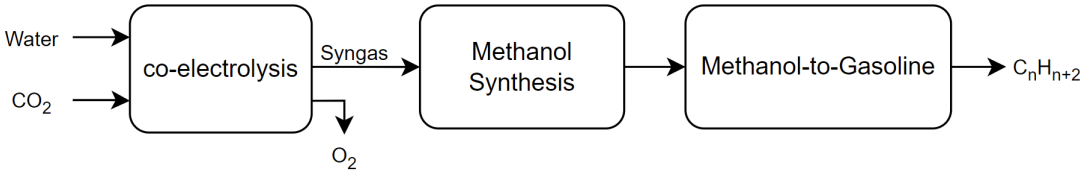

Water electrolysis - Methanol from CO_2 - MtG

As seen in section 2, methanol can be synthesised either from syngas or from a mixture of CO_2 and H_2. The second alternative removes the need of a CO_2 conversion in the process, effectively increasing the efficiency. In this case, a water-electrolysis alone is sufficient for the feed gas preparation, allowing more flexibility in the process thanks to the wide variety of electrolyser choice (PEM, alkaline, SOEC). The change in feed composition for the methanol synthesis only has a small impact on the product, the most notable difference being the amount of heat released by the process. The rest of the pathway remains the same, the resulting methanol is sent to a MtG unit for further fuel upgrading.

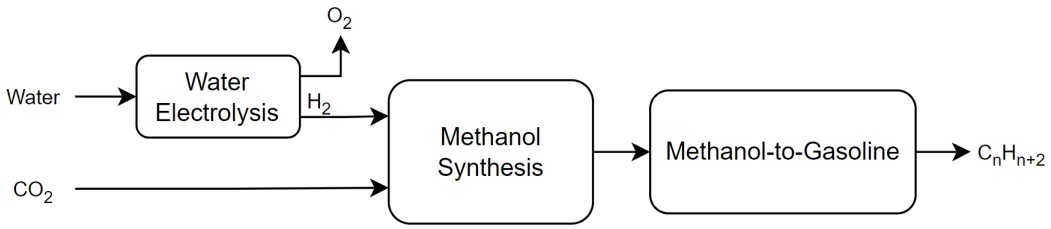

Summary table of the characteristics of the different Power-to-Fuel routes

When substituting in all the different pathways, the characteristics of their components discussed in the previous sections, a global summary of the different Power-to-Fuel routes can be created. This summary is available in the form of a table on the next page. This table allows to effectively compare different CCU possible routes for the e-fuel production regarding their efficiency, selectivity and operational conditions. The production capabilities (in quantity) of theses different pathways are studied in the following section.

Production pathway	Efficiency (on an LHV basis)	Selectivity	Operability
Water electrolysis followed by a RWGS for syngas production and FT reactor for hydrocarbon synthesis	-Efficiency of the **FT** reaction: 57.1 - 71% -Efficiency of the **RWGS reactor**: 100% -Using an **alkaline** electrolyser: η_{elec} = 51-60% ⇨ $\eta = \eta_{elec} \times 1 \times (0.57\text{-}0.71) = 29.1 – 42.6$ % -Using an **PEM** electrolyser: η_{elec} = 46-60% ⇨ $\eta = 26.2 – 42.6$% -Using an **SOEC** electrolyser: η_{elec} = 76.8-84.6% ⇨ $\eta = 43.8 – 60$%	- Purity of the H_2 produced by electrolysis: ⇨ **AEL**: 99.5 – 99.9% ⇨ **PEM**: >99.99% ⇨ **SOEC**: >99.9% - **RWGS** selectivity towards syngas production: up to 100% (CO_2 => CO) but require separation since CO_2 => CO conversion is not 100% - **LTFT**: three-phase mixture composed for the most part of long paraffin chains - **HTFT**: two-phase mixture, composed mainly of short olefins Refining of the crude leaving the FT require to obtain the right product type in quantity (distillation, hydrocracking, isomerization, etc)	- **Alkaline**: 1.8–2.4V ; 0.1–0.45A/cm² ; 60-90°C; <30 bar **PEM**: 1.8–2.2V ; 1–2A/cm² ; 50-80°C ; <200 bar **SOEC**: 0.7-1.5V ; 0.3-1A/cm² ; 650-1000°C ; <15 bar - **RWGS reactor**: Endothermic process, operational point depending on the catalyst used; in the case of the NiO/SBA-15 (used in the efficiency calculation), the reactor is operating at 900°C ; 1 bar ; H_2/CO_2 = 1 - **LTFT**: 220-240°C ; 20-30 bar ; Co-catalysts ; H_2/CO = 2 ; Fixed-bed reactor, slurry bed reactor, microchannel reactor ; Exothermic process - **HTFT**: 320-350°C ; 20-40 bar ; Fe-catalyst ; H_2/CO = 1.8-2.2 ; Fixed fluidized bed reactor, Circulating fluidized bed reactor, microchannel reactor ; Exothermic process
Parallel Electrolysis to produce syngas followed by a FT reactor	-Efficiency of the **CO_2 electrolysis**: 70 - 80% (stack efficiency, not system) -Efficiency of the **FT** reaction: 57.1 - 71% -Using an **alkaline** electrolyser: η_{elec} = 51-60% ⇨ $\eta = \eta_{elec} \times (0.57\text{-}0.71) = 29.1 – 42.6$% -Using an **PEM** electrolyser: η_{elec} = 46-60% ⇨ $\eta = 26.3 – 42.6$% -Using an **SOEC** electrolyser: η_{elec} = 76.8-84.6% ⇨ $\eta = 40 – 56.8$%	- Purity of the H_2 produced by electrolysis: ⇨ **AEL**: 99.5 – 99.9% ⇨ **PEM**: >99.99% ⇨ **SOEC**: >99.9% - Purity of the CO produced by **CO_2 electrolysis** in SOEC: 100% - **LTFT**: three-phase mixture composed for the most part of long paraffin chains - **HTFT**: two-phase mixture, composed mainly of short olefins Refining of the crude leaving the FT require to obtain the right product type in quantity (distillation, hydrocracking, isomerization, etc)	- **Alkaline**: 1.8–2.4V ; 0.1–0.45A/cm² ; 60-90°C ; <30 bar **PEM**: 1.8–2.2V ; 1–2A/cm² ; 50-80°C ; <200 bar **SOEC**: 0.7-1.5V ; 0.3-1A/cm² ; 650-1000°C ; <15 bar - **SOEC (CO_2)**: 1-1.4V ; >0.75A/cm² ; 700-900°C ; pressure limited due to carbon formation - **LTFT**: 220-240°C ; 20-30 bar ; Co-catalysts ; H_2/CO = 2 ; Fixed-bed reactor, slurry bed reactor, microchannel reactor ; Exothermic process - **HTFT**: 320-350°C ; 20-40 bar ; Fe-catalyst ; H_2/CO = 1.8-2.2 ; Fixed fluidized bed reactor, Circulating fluidized bed reactor, microchannel reactor ; Exothermic process
Co-electrolysis of water and CO_2 followed by a FT reactor	-Efficiency of the **co-electrolysis**: 73.5 – 78.6% -Efficiency of the **FT** reaction: 57.1 - 71% ⇨ $\eta = 42 – 55.8$%	- Selectivity of the **co-electrolysis** toward CO and H_2: up to 100% if the current density and pressure are limited to limit the methane production - **LTFT**: three-phase mixture composed for the most part of long paraffin chains - **HTFT**: two-phase mixture, composed mainly of short olefins Refining of the crude leaving the FT require to obtain the right product type in quantity (distillation, hydrocracking, isomerization, etc)	- **SOEC co-electrolysis**: 1-1.4V; >0.75A/cm²; 700-900°C; <3 bar - **LTFT**: 220-240°C ; 20-30 bar ; Co-catalysts ; H_2/CO = 2 ; Fixed-bed , slurry-bed, microchannel reactor ; Exothermic process - **HTFT**: 320-350°C ; 20-40 bar ; Fe-catalyst ; H_2/CO = 1.8-2.2 ; Fixed fluidized bed, Circulating fluidized bed, microchannel reactor ; Exothermic process
Water electrolysis in parallel to a methanol synthesis from CO_2 and H_2 followed by a MtG unit	-Efficiency of the **methanol synthesis**: 95.75% -Efficiency of the **methanol-to-hydrocarbons** unit: 96.8%* -Using an **alkaline** electrolyser: η_{elec} = 51-60% ⇨ $\eta = \eta_{elec} \times 0.957 \times 0.968 = 47.2 – 55.6$% -Using an **PEM** electrolyser: η_{elec} = 46-60% ⇨ $\eta = 42.6 – 55.6$% -Using an **SOEC** electrolyser: η_{elec} = 76.8-84.6% ⇨ $\eta = 71.1 – 78.4$% *96.8% efficiency used for the MtG since it is the mean of the two processes studied (96 and 97.6) and they are close to each other	- Purity of the H_2 produced by electrolysis: ⇨ **AEL**: 99.5 – 99.9% ⇨ **PEM**: >99.99% ⇨ **SOEC**: >99.9% - **Methanol** selectivity from CO_2 and H_2 mainly depends on the catalyst used, if the catalyst is ZrO_2-Cu/ZnO (used in the excel file): ⇨ 68% selectivity from CO_2 to CH_3OH and 31% towards CO* ⇨ CO converts to CH_3OH in presence of H_2 with a selectivity of 99%* - The selectivity of the methanol to hydrocarbon depends on the process used: ⇨ **MtG** (dry composition): 80% C_{5+} gasoline; 8.6% Isobutane; 5.5% Propane; 3.3% n-Butane ⇨ **MTO-MOGD** (dry composition): 45% Diesel; 27% Kerosene; 17% Gasoline; 7.4% Fuel gas; 4.5% LPG *Conversion of CO_2/CO of 94%	- **Alkaline**: 1.8–2.4V ; 0.1–0.45A/cm² ; 60-90°C; <30 bar **PEM**: 1.8–2.2V ; 1–2A/cm² ; 50-80°C ; <200 bar **SOEC**: 0.7-1.5V ; 0.3-1A/cm² ; 650-1000°C ; <15 bar - **Methanol (CO_2)**: 240-300°C ; Exothermic process ; 50-150 bar ; H_2/CO_2 = 3 ; Cu/ZnO catalyst ; fixed-bed reactor or slurry-bed reactor - Methanol-to-hydrocarbons: ⇨ **MtG**: 1st reactor: Exothermic ; 300 – 320°C ; 2 bar when using an alumina catalyst 2nd reactor: Exothermic ; 400 – 420°C ; ZSM catalyst Distillation column ⇨ **MTO-MOGD**: 1st reactor: Exothermic ; 450°C ; 2 bar ; ZSM-5 catalyst Three-phase separator 2nd reactor: Exothermic ; 200°C ; 40 bar Distillation column 3rd reactor: Exothermic ; 300°C ; 40 bar
Co-electrolysis for syngas production followed by methanol synthesis and MtG unit	-Efficiency of the **co-electrolysis**: 73.5 – 78.6% -Efficiency of the **methanol synthesis**: 92.5% -Efficiency of the **methanol-to-hydrocarbons** unit: 96.8%* ⇨ $\eta = 65.8 – 70.4$% *96.8% efficiency used for the MtG since it is the mean of the two processes studied (96 and 97.6) and they are close to each other	- Selectivity of the **co-electrolysis** toward CO and H_2: up to 100% if the current density and pressure are limited to limit the methane production - **Methanol** selectivity from syngas is mainly dependent on the catalyst used, for Cu/ZnO (used in the excel file): ⇨ 99% selectivity from CO to CH_3OH* - The selectivity of the methanol to hydrocarbon depends on the process used: ⇨ **MtG** (dry composition): 80% C_{5+} gasoline; 8.6% Isobutane; 5.5% Propane; 3.3% n-Butane ⇨ **MTO-MOGD** (dry composition): 45% Diesel; 27% Kerosene; 17% Gasoline; 7.4% Fuel gas; 4.5% LPG *Conversion of CO_2/CO of 94%	- **SOEC co-electrolysis**: 1-1.4V; >0.75A/cm²; 700-900°C; <3 bar - **Methanol (syngas)**: 215°C ; Exothermic process ; 30-50 bar ; H_2/CO = 2 ; Cu/ZnO catalyst ; slurry-bed reactor - Methanol-to-hydrocarbons: ⇨ **MtG**: 1st reactor: Exothermic ; 300 – 320°C ; 2 bar when using an alumina catalyst 2nd reactor: Exothermic ; 400 – 420°C ; ZSM catalyst Distillation column ⇨ **MTO-MOGD**: 1st reactor: Exothermic ; 450°C ; 2 bar ; ZSM-5 catalyst Three-phase separator 2nd reactor: Exothermic ; 200°C ; 40 bar Distillation column 3rd reactor: Exothermic ; 300°C ; 40 bar

Simulation of a full CCU/Power-to-Fuel chain based on a renewable feedstock

1 Simulation context and hypothesis

In this section, most of different pathways mentioned in this previous section will be tested theoretically, using Python, based on a specific scenario to compare their performances, both in terms of production capabilities, cost, and operability.
To do so, a fictional CCU chain for Power-to-Fuel application has been imagined. The installation is composed of a syngas generation unit, followed by storage and conditioning units and then a hydrocarbons synthesis part, in the form of a Fisher-Tropsch reactor or a Methanol-to-Gasoline unit. This theoretical installation is configured to be supplied only by using renewable sources, since the production of fuel from other fuels burned would be somewhat cyclical and inefficient... Therefore, to supply the installation, and mainly the electrolysers, solar panels will be installed in parallel with the other installations. The power of this PV field is set to be of 10MW_p in order to evaluate the potential production capacity of large industrial installation in the future.
The purpose of the simulations carried out in this section are multiple: first of all, they will allow to evaluate (in order of magnitude) the quantity of hydrocarbons that it is possible to extract from a CCU installation of this size based entirely on renewable energy sources. Then, as several production routes will be simulated. It will be possible to compare the production capacity of each route when subjected to the same energy profile.

For the simulation, some hypothesis were taken. First of all, it is important to mention that, in the different production pathways that will be tested, their will be no mention of one using a CO_2 electrolysis for the syngas generation. This choice is supported by the fact that, currently, the technology still has a technology readiness level too low to be commercially available at scales sufficient for the following simulations ($10\ \text{MW}_p$).
Then, when dealing with the different chemical processes used in the chains, no reactor technology has been specifically chosen for the simulation since it will not change drastically the results and, depending on the installation (the localisation, the industrial environment of the CCU chain, ect), some technologies may be preferable over other.
Finally, in this simulation, the first part of the CCU chain, the capture of carbon dioxide, will be omitted. This choice was made based on the difficulty that it is to represent a typical scenario of CO_2 capture given the span of the technology and the great dependency on where it is implemented. Indeed, the amount of carbon dioxide captured, its purity and the amount of electricity required for the separation in a post-combustion capture unit varies greatly depending on the flues gas feed from which the CO_2 is separated: in gas mixture where the concentration of carbon dioxide is high (such as in the cement, iron and steel production process) the separation will required less filtration and therefore required less energy while capturing more CO_2, whereas in a low concentration feed, the equipment needed will be more energy demanding and the amount of CO_2 capture for unit mass of flue gas will be less. Another factor influencing the capture performance and cost is the choice of technology used for the separation: some technologies, such as membrane separation for example, are relatively energy efficient but at the cost of low CO_2 purity, some are only usable in specific flue gases conditions, and other while having good performance and purity values are very energy demanding and complex, increasing the operating cost. These different reasons explain the choice of considering the CO_2 used in the Power-to-Fuel process as "given" and "pure" such that this simulation can represent a typical production profile of a CCU chain without being restricted to some cases due to a choice of carbon capture technology and location.

2 Equipment choice

In this section, the different technologies used within the Power-to-Fuel chains are listed. These choices of commercially available device allow the simulations to be more precise by referring to existing value of consumption, production capabilities and constrains.
The devices presented here are obviously not the only ones available for each operation, others are available in other sizes and by other suppliers. However, the purpose here is to represent what the technology is capable in general.

2.1 Solar photovoltaic generation

As explained in the introduction, PV generation will be the only source of power for the complete CCU installation. The amount of installed PV has a cumulative peak power generation of 10MW$_p$, distributed over 25 000 solar panels.
The selected PV module is based on higher-end Crystalline silicon cells such as monocrystalline cell technology in order to take advantage of higher conversion efficiency. To this end, SM400M(BF) PV module developed by Peimar Company was selected for this application [113]. The suggested PV modules are made of 72 5BB Monocrystalline cell technology. The technical properties are provided in Table 13. For the simulation, the PV modules are supposed to be installed on tilted racks (at an optimum angle of 41° if placed in Belgium) with east to west tracking capability.
The Global Horizontal Irradiance (GHI) values, required for the calculation of the hourly energy generation were imported from EU Science Hub established by European Commission [114]. GHI is an indicator that measures the total solar irradiance from the sun on a horizontal surface, in which its value is of interest in PV systems. The resulting electrical energy produced by PV panels can be calculated using eq.57 where A$_p$ is the panel area, η is the conversion efficiency and P_r is the performance ratio of the panel which includes the losses due to the electricity consumption of the auxiliaries and due to environmental factors such as the shades, dust, cable losses, etc. This coefficient is often set to a default value of 0.75.

$$E_{panel} = A_p \times P_r \times GHI \times \eta \tag{57}$$

Nominal Power	Efficiency	Module area	Voltage P$_{max}$	Current P$_{max}$	NMOT
400 W	20.09%	1900×1048mm	38 V	10.53 A	45°C±2

Table 13: Technical Properties of PV module; Peimar SF400M(BF) [113]

2.2 Electricity storage using batteries

Supporting the electricity production by the solar panels, batteries will be considered in some of the discussed scenarios, depending on the technology used for the hydrogen production. This battery system will be used to smooth hydrogen production throughout the day, avoiding constant change in electrolyser regimes since, depending on the electrolysis technology used, the fluctuating energy source may or may not be an issue (regarding the cold/hot start-up time and load flexibility, for example).

In this report, the implementation of Sodium-Sulfur (NaS) energy storage technology was considered. The NaS batteries operate on the principle of reversible redox reaction between sodium and sulfur (Fig.46), in which the operating temperature can reach as high as 300-350℃. High energy density, long life span (∼15 years at a usage of 300 cycles at >80% - depth of discharge - per year), low maintenance, fast response time (1ms), and high round-trip efficiency are significant advantages of this battery technology [115]. Moreover, the long

duration discharge ability of this battery ensures that it can supply electrical power as much as 6 hours (when operating at nominal power). However, a drawback of NaS is that relatively high temperatures (300-350 °C) are required for the reaction to take place and that the molten electroldes must be kept at temperature or they will solidify, reducing the battery longevity. For the application described here (a Power-to-Fuel chain), this heating constrain should not be as much of a problem than in other applications because most of the processes used during the e-crude synthesis are highly exothermic.
The model of NaS battery selected to perform the simulations is the one developed by the company NGK Insulators. A product of NGK's Company advanced ceramic technologies, the NaS battery was the world's first commercialized battery system capable of megawatt-level electric power storage [116]. The technical properties are provided in Table 14. The NAS batteries from NGK are shipped in the form of big containers each of which with the following characteristics:

Rated Power	Energy Capacity	DC Voltage	Round-Trip Efficiency	Footprint	Weight
200 kW	1,200 kWh	192 V	96 %	6.1 $\times 2.4m$	21 tons

Table 14: Technical Properties of NGK's NAS Battery system

To ensure the constant operation of the electrolyser during the year and supply the installation long enough during the night and winter, the cumulative batteries capacity of 36 MWh should be installed. This represents the capacity of 30 of the NGK's batteries containers.

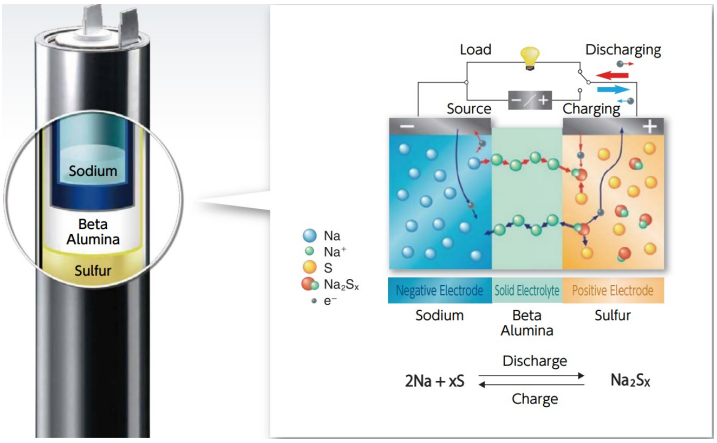

Figure 46: NaS technology energy storage concept [116]

2.3 Electrolyser choice

The electrolyser choice is crucial in a Power-to-Fuel chain since it is the element consuming the most energy as well as the one providing the hydrogen, essential to the process. In this report, the three main electrolysis technology will be tested.

2.3.1 PEM electrolyser

The PEM electrolyser is set to be used continuously during the year. This means that it will produce hydrogen as soon as electricity is provided to it without relying on a battery system. This is possible because this electrolyser technology is well suited for intermittent application thanks to its very low response time and large load variation capabilities. This ability not to be dependent on a battery system allows the PEM electrolyser to fill the efficiency deficit that it has compared to the other two electrolysis technologies, which are battery dependent.

The model of electrolyser selected for this simulations is developed by Cummins, the HyLYZER1000 [117]. In the theoritical test of the 10MW Power-to-Fuel installation, two of these electrolysers were used. The technical specifications of this system are listed in the table here below:

H_2 Production	Operating range	DC power consumption (stack)	H_2 delivery pressure	H_2 purity	Footprint
1000 Nm^3/h	5-125%	4.3 kWh/Nm^3	99.99%	30 barg	$8.4 \times 2.3m$
2160 kg/day		48 kWh/kg			

Table 15: Technical Properties of HyLYZER1000 electrolyser [117]

2.3.2 Alkaline electrolyser

The alkaline electrolyser as explained above will be operated through the use of a battery system, this will allow the electrolyser to constantly produce hydrogen during the year no matter what the weather conditions are. The battery solution is implemented in the case of the alkaline electrolyser because, in contrary to the PEM electrolyser, the alkaline technology has a significant start-up time (even when already at temperature) and a rather high minimum load required for H_2 production making it hard to implement based on an fluctuating energy source.
For the simulations, two different models of electrolyser have been selected, both from the same company but with different production capacities, depending on the period of the year. The selected models are the A485 and A1000 from the NEL company [118], one of the leading manufacturers of hydrogen generators. The specifications of theses two models are provided in the following tables:

H_2 Production	Operating range	DC power consumption (stack)	H_2 delivery pressure	H_2 purity	Footprint
300-485 Nm^3/h	15-100%	3.8-4.4 kWh/Nm^3	99.99-99.999%	1-200 barg	$\sim 225m^2$
647-1046 kg/day		4 kWh/Nm^3 used in the simulations			

Table 16: Technical Properties of NELA485 electrolyser [118]

H_2 Production	Operating range	DC power consumption (stack)	H_2 delivery pressure	H_2 purity	Footprint
600-970 Nm^3/h	15-100%	3.8-4.4 kWh/Nm^3	99.99-99.999%	1-200 barg	$\sim 350m^2$
1295-2094 kg/day		4 kWh/Nm^3 used in the simulations			

Table 17: Technical Properties of NELA1000 electrolyser [118]

2.3.3 SOEC electrolyser for water electrolysis

As for the alkaline electrolyser, the SOEC electrolyser power supply will be assisted by batteries to overcome the issues of transient behaviour that would come with a fluctuating power source (due to the slow response time of the technology and the high temperature to maintain). The model used for the simulation is the HyLink, developed by Sunfire [119]. This electrolyser uses pressurised steam as hydrogen source. The important specifications of the electrolyser are listed in the following table :

H_2 Production	Operating range	DC power consumption (stack)	H_2 delivery pressure	H_2 purity	Footprint
750 Nm^3/h	5-100%	3.3 kWh/Nm^3	99.99%	0 barg	$\sim 300m^2$

Table 18: Technical Properties of the HyLink electrolyser [119]

2.3.4 SOEC electrolyser for CO_2 electrolysis

As for water electrolysis, the SOEC used for water and CO_2 co-electrolysis will be powered both by the PV field and the batteries. The electrolyser selected for the simulations is the SynLink, developed by Sunfire.

It uses both pressurised steam and carbon dioxide as input feedstock for the syngas production. The technical specifications of this unit are provided in the table here below:

Syngas Production	Operating range	DC power consumption (stack)	H_2/CO ratios	delivery pressure	Footprint
750 Nm^3/h	5-100%	3.3 kWh/Nm^3	1.5-3.5	0 barg	$\sim 300m^2$

Table 19: Technical Properties of the SynLink co-electrolyser [120]

2.4 Gas storage (H_2, CO_2, CO)

2.4.1 Hydrogen storage

The hydrogen produced by the different electrolysers can not be directly utilised in the different reactor for fuel synthesis. It must firstly be conditioned for the processes downstream. This conditioning will make possible to feed hydrogen to the different reactors at the right temperature and pressure values while delivering it at constant flow, insuring smooth operation of the production chain and avoiding any transient effects inside the reactors. Therefore, in order to implement this hydrogen conditioning, H_2 must firstly be stored.
However, storing hydrogen is not a trivial thing to do. Indeed, since hydrogen is a very light gas, its storage is an essential obstacle to overcome. At atmospheric pressure, storing 1kg of gaseous hydrogen would required a tank of 11 000 liters (or $11m^3$).

Nowadays, it exists six methods or phenomena to more efficiently store hydrogen: high-pressure gas cylinders, liquid hydrogen storage in cryogenic tanks, adsorbed hydrogen on materials with a large specific surface area, absorbed on interstitial sites in a host metal (at ambient conditions), chemically bonded in covalent and ionic compounds (at ambient pressure), or through oxidation of reactive metals (like Li, Na, Mg, Al and Zn) with water, with the two most common being the high-pressure cylinder storage and the liquid hydrogen storage. Both of these techniques are quite energy expensive, requiring high pressure compression (up to 800/900 MPa) or intensive gas cooling due to the extremely low boiling temperature of hydrogen (20.2K at atmospheric pressure). These extreme storage conditions are required to overcome the low density of hydrogen at standard conditions ($\sim$0.08 kg/m^3), doing so, the high-pressure storage can reach volumetric densities of 36 kg/m^3, half of what is possible with the liquid hydrogen storage at around 70.8 kg/m^3 (note that the highest volumetric densities of hydrogen are found in metal hybrides) [121].

Although more compact and secure solutions are available for hydrogen storage, high pressure cylinders seem to be the most appropriate one for the Power-to-Fuel application. Indeed, having the hydrogen available directly in gaseous state and at the right pressure will facilitate its homogeneous mixing with CO for the production of syngas.

Therefore, the H_2 produced by the electrolysers will be stored at high pressure (500-700 bars) in order to maximises its volumetric density. Such pressures are obtained by the use of specific compressors. The selected compressor for this application is an ionic compressor, developed by Linde Hydrogen Fueltech. This compressor uses hydraulic pistons to gradually compress hydrogen to the right pressure. Highlights of this compressor include the use of an ionic liquid, which does not bond with the gas. This ionic liquid also act as both a lubricant and coolant inside the piston shell, increasing its efficiency, cooling and reducing its wear and tear. At the end of the compression, the ionic liquid molecules are separated from the hydrogen and fed back to the process flow [122]. This compression unit is bound to an H_2 storage reservoir, the one chosen for this application is the IC P/140-XL developed by Linde Hydrogen FuelTech, the technical specification of this model are available in Table 20:

Unit number	Outlet pressure	Output capacity	Maximum capacity	Power consumption	Type of hydrogen
IC P/140-XL	20/50/150/500 bar	140 kg/h	3360 kg %	0.68-2.7 kWh/kg	GH_2

Table 20: Technical Properties of the storage unit by Linde Hydrogen FuelTech [122]

It is important, during the simulations of the Power-to-Fuel chains, to be aware of the maximum flow rate at which the compressor can handle the incoming hydrogen from the electrolyser. This flow being highly variable during the year, the overall electrical consumption of the compression and storage of H_2 is set to be constant at an average value of 1.5kWh/kg_{H_2} due to the lack of indication regarding the consumption variation with the mass flow.

2.4.2 Carbon Dioxide storage

A carbon dioxide storage should be necessary if a carbon capture unit is implemented, which is not the case here, as explained in the hypothesis. However, if a CO_2 storage unit was necessary, the storage could easily be handle by a gas compressor followed by a storage vessel in which the CO_2 will be contained before used in the chain. The pressure at which CO_2 has to be stored is much lower than in the case of hydrogen since its volumetric density is 22 times higher.

2.4.3 Carbon Monoxide storage

As for the CO_2 storage, carbon monoxide can be stored in pressurised vessel. The amount of CO storage used in the simulations is set to be of 10 000 kg. The electrical consumption associated to the gas compression is set to be the same as the one used for the hydrogen storage (∼1.5kWh/kg). This assumption is made because no commercial example of specific CO storage compressor as been found online from which informations about the storage capacity and energetic cost could have been extracted.

2.5 Heat management

The heat management inside the different CCU routes can be done by balancing the heat produced by the exothermic processes (FT, MtG, methanol syntehsis) with the heat requirement of the endothermic processes (RWGS reaction, syngas conditioning). In each of the Power-to-Fuel route studied, the number and strength of the exothermic processes exceed the endothermic ones. This means that considering an efficient enough heat exchanger system, no external heat generation is required; the global process is self-sufficient. An example of such heat balance within a Power-to-Fuel pathway is available on Fig.47:

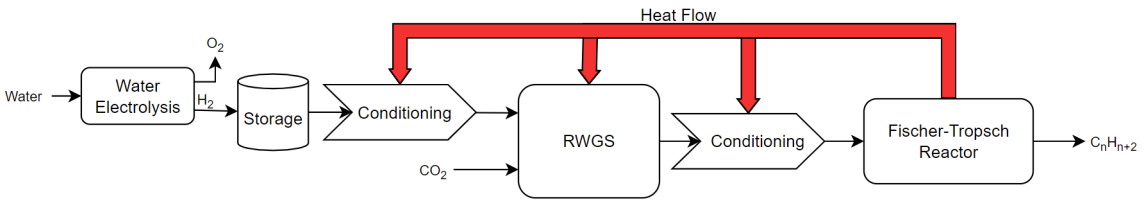

Figure 47: Example of heat management for the route using an electrolysis, a RWGS reactor and a FT synthesis

More precisely, the heat transfer between the different installations can be operated by steam (high and low pressure), generated in the heat exchanger of the exothermic processes and condensed in the heat exchanger of the endothermic processes. The steam excess can even be used in turbines for electricity generation (not taken into account here). No water consumption is associated to the heating/cooling of the installation since this circuit works in close loop.

The electrolysers are not considered in the heat system of the different installations since they do not required heating once the electrolysis as started, only at startup (provided by the electricity supply). Besides, most of the electrolysers used in the simulations are operating continuously thanks to the use of a battery system.

3 Description of the different algorithms used depending on the technology applied

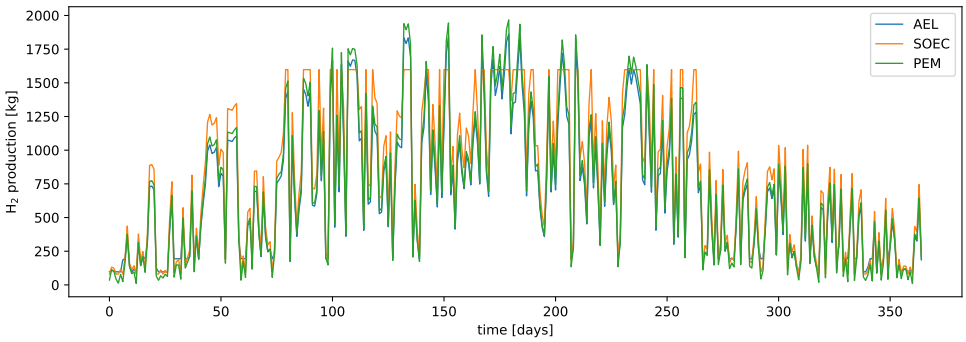

Figure 48: Comparison of the different electrolyser H_2 production profiles

3.1 When using PEM electrolysers

In the case where hydrogen production is handled by 2 PEM electrolysers, the H_2 production profile is rather simple. When electricity is generated by the solar panels, the electrolysers is turned on and produce H_2 as long as the electricity generated is bigger than the electrolysers lower limit of production (f.e. $5\%_N$ in the case of the electrolysers used in the simulation). An example of this production profile is available on Fig.49
The produced hydrogen is then sent to a storage unit which compresses it to 500 bar, in order to maximise its volumetric density. The hydrogen usage throughout the year is set in a way to minimise the storage necessary while smoothing as much as possible the H_2 utilisation in the chain to avoid transient effects in the reactor. To do so, the hydrogen use is set to be constant during each day, and the mass flow is determined by the amount produced during the same day (based on the PV generation, hence the weather forecast). If the average hydrogen production ($H_{average}$) during the day is bigger than a set limit (fixed as being two times the minimum production capable by the electrolysers, $2\times H_{min}$), the production chain will use $H_{average}$ for the next 24 hours. Otherwise, if $H_{average}$ is smaller than the limit, the storage unit will be depleted in order to provide a constant, minimum hydrogen flow in the chain of H_{min}, being the minimum production rate of the electrolysers.

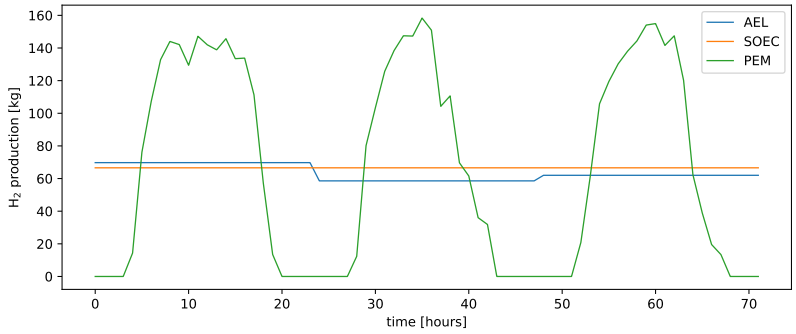

Figure 49: H_2 production for June 22, 23 and 24 (2019) of the electrolysers as implemented in the algorithm

3.2 When using Alkaline electrolysers (AEL)

In the case where hydrogen is produced using an alkaline electrolysis, as already mentioned, batteries will be implemented to support the electrolyser electricity supply, allowing a smoother production profile during the year.
To maximise the production time of H_2 and counter balance the relatively poor load flexibility of the alkaline technology, two electrolysers were chosen for the simulations: One smaller (up to 485 Nm^3/h) when little to no sun is expected and one bigger (up to 970 Nm^3/h) when the solar predictions are favorable. The choice of using one or the other is decided by the algorithm and is based on the weather forecast of the next 5 days: if the average electricity production by the PV field during the 120h (= 5 days) prediction period is estimated to be bigger than the lower limit of production of the bigger electrolyser (15% of the nominal load), this one will be used continuously during the prediction period. If the average electricity production is below this minimum load value, the smaller electrolyser will be used.
The choice of utilisation periods of 5 days was chosen because it allows to have relatively accurate weather forecast, while not changing too often electrolysers, reducing the energy and time demand of start up. This selection technique also allows to maximize the use of the electrolyser without being limited by the maximum production capabilities of a small electrolyser during sunny periods and the minimum production capabilities of a large electrolyser during winter or more cloudy periods.
The electrolyser load is set to be constant during each day, equal to the mean value of the energy produced during the next 24h (see Fig.49). This constant production is possible thanks to the battery implementation, supplying electricity to the electrolyser when PV production is not sufficient. The electrolyser load being set by the energy produced during the day will ensure that the energy depleted from the batteries will be at some point in the day recovered.
Then, once the hydrogen is produced, the path from the storage unit to the hydrocarbons synthesis will be equivalent as the one used in the case of a PEM electrolyser: H_2 use determined by the total daily production and constant throughout the day to limit the transient effect in the reactor and minimize the amount of storage needed.

3.3 When using a SOEC electrolyser

As for the alkaline electrolyser, the SOEC will use batteries as support for its electricity supply. However, in contrary to the hydrogen from alkaline case, only one model of SOEC electrolyser is used, which removes the need of a production forecast as used with the alkiline electrolysers. This is possible thanks to the increased load flexibility of the SOEC technology compared to the alkaline (5% versur 15% minimlum load).
The algorithm is set to produce hydrogen during every hour of the year, with a production profile determined by the PV production forecast of the day. If the average hourly PV production of the day $E_{average}$ is above the maximum load of the electrolyser, H_2 will be produced at the maximum rate of the electrolyser with the energy overflow going to the batteries (as happening in Fig.49). If $E_{average}$ is below the minimum load of the electrolyser, the batteries will be depleted to ensure a minimum hydrogen production, keeping the electrolyser at temperature. Finally, if $E_{average}$ is in the range of production of the electrolyser, it will work at constant load during the day, with the batteries either filling up or depleting depending on the current PV production.
The resulting H_2 produced will be treated in the same way as for the PEM and alkaline case: the H_2 use is determined by the total daily production, its is set constant throughout the day to limit the transient effect in the reactor and minimize the amount of storage needed.

3.4 When using a SOEC electrolyser for water and CO_2 co-electrolysis

In the case of syngas production by co-electrolysis in a SOEC electrolyser, the algorithm used for the production is essentially the same as the one used for the water electrolysis using SOEC: the electrolyser use is determined by the average electricity generation from the PV field, with adjustment made hour by hour via the battery system. The syngas usage is handle in the same way as the hydrogen use in the other electrolysis scenarios.

4 Production capabilities and comparison of the different pathways during a year

In this section, the simulation results of the production capabilities of the different Power-to-Fuel routes introduced at the beginning of this part (see part III) will be presented, discussed and compared. The CCU chain studied will be separated in two groups since two main hydrocarbons synthesis process were selected: the ones using a Fischer-Tropsch reactor and the ones using a methanol-to-gasoline unit. The results obtained from the Python simulation were based on the solar data of the year 2019 in Louvain-La-Neuve. The global simulations results are available at the end of the section, in Table 25, on page 96.

4.1 Fischer-Tropsch route

The first step in the Fischer-Tropsch (FT) route is the syngas synthesis. Syngas, a mixture of hydrogen and carbon monoxide, is either obtained by combining a water electrolysis and a reverse water gas shift (RWGS) reactor, or by using a co-electrolysis of H_2 and CO_2. In this section, the focus will be made on the route using a water electrolysis in combination with a RWGS reactor, the co-electrolyser being explored in the next section (4.2.1). The produced syngas, after its conditioning is sent to the FT reactor in which happen the reactions for the production of alkanes, alkenes, alcohols, etc. The FT synthesis part is the same regardless of the syngas production pathway.

4.1.1 Water electrolysis

The hydrogen production is done by using an electrolyser (either PEM, Alkaline or SOEC), on Fig.50a is drawn the H_2 production profile of the two alkaline electrolysers chosen for the simulations (see subsection 2.3) in parallel to the NAS batteries state of charge (SoC). As planned by the algorithm, the hydrogen production is continuous during the year, with minimum production of 4kg/h when the smaller electrolyser is used (mostly at the beginning and end of the year). For most of the year, the bigger electrolyser (chosen to be the NEL A1000) is handling the electrolysis, the resulting average hydrogen production for the year is 29.7kg/h, with a maximum at around 90% of the electrolyser nominal production capabilities, 77.5kg/h. The histogram of the hydrogen production during the year is plotted on Fig.50b.
During the year, the battery system is enough to allow the constant H_2 production. As expected, it is in the winter months that the batteries are the most used, with some power surge required during summer due to the algorithm definition. During the test, the batteries were empty for a total of 15 hours and full for 513. At no point during the year, batteries reached their maximum rated output power of 6MW.
However, as seen in Fig.50a, the batteries SoC at the last hour of the year is not greater or equal to the SoC when starting the year, meaning that theoretically, the system will fail if applied to more than 1 year. To compensate this deficit, the hydrogen excess (see Fig.51) available in storage could be used to generate electricity, either in a fuel cell generator or in a small gas turbine, thereby filling the batteries.

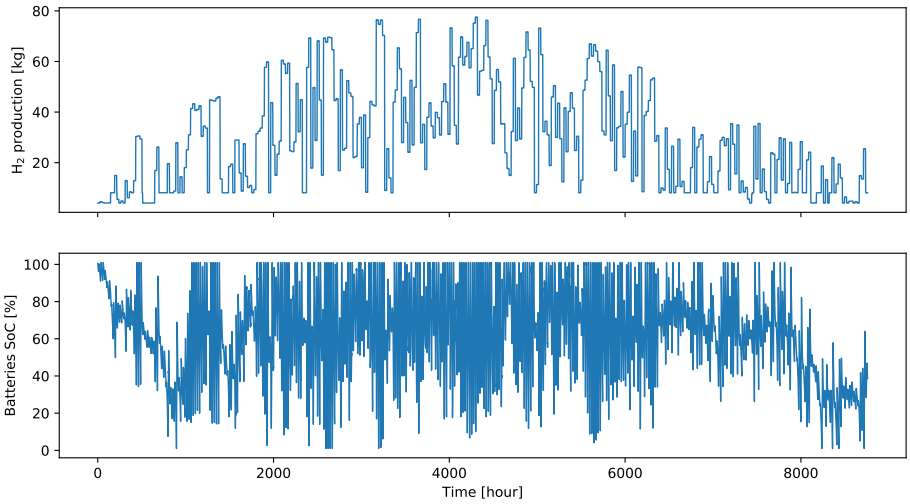

(a) Hydrogen production profile of the NEL A1000 and A485 electrolyser in parallel to the NAS batteries state of charge (SoC)

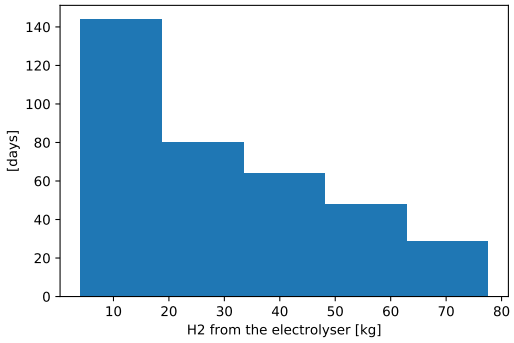

(b) Distribution of the hourly H_2 production during the year

Figure 50: Hydrogen production by the Alkaline electrolyser during the year 2019

The hydrogen production profile using alkaline electrolysers can be compared to the production that would be obtained using other electrolysis techniques, based on the same PV production.
Firstly, when two PEM electrolysers are used (as well as the associated algorithm), the hourly average H_2 production increases to 30.58kg/h as well as the maximum production at 169.2kg/h, while the minimum decreases to 0kg/h due to the PEM usage definition and the fact that its operation is not supported by a battery system.
The SOEC electrolyser, on the other hand, is much more similar to the alkaline electrolyser regarding its utilisation, the minimum hourly H_2 production is 3.33kg/h, which is the electrolyser minimum load ($5\%_N$), the hourly average production is higher than the one of the alkaline at 33.9kg/h and the maximum production is limited by the SOEC nominal load, at 66.6kg/h.
When using the SOEC electrolyser couple with batteries, the H_2 generation is limited by its maximal production capabilities. Indeed, during the year, it happens for about 400 hours that the HyLink electrolyser is asked to work at nominal power while the batteries are full. This results in a potential loss of H_2 production compared to other implementations where such a scenario does not occur. Installing a second, smaller, SOEC electrolyser (as done for the alkaline electrolysis) would not be an effective solution since their is only one available size for this technology (at least in the Sunfire catalog). Therefore, the cost compared to the benefits would not be interesting (only a 5% increase in H_2 production when using 2 Hylink electrolysers). Moreover, while being cap

in production capabilities, the SOEC electrolysis still produces the most hydrogen during the year compared to the other two technologies:

- 2 PEM electrolysis (2×1000Nm^3/h) : 267 878 kg_{H_2} produced in 2019 with a 10 MW_p PV installation and no batteries
- 2 Alkaline electrolyser (970 and 485Nm^3/h): 260 216 kg_{H_2} produced in 2019 with a 10 MW_p PV installation and 36MWh of batteries storage
- 1 SOEC electrolyser (750Nm^3/h) : 297 075 kg_{H_2} produced in 2019 with a 10 MW_p PV installation and 36MWh of batteries storage

4.1.2 Reverse water gas shift reaction (RWGS)

The hydrogen, once produced, will firstly be stored before being sent to a conditioning unit in which it will be mixed with CO_2, and prepared for the RWGS reaction. The hydrogen storage unit (IC P/140-XL) is capable of supplying H_2 at pressures up to 500 bar and store up to 3360kg_{H_2}. This hydrogen storage will be used accordingly to the daily hydrogen production by the electrolysers, the CO_2 usage is then fixed by the hydrogen availability (in this case, where the CO_2 is considered as a base product and where the carbon capture part is not implemented).
On Fig.51 is plotted the hourly hydrogen utilisation (going from the storage to the conditioning unit and therefore the RWGS reactor) in parallel to the hydrogen storage capacity. This profile represents the H_2 utilisation in the case where H_2 is being produced by the alkaline electrolysers. The storage state, at the start of the year, is set to be at 1/3 of the capacity, with the H_2 utilisation being based on the amount produced during the day by the electrolyser. During the year, the minimum quantity of hydrogen inside the reservoir is around 216kg and the storage state, at the end of the year, is greater than where the year started meaning that this utilisation algorithm is sustainable. However, the maximum storage capacity in the reservoir is reached for 262 hours during the year, this represents an hydrogen loss of 107kg (or 0.04%) over the year if the H_2 utilisation profile is not adapted to account for this scenario.
It is important to note that the hourly H_2 utilisation is considered to be the combination of the H_2 used in the RWGS reactor as well as the one used in the Fischer-Tropsch reactor (with the non-reacting hydrogen not taken into account: $H_{2,used} = (H_{2,RWGS} + H_{2,FT})_{in}$-$(H_{2,RWGS} + H_{2,FT})_{out}$)

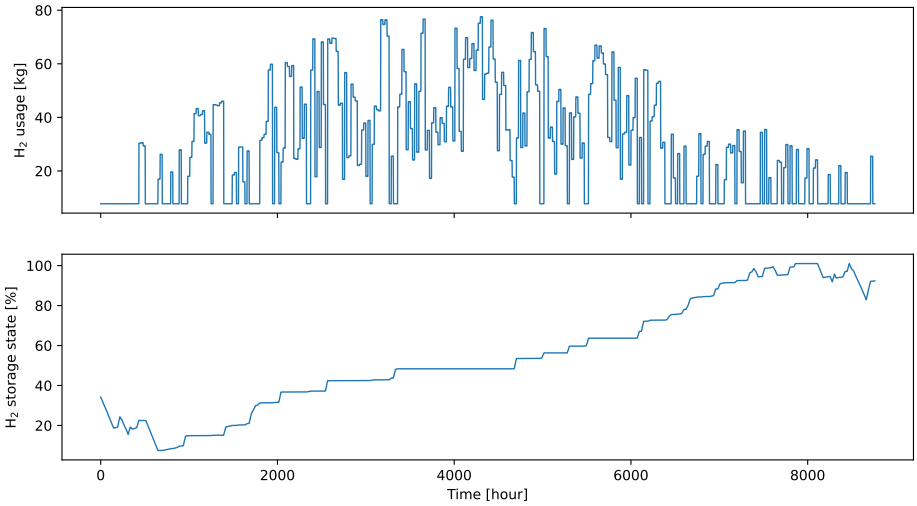

Figure 51: Hourly hydrogen usage by the chain, this include the feed flow to the RWGS reactor as well as the one for the FT reactor

The gas mixture composed of hydrogen and carbon dioxide, after conditioning, will be sent to the RWGS reactor(s). The chosen operating conditions for the reactor(s) are the following: the reaction, endothermic, is operated at a temperature of 900°C, under a pressure of 1 bar, over a NiO/SBA-15 catalyst, and with a unitary inlet molar ratio (H_2/CO_2=1). The resulting carbon dioxide conversion is 55% and the selectivity of the reaction towards CO is assumed to be close to 100% (as used in section 5.4).
The hourly carbon monoxide production is plotted on Fig.52a and the CO production histogram is drawn in Fig.52b. Thanks to the hydrogen storage (and carbon dioxide storage if the carbon capture unit were to be implemented), the reactor can operate continuously during the year, with a production mass flow varying between 35.9 and 359kg/h, with an average hourly production of 136.5kg/h.
To account for this wide variation in intake flow rate, the RWGS reaction must be split in several reactors, this will allow to operate more efficiently, preventing the huge energy cost that would come with the use of an oversized reactor (in the winter months, for example). To maximise the efficiency of the reaction, several reactors must be used throughout the year in order to better suit the gas mixture intake variation. The choice of reactors number and size can be made by looking at the H_2 production histogram (on Fig.50b), proportional to the one at the RWGS intake.

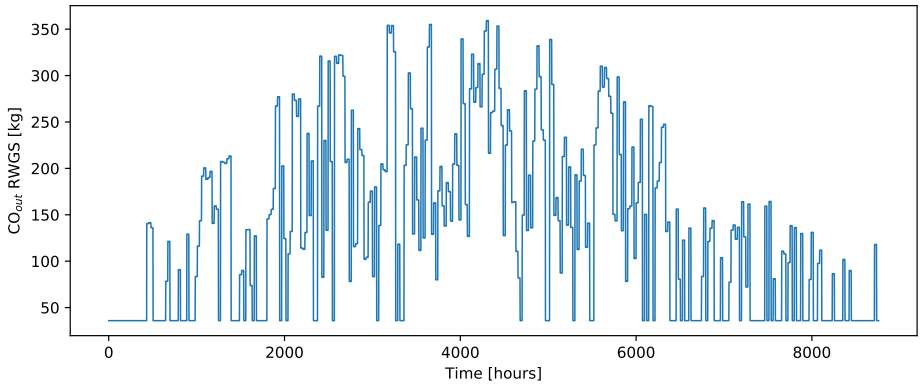

(a) Hourly production of Carbon monoxide in the RWGS reactor

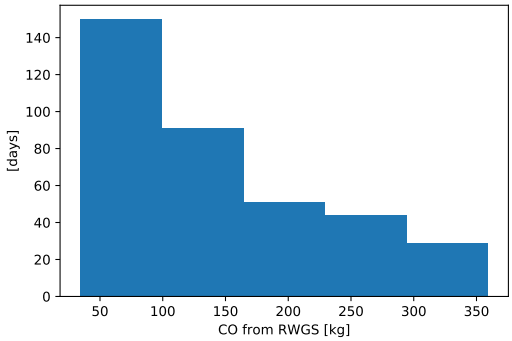

(b) Distribution of the quantity of CO produced per hour over the year

Figure 52: CO synthesis by the RWGS reactor during the year, based on the H_2 production of the alkaline electrolysers

4.1.3 Fischer-Tropsch synthesis

The FT reaction uses, as input flow, a syngas with a molar ratio bewteen the hydrogen and carbon dioxide of 2, a pressure of around 25 bar and a temperature of 220°C. To obtain such syngas, the carbon monoxide, coming from the RWGS reactor (after separation from the other gases), is mixed with hydrogen from the

hydrogen storage in a conditioning unit. This unit is used to pressurise and heat the gas mixture up to the specifications, the heating is made mostly using the heat from the FT synthesis.
In the reactor, a "low-temperature Fischer-Tropsch" reaction (or LTFT, see in section 1.2) was implemented, due to its higher yield towards the longer hydrocarbon chains. The number of reactors used for the synthesis is, as for the RWGS reaction, determined by the syngas production histogram (proportional to the CO production histogram in Fig.52b). This allows to take into account the wide intake flow variation throughout the year and, therefore, limits losses due to the operational cost of an oversized reactor.
With the CO production profile (on Fig.52a), being the same as the CO utilisation profile in the FT reactor, the total amount of syncrude produced during the year can be calculated. This number is compared, here below, with the production quantity expected from the other two electrolysis techniques, independently of the electrolyser used, the composition of the syncrude between the simulations remains the same at 41.35% of wax, 30.73% of naphta and 28.02% of diesel [1].

- When using the 2 PEM electrolysers, the global hydrocarbons production is 604 409 kg. This was produced using, as base feedstock, 2 410 907 kg of demineralised water (of which 1 930 876 are retrieved in the RWGS and FT products) and 1 949 285 kg of CO_2.
- When using a combination of 2 alkaline electrolysers coupled to a battery system, the global chain produces a total of 582 467 kg of hydrocarbons, based on a feedstock of 2 602 162 [2] kg of water (of which 1 860 781 are retrieved in the RWGS and FT products) and 1 878 522 kg of CO_2.
- Finally, when the electrolysis is performed using a SOEC electrolyser, also coupled to a battery system, the global hydrocarbon production is 670 275 kg, when using as base feedstock 3 837 289 kg of steam (of which 2 141 294 are retrieved in the RWGS and FT products) and 2 161 709 kg of CO_2.

As mentioned in the beginning of this section, in parallel to this FT route using a water electrolysis and a RWGS reaction is the pathway using a direct syngas synthesis by the use of a co-electrolysis. The production capabilities of this route can also be compared to ones using a RWGS reactor:

- When using a co-electrolysis for direct syngas production, the global hydrocarbon production of the chain for the year is 585 461 kg, this was produced using as base feedstock 2 182 572 kg of steam (of which 1 097 422 are retrieved in the FT products) and 2 845 138 kg of CO_2.

4.2 Methanol to gasoline route

The methanol to gasoline route, although generally made up of the same blocks, includes several variations: the methanol synthesis can either be performed based on a CO_2 or CO feedstock, and the products coming out of the methanol-to-gasoline process will depend on the type of unit used (either MTG or MTO-MOGD). The discussion in this section will focus on the pathway that uses the methanol synthesis from syngas, the one being produced by a co-electrolysis (the water electrolysis being already detailed in the FT route).

4.2.1 Syngas generation

The direct syngas generation is done by using a co-electrolysis. The production profile of the one implemented in the simulation is plotted on Fig.53a. The syngas produced by the electrolyser is expected to provide a molar H_2/CO ratio of 2. In parallel to this profile, is also plotted the batteries state during the year. This system is used to support the power source and provide a steady supply to the electrolyser. As expected, by the energy utilisation algorithm, the syngas production during the year is constant (no hour without production), allowing

[1] The product composition has been extracted from an industrial process utilising a Fischer-Tropsch reactor for LTFT synthesis, for reasons of confidentiality the name of the company will not be revealed

[2] No information is given by the electrolyser manufacturer, therefore, a value of 10 l/kg_{H_2} was considered [123]

the electrolyser (SynLink) to keep its operating temperature constant, avoiding production losses due to the start-up time of the electrolyser. The minimum amount of syngas produced per hour by the electrolyser is 17.64 kg which corresponds to its minimum load, the maximum is 352.73 kg and the mean hourly production during the year is equal to 156.93 kg (of which 137.19 are CO and 19.74 are H_2).
The maximum syngas production by the electrolyser corresponds to its nominal power operation. This occurs for 1008 hours during the year, of which 190 are simultaneous to a full battery capacity. During these 190 hours, the maximum energy utilisation of the system is reached, meaning that production is "lost" since the extra energy given to the system by the PV generation can not produce more hydrogen or being stored in the batteries. This "problem" could be elevated by either increasing the number of batteries or by having more/bigger electrolysers. However, the cost associated to these solutions is high compared to the benefits expected: in the situation presented (1 SynLink electrolyser and 36MWh of battery storage), the total amount of syngas produced during the year is 1 374 766 kg, while when the upper production limit of the electrolyser is removed, the expected syngas production will be 1 384 866 kg, or a production increase of 0.73%.

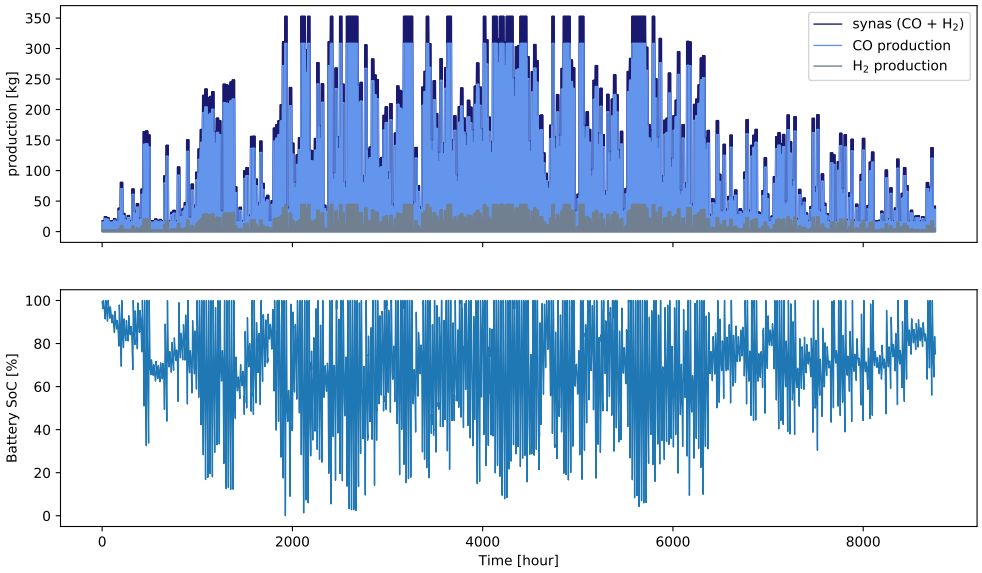

(a) Syngas production profile over 2019 by the SynLink electrolyser in parallel to the NAS batteries state of charge

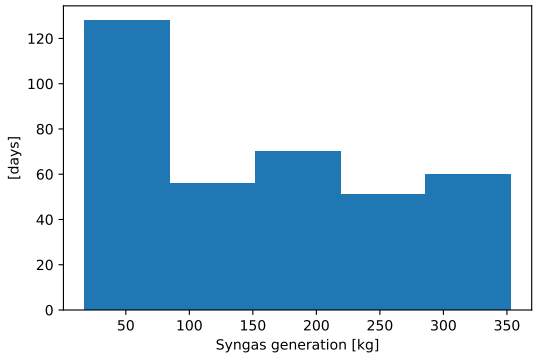

(b) Distribution of the quantity of syngas produced per hour over the year

Figure 53: Hourly syngas generation by the SynLink electrolyser and its battery support for the year 2019

The produced syngas by the electrolyser will not be directly used in the methanol synthesis reactor, as for the FT route, the electrolysis products will first be stored and conditioned before being used in other processes. Therefore, storage units are required for both the CO and H_2 leaving the electrolyser. The hydrogen storage is realised by the IC P/140-XL capable of storing up to 3 360 kg, at a filling rate of 140kg/h and up to a pressure of 500 bar. The CO storage is handled by a pressurized tank, capable of storing 10 000 kg of CO.

4.2.2 Methanol synthesis

The methanol synthesis from syngas is realised using, as inlet flow, a previously conditioned mixture of carbon dioxide (CO_2) and hydrogen (H_2) with a molar ratio H_2/CO of 2. In the reactor(s), the syngas utilisation is determined by the amount of syngas produced during the day. Its hourly utilisation during the simulation is shown on Fig.54. This utilisation is put in parallel to the storage state of both the hydrogen and carbon dioxide. The minimum syngas flow, inside the reactor, is 31.4 kg/h, the maximum is of 352.73 kg and the average hourly syngas usage of 157.03 kg. This utilisation distribution allows the storage to stay within limit during the year and to have, at the end of the year, more in storage than when starting. Moreover, this curve, in parallel to the distribution histogram of syngas production by the electrolyser (Fig.53b) will provide a way to size the methanol reactor(s) by taking into account the syngas inlet flow variations as well as the duration for which it remains at a certain mass flow.

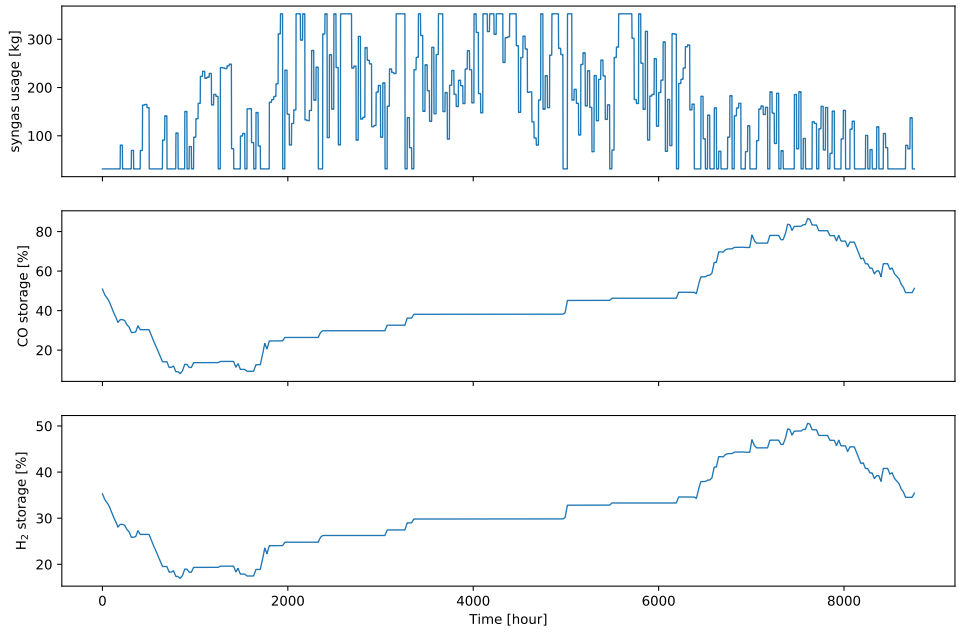

Figure 54: syngas utilisation over the year in parallel to the storage state of the CO and H_2 reservoirs

On Fig.55a is plotted the global methanol production during the year. This production is based on the syngas utilisation profile plotted on Fig.54 and the conversion value of the synthesis, determined by the reaction operating parameters. Here, the reaction is set be be operated at 250°C, high pressure (>50 bar) and over a Cu/ZnO catalyst, providing a CO conversion around 94% and a methanol selectivity of 99%. The amount of methanol produced during the year varies from 31 to 349 kg/h, with an average production value of 155.3 kg/h. The histogram of the hourly methanol production over the year is available on Fig.55b, this figure will be useful to determinate the number and size of the reactors downstream.

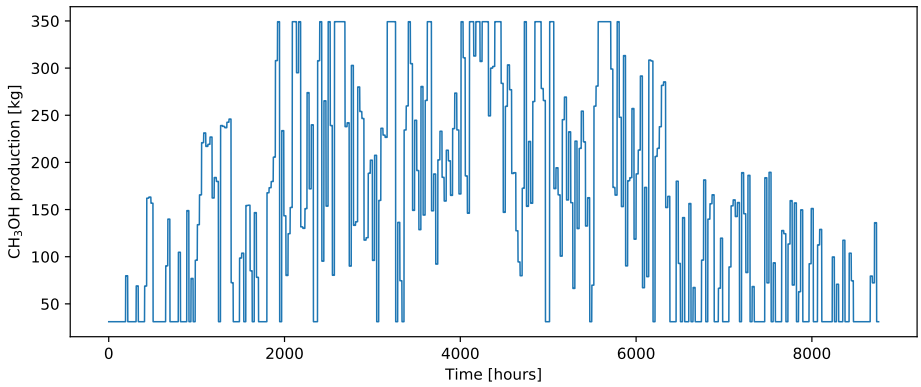

(a) Hourly production of methanol in the reactor

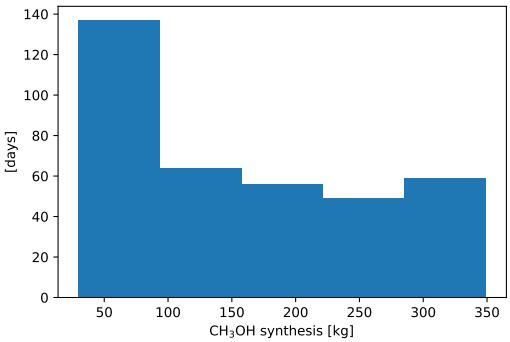

(b) Distribution of the quantity of methanol synthesised per hour over the year

Figure 55: Hourly methanol production from syngas

This production of methanol can be compared to the production that would be expected if the route using a water electrolysis followed by a methanol synthesis using carbon dioxide (CO_2) and hydrogen was taken. The water electrolysis can be operated in several ways, either by a PEM electrolysis, an alkaline electrolysis or a high temperature steam electrolysis. The choice will impact the hydrogen production and, therefore, the methanol production. The reactor conditions used for this synthesis are the same as ones used for the efficiency determination in section 2.6. Finally, the amount of methanol produced during the year depending on the electrolysis type used can be calculated:

- Using a PEM electrolyser, the global methanol production is equal to 1 407 658 kg with an average production during the year of 160.7 kg/h
- Using a alkaline electrolyser, the global methanol production is equal to 1 356 557 kg with an average production during the year of 154.8 kg/h
- Using a SOEC for water electrolysis, the global methanol production is equal to 1 561 058 kg with an average production during the year of 178.2 kg/h

4.2.3 Methanol to gasoline

As explained in the section specifically dedicated to the MtG process (see section 3), the unit responsible for the conversion of methanol to gasoline can either be a classical MTG, for the synthesis of gasoline, or a MTO-MOGD unit for the synthesis of diesel, kerosene and gasoline. Both the processes were simulated and the results depending on the methanol synthesis process are shown here below.

MTG unit (section 3.1) The MTG unit takes as inlet flow a combination of methanol and hydrogen (at a mass ratio of $\approx 400/1$), this mixture comes from a conditioning unit, responsible of mixing and preparing the reactants before entering the first MTG reactor. The methanol entering the conditioning unit directly comes from the methanol synthesis reactor (after separation) while hydrogen is extracted from its storage reservoir. The hydrocarbon flow leaving the MTG is directly proportional to the methanol produced in the methanol reactor, it follows its production profile throughout the year. From this production profile, the total amount of hydrocarbons produced during the year can be calculated. This production is placed here below in comparison to the total production capabilities of the other methanol to gasoline route, using a water electrolysis followed by a methanol synthesis from H_2 and CO_2:

Table 21: MTG production using methanol from syngas synthesis as feedstock

Electrolyser	Hydrocarbons production [kg]	Gasoline production [kg][3]
SOEC for co-electrolysis	600 305.5	479 644

Table 22: MTG production using methanol synthesis from CO_2 and H_2

Electrolyser	Hydrocarbons production [kg]	Gasoline production [kg][3]
PEM	620 889	496 090
Alkaline	598 349	478 081
SOEC for water electrolysis	688 550.5	550 152

MTO - MOGD unit (section 3.2) The MTO-MOGD operates in the same way as its MTG counterpart in the way the inlet flow is treated: the flow is mainly composed of methanol with a small quantity of hydrogen, preconditioned, and the production profile during the year is proportional to the one of the methanol synthesis. The total amount of hydrocarbons produced by the process can be calculated and compared between the different production routes:

Table 23: MTO-MOGD production using methanol from syngas synthesis as feedstock

Electrolyser	Hydrocarbons production [kg]	Detailed production [kg][4]
SOEC for co-electrolysis	602 556	Diesel: 268 115
		Kerosene: 161 504
		Gasoline: 101 621

Table 24: MTO-MOGD production using methanol synthesis from CO_2 and H_2

Electrolyser	Hydrocarbons production [kg]	Detailed production [kg][4]
PEM	623 217	Diesel: 277 309
		Kerosene: 167 042
		Gasoline: 105 105
Alkaline	600 593	Diesel: 267 241
		Kerosene: 160 978
		Gasoline: 101 289
SOEC for water electrolysis	691 132	Diesel: 307 528
		Kerosene: 185 245.5
		Gasoline: 116 559

[3]The ratios of hydrocarbons cuts are the same as the one used in Table11
[4]The ratios of hydrocarbons cuts are the same as the one used in Table12

4.3 Results discussion

Regarding the different process simulated, SOEC for co-electrolysis seems to be the one performing the best overall when compared to the other water electrolysis techniques thanks to its very high efficiency. However, due to the technology being relatively new, only few suppliers and sizes are available, making it harder to have a perfect fit for the size of the installation on which we want to deploy it. Also, the use of a SOEC electrolyser requires the use of batteries, this will add a significant cost to the potential CCU installation.
The hydrogen production using a combination of two alkaline electrolyser and a battery system, on the other hand, is clearly the least effective of the processes. Both regarding the production capabilities and the overall cost of the installation since two electrolysers are required to account for the limited load flexibility and to have an efficient production profile, a battery system would be installed.
H_2 production using PEM electrolysis looks to be the best compromise between the production capabilities and the cost of the installation. Indeed, using Table 25, it is clear that using 2 PEM electrolysers would be the best of the studied options regarding the production capabilities and cost (since it does require a battery system as the SOEC and alkaline scenario).

In the case of syngas production using a co-electrolysis, the overall production compared to the other pathway is smaller. This can be explained because the electricity produced by the PV field is used for both water electrolysis and CO_2 electrolysis whereas, for the other pathways, a combination of water electrolysis and chemical reactions is used. The water electrolysis is therefore allowed to use all the electricity available for the H_2 production while the CO synthesis only required heat to be operated. Besides, due to the nature of the electrodes used in the SOECs for co-electrolysis, the technology is very sensitive to the contamination for the inlet CO_2 and water flow, and may require additional care to the purity of these feedstocks compared to the other production routes.
In conclusion, this technology does not seem to be the best suited for this particular case of Power-to-Fuel chain, where the electricity supply is limited (here by the number of renewable production) and where the purity of the CO_2 and water feedstock is critical. However, since the syngas can be produced in a single step, it allows to have a simpler production chain, reducing the number of reactors, pumps, cooling system, etc. making the technology more robust (less failure points).

When comparing the different processes for the hydrocarbons synthesis (FT, MTG, MTO-MOGD), none seems to come out ahead of the other. They all are used for different products synthesis, the MTG unit can produces large amount of gasoline with only a little amount of side products, the MTO-MOGD has a product composition well suited for upgrading towards jet fuel, for example, and Fisher-Tropsch can produced a wide variety of products depending on the conditions set inside the reactor.
A global summary of all the different production route production capabilities, consumption of water/carbon dioxide and battery/storage utilisation is available in Table 25.

Production Pathways	Electrolyser Technology	Water/CO_2 consumption[1] [kg/a]	H_2/CO produced [kg/a]	Batteries[2]			H_2 Storage[3] [kg]			H_2 Utilisation [kg]			Hydrocarbons produced [kg/a]	
				Empty hours	Full hours	SoC last hour of the year [%]	Minimun	Maximum	Last hour of the year	Minimum	Maximum	Average	Global	Detailed
Pathway 1	PEM	480 030[4] / 1 949 285	267 878 / 0	/	/	/	406	1824	1115	4.1	81.96	30.58	604 409	Wax: 249 878 Diesel: 168 764 Naphta: 185 771
	Alkaline	741 381 / 1 878 521	260 216 /0	15	513	37.6%	216.5	3360	3070	7.75	29.47	77.55	582 468	Wax: 240 803 Diesel: 162 637 Naphta: 179 026
	SOEC	1 695 995[5] / 2 161 708	297 075 / 0	0	698	75%	126	2124	1119	6.66	66.66	33.91	670 275	Wax: 277 104 Diesel: 187 154 Naphta: 206 015
Pathway 2	SOEC for co-electrolysis	1 085 149[5] / 2 845 138	172 993 / 1 201 773	1	567	75%	502	1632	1123	3.95	44.38	19.75	585 461	Wax: 242 041 Diesel: 163 472 Naphta: 179 946
Pathway 3	PEM	MTG: 812 611[4] / 1 995 130	267 878 / 0	/	/	/	406	1824	1115	4.09	81.96	30.58	MTG :620 889	Gasoline: 496 090
		MTO-MOGD: 815 013 / 1 995 130											MTO-MOGD: 623 217	Diesel: 277 308 Kerosene: 167 042 Gasoline: 105 105
	Alkaline	MTG: 1 060 986 / 1 923 829	260 216 / 0	15	513	37.6%	216.5	3360	3070	7.75	29.47	77.55	MTG : 598 349.3	Gasoline: 478 081
		MTO-MOGD: 1 063 302 / 1 923 829											MTO-MOGD: 600 593	Diesel: 267 241 Kerosene: 160 978 Gasoline: 101 290
	SOEC	MTG: 2 063 780[5] / 2 213 846	297 075 / 0	0	698	75%	126	2124	1119	6.66	66.66	33.91	MTG : 688 550	Gasoline: 550 152
		MTO-MOGD: 2 066 445[5] / 2 213 846											MTO-MOGD: 691 132	Diesel: 307 528 Kerosene: 185 245 Gasoline: 116 559
pathway 4	SOEC for co-electrolysis	MTG: 1 418 546[5] / 2 845 138	172 993 / 1 201 773	1	567	75%	502	1632	1123	3.95	44.38	19.75	MTG : 600 305	Gasoline: 479 644
		MTO-MOGD: 1 420 870[5] / 2 845 138											MTO-MOGD: 602 556	Diesel: 268 115 Kerosene: 161 504 Gasoline: 101 621

Table 25: Global simulation results of the different hydrocarbons production pathways in which the electricity required by the electrolyser is supplied by a 10MWp PV field.

Pathway 1: Water electrolysis followed by a RWGS for syngas production and FT syntehsis for hydrocarbon synthesis;

Pathway 2: co-electrolysis of water and CO_2 followed by a FT synthesis;

Pathway 3: Water electrolysis in parallel to a methanol synthesis from CO2 and H2 followed by a MtG unit;

Pathway 4: Co-electrolysis for syngas production followed by methanol synthesis and MtG unit;

[1]The consumption represent the overall water and CO_2 used during the year, meaning what enters the processes minus what leaves it.

[2]The chain simulation starts with the batteries full (at 36MWh). [3]The hydrogen storage is at 1/3 of its capacity at the start of the year.

[4]Demineralized water.

[5]Steam input.

Conclusion

The goal of this document was to provide a preliminary study of at some possible CCU chains in the case of a Power-to-Fuel application in order to have, at the end, a global view of the production routes and the different elements composing them, regarding their efficiency, selectivity, operability and production capabilities when powered only by renewable sources.

Hydrogen is one of the two main reactants in PtF application. To obtain it based on a water feedstock, an electrolysis must be used. The electrolyser is crucial in such installation since it is the element consuming the most energy of the chain; the different type used were the alkaline, PEM and SOEC electrolyser.
The alkaline electrolysis technology is the most mature of the three and, therefore, the least expensive to install. However, the low load flexibility, combined to the relatively poor efficiency makes it not a very compelling option for an hydrogen production considering renewable sources. The SOEC electrolyser, thanks to its very high efficiency and its high load flexibility, is able to produce very large amount of hydrogen. However, the technology suffers from several problems, most of them linked to its relatively low technology readiness level: the capital cost of the technology and materials is, nowadays, still high, and, its starting time and high operating temperature make it unusable when based on fluctuating energy sources without using batteries. The PEM electrolysis seems to the best option regarding the production of hydrogen based on a renewable sources. From all the electrolysis technologies, it is the only one where a battery system is not required thanks to its very fast starting time. Moreover, its high load flexibility better allows it to follow the sun/wind production profile, even at low power. Therefore, PEM seems to be the best option for H_2 production: good production capabilities thanks to the high load variation and relatively good efficiency while having a lower capital cost since only little to no battery system is required.

The second main reactant for the syngas is the carbon monoxide. To obtain it based on CO_2, either the electrochemical or chemical pathway can be used. However, using a CO_2 electrolysis (in SOEC) does not seem to be the solution since, nowadays, the technology still has a TRL too low making the technology expensive, with low production capabilities and still very prone to contamination from the CO_2 feedstock. Syngas can also directly be produced from CO_2 and water by using a co-electrolyser. Even if this technology seems promising, in the case of limited electricity source, the overall syngas production will be smaller than other syngas production techniques because electricity will be used for both the H_2 and CO generation, effectively decreasing the global amount of syngas produced compared to the other processes using a chemical reaction for the CO synthesis. Beside, this technology (as for the CO_2 electrolysis) being relatively new, is still very expensive to implement and prone to degradation from impurities present in the CO_2 feed flow (reducing its efficiency and consequently lifetime). Therefore, the best way to produce CO for the syngas production is by using a RWGS reactor: The reaction does not consume much energy and can fully be supplied by the other processes in the chain.

Regarding the different syngas upgrading units (FT, methanol synthesis, methanol-to-gasoline), none seems to stand out particularly as better than the others. They all produced different product types and with efficiency relatively similar. Of all the processes, the methanol synthesis is the more versatile. Methanol can either be used as such, or upgraded to DME or gasoline for use as fuels. The Fischer-Tropsch synthesis is also versatile since the products selected by tuning the reactor conditions and catalyst. And the methanol to gasoline unit, depending on its implementation, can be used to synthesise many products, from gasoline for cars to kerosene and jet fuel.

In conclusion, this document can serve as a preliminary study for potential CCU and PtF applications depending on the type of products wanted by the chain and the type of electrical sources available while proposing research leads for different processes that could be used in these chains.

References

[1] Mofarahi, Masoud, Yaser Khojasteh, Hiwa Khaledi, and Arsalan Farahnak. 'Design of CO2 Absorption Plant for Recovery of CO2 from Flue Gases of Gas Turbine'. Energy 33, no. 8 (1 August 2008): 1311–19. https://doi.org/10.1016/j.energy.2008.02.013.

[2] Songolzadeh, Mohammad, Mansooreh Soleimani, Maryam Takht Ravanchi, and Reza Songolzadeh. 'Carbon Dioxide Separation from Flue Gases: A Technological Review Emphasizing Reduction in Greenhouse Gas Emissions'. TheScientificWorldJournal 2014 (2014): 828131. https://doi.org/10.1155/2014/828131.

[3] Futura, la rédaction de. « L'air: quelle en est sa composition? » Futura. Consulté le 3 juin 2022. https://www.futura-sciences.com/planete/questions-reponses/environnement-air-composition-57/.

[4] Global CCS Institute. 'CO2 Capture Technologies: Technology Options for CO2 Capture'. Accessed 5 May 2022. https://www.globalccsinstitute.com/resources/publications-reports-research/co2-capture-technologies-technology-options-for-co2-capture/.

[5] Xu, Gang, Le Li, Yongping Yang, Longhu Tian, Tong Liu, and Kai Zhang. 'A Novel CO2 Cryogenic Liquefaction and Separation System'. Energy, 8th World Energy System Conference, WESC 2010, 42, no. 1 (1 June 2012): 522–29. https://doi.org/10.1016/j.energy.2012.02.048.

[6] 'High Temperature Electrolysis Cell (SOEC)'. Accessed 27 April 2022. http://www.helmeth.eu/index.php/technologies/high-temperature-electrolysis-cell-soec.

[7] Buttler, Alexander, and Hartmut Spliethoff. 'Current Status of Water Electrolysis for Energy Storage, Grid Balancing and Sector Coupling via Power-to-Gas and Power-to-Liquids: A Review'. Renewable and Sustainable Energy Reviews 82 (1 February 2018): 2440–54. https://doi.org/10.1016/j.rser.2017.09.003.

[8] Shiva Kumar, S., and V. Himabindu. 'Hydrogen Production by PEM Water Electrolysis – A Review'. Materials Science for Energy Technologies 2, no. 3 (1 December 2019): 442–54. https://doi.org/10.1016/j.mset.2019.03.002.

[9] 'Proton-Exchange Membrane'. In Wikipedia, 9 October 2021. https://en.wikipedia.org/w/index.php?title=Proton-exchange_membrane&oldid=1049051602.

[10] Hauch, A., R. Küngas, P. Blennow, A. B. Hansen, J. B. Hansen, B. V. Mathiesen, and M. B. Mogensen. 'Recent Advances in Solid Oxide Cell Technology for Electrolysis'. Science 370, no. 6513 (9 October 2020): eaba6118. https://doi.org/10.1126/science.aba6118.

[11] 'Électrolyse à oxyde solide'. In Wikipédia, 30 March 2022. https://fr.wikipedia.org/w/index.php?title=%C3%89lectrolyse_%C3%A0_oxyde_solide&oldid=192425406.

[12] Chen, Ming, Peter Blennow, Brian Mathiesen, and Zhe Zhang. Towards Solid Oxide Electrolysis Plants in 2020, 2017.

[13] Wang, Ligang, Mar Pérez-Fortes, Hossein Madi, Stefan Diethelm, Jan Van herle, and François Maréchal. 'Optimal Design of Solid-Oxide Electrolyzer Based Power-to-Methane Systems: A Comprehensive Comparison between Steam Electrolysis and Co-Electrolysis'. Applied Energy 211 (1 February 2018): 1060–79. https://doi.org/10.1016/j.apenergy.2017.11.050.

[14] Carmo, Marcelo, David L. Fritz, Jürgen Mergel, and Detlef Stolten. 'A Comprehensive Review on PEM Water Electrolysis'. International Journal of Hydrogen Energy 38, no. 12 (22 April 2013): 4901–34. https://doi.org/10.1016/j.ijhydene.2013.01.151.

[15] Burton, N. A., R. V. Padilla, A. Rose, and H. Habibullah. 'Increasing the Efficiency of Hydrogen Production from Solar Powered Water Electrolysis'. Renewable and Sustainable Energy Reviews 135 (1 January 2021): 110255. https://doi.org/10.1016/j.rser.2020.110255.

[16] Felgenhauer, Markus, and Thomas Hamacher. 'State-of-the-Art of Commercial Electrolyzers and on-Site Hydrogen Generation for Logistic Vehicles in South Carolina'. International Journal of Hydrogen Energy 40, no. 5 (9 February 2015): 2084–90. https://doi.org/10.1016/j.ijhydene.2014.12.043.

[17] Lehner, Markus, Robert Tichler, Horst Steinmüller, and Markus Koppe. 'Water Electrolysis'. In Power-to-Gas: Technology and Business Models, edited by Markus Lehner, Robert Tichler, Horst Steinmüller, and Markus Koppe, 19–39. SpringerBriefs in Energy. Cham: Springer International Publishing, 2014. https://doi.org/10.1007/978-3-319-03995-4_3.

[18] Zeng, Kai, and Dongke Zhang. 'Recent Progress in Alkaline Water Electrolysis for Hydrogen Production and Applications'. Progress in Energy and Combustion Science 36, no. 3 (1 June 2010): 307–26. https://doi.org/10.1016/j.pecs.2009.11.002.

[19] Fu, Qingxi, Corentin Mabilat, Mohsine Zahid, Annabelle Brisse, and Ludmila Gautier. 'Syngas Production via High-Temperature Steam/CO2 Co-Electrolysis: An Economic Assessment'. Energy Environmental Science 3, no. 10 (29 September 2010): 1382–97. https://doi.org/10.1039/C0EE00092B.

[20] Skafte, Theis, Johan Hjelm, Peter Blennow, and Christopher Graves. Quantitative Review of Degradation and Lifetime of Solid Oxide Cells and Stacks, 2016.

[21] Hansen, John Bøgild. 'Solid Oxide Electrolysis – a Key Enabling Technology for Sustainable Energy Scenarios'. Faraday Discussions 182, no. 0 (3 November 2015): 9–48. https://doi.org/10.1039/C5FD90071A.

[22] Küngas, Rainer. 'Review—Electrochemical COsub2/Sub Reduction for CO Production: Comparison of Low- and High-Temperature Electrolysis Technologies'. Journal of The Electrochemical Society 167, no. 4 (January 2020): 044508. https://doi.org/10.1149/1945-7111/ab7099.

[23] Ma, Z., J. Zhou, Y. Li, C. Liu, J. Pu, and X. Chen. 'Developments in CO2 Electrolysis of Solid Oxide Electrolysis Cell with Different Cathodes'. Fuel Cells 20, no. 6 (2020): 650–60. https://doi.org/10.1002/fuce.201900240.

[24] Zheng, Yun, Jianchen Wang, Bo Yu, Wenqiang Zhang, Jing Chen, Jinli Qiao, and Jiujun Zhang. 'A Review of High Temperature Co-Electrolysis of H2O and CO2 to Produce Sustainable Fuels Using Solid Oxide Electrolysis Cells (SOECs): Advanced Materials and Technology'. Chemical Society Reviews 46, no. 5 (6 March 2017): 1427–63. https://doi.org/10.1039/C6CS00403B.

[25] Hauch, A., R. Küngas, P. Blennow, A. B. Hansen, J. B. Hansen, B. V. Mathiesen, and M. B. Mogensen. 'Recent Advances in Solid Oxide Cell Technology for Electrolysis'. Science 370, no. 6513 (9 October 2020): eaba6118. https://doi.org/10.1126/science.aba6118.

[26] Küngas, Rainer, Peter Blennow, Thomas Heiredal-Clausen, Tobias Holt Nørby, Jeppe Rass-Hansen, John Bøgild Hansen, and Poul Georg Moses. 'Progress in SOEC Development Activities at Haldor Topsøe'. ECS Transactions 91, no. 1 (10 July 2019): 215. https://doi.org/10.1149/09101.0215ecst.

[27] Küngas, Rainer, et al. 'Increasing the lifetime of stacks in CO2 electrolysis.' Proceedings of the 13th European SOFC and SOEC Forum (Lucerne) B. Vol. 1503. (2018).

[28] Skafte, Theis, Johan Hjelm, Peter Blennow, and Christopher Graves. Quantitative Review of Degradation and Lifetime of Solid Oxide Cells and Stacks, 2016.

[29] Fu, Qingxi, Corentin Mabilat, Mohsine Zahid, Annabelle Brisse, and Ludmila Gautier. 'Syngas Production via High-Temperature Steam/CO2 Co-Electrolysis: An Economic Assessment'. Energy Environmental Science 3, no. 10 (29 September 2010): 1382–97. https://doi.org/10.1039/C0EE00092B.

[30] Nechache, Aziz, and Stéphane Hody. 'Alternative and Innovative Solid Oxide Electrolysis Cell Materials: A Short Review'. Renewable and Sustainable Energy Reviews 149 (1 October 2021): 111322. https://doi.org/10.1016/j.rser.2021.111322.

[31] Mogensen, M B, M Chen, H L Frandsen, C Graves, J B Hansen, K V Hansen, A Hauch, et al. 'Reversible Solid-Oxide Cells for Clean and Sustainable Energy'. Clean Energy 3, no. 3 (7 November 2019): 175–201. https://doi.org/10.1093/ce/zkz023.

[32] Hauch, A., R. Küngas, P. Blennow, A. B. Hansen, J. B. Hansen, B. V. Mathiesen, and M. B. Mogensen. 'Recent Advances in Solid Oxide Cell Technology for Electrolysis'. Science 370, no. 6513 (9 October 2020): eaba6118. https://doi.org/10.1126/science.aba6118.

[33] Stoots, Carl M., James E. O'Brien, J. Stephen Herring, and Joseph J. Hartvigsen. 'Syngas Production via High-Temperature Coelectrolysis of Steam and Carbon Dioxide'. Journal of Fuel Cell Science and Technology 6, no. 1 (7 November 2008). https://doi.org/10.1115/1.2971061.

[34] Hansen, John Bøgild. 'Solid Oxide Electrolysis – a Key Enabling Technology for Sustainable Energy Scenarios'. Faraday Discussions 182, no. 0 (3 November 2015): 9–48. https://doi.org/10.1039/C5FD90071A.

[35] Becker, William L. 'DESIGN, PERFORMANCE, AND ECONOMIC ASSESSMENT OF RENEWABLE AND ALTERNATIVE FUEL PRODUCTION PATHWAYS', n.d., 203.

[36] Becker, W. L., R. J. Braun, M. Penev, and M. Melaina. 'Production of Fischer–Tropsch Liquid Fuels from High Temperature Solid Oxide Co-Electrolysis Units'. Energy, Asia-Pacific Forum on Renewable Energy 2011, 47, no. 1 (1 November 2012): 99–115. https://doi.org/10.1016/j.energy.2012.08.047.

[37] Du, Yingmeng, Yanzhou Qin, Guobin Zhang, Yan Yin, Kui Jiao, and Qing Du. 'Modelling of Effect of Pressure on Co-Electrolysis of Water and Carbon Dioxide in Solid Oxide Electrolysis Cell'. International Journal of Hydrogen Energy 44, no. 7 (5 February 2019): 3456–69. https://doi.org/10.1016/j.ijhydene.2018.12.078.

[38] Hauch, Anne, Karen Brodersen, Ming Chen, Christopher Graves, Søren Højgaard Jensen, Peter Stanley Jørgensen, Peter Vang Hendriksen, Mogens Bjerg Mogensen, Simona Ovtar, and Xiufu Sun. 'A Decade of Solid Oxide Electrolysis Improvements at DTU Energy'. ECS Transactions 75, no. 42 (11 January 2017): 3–14. https://doi.org/10.1149/07542.0003ecst.

[39] Wang, Yao, Tong Liu, Shumin Fang, Guoliang Xiao, Huanting Wang, and Fanglin Chen. 'A Novel Clean and Effective Syngas Production System Based on Partial Oxidation of Methane Assisted Solid Oxide Co-Electrolysis Process'. Journal of Power Sources 277 (1 March 2015): 261–67. https://doi.org/10.1016/j.jpowsour.2014.11.092.

[40] Lo Faro, M., S. C. Zignani, S. Trocino, V. Antonucci, and A. S. Aricò. 'New Insights on the Co-Electrolysis of CO2 and H2O through a Solid Oxide Electrolyser Operating at Intermediate Temperatures'. Electrochimica Acta 296 (10 February 2019): 458–64. https://doi.org/10.1016/j.electacta.2018.11.079.

[41] N. P. Brandon, E. Ruiz-Trejo, P. Boldrin, Solid oxide fuel cell lifetime and reliability (Elsevier Academic Press, 2017).

[42] Boldrin, Paul, and Nigel Brandon. 'Progress and Outlook for Solid Oxide Fuel Cells for Transportation Applications'. Nature Catalysis 2 (1 July 2019): 571–77. https://doi.org/10.1038/s41929-019-0310-y.

[43] Cinti, G., G. Discepoli, G. Bidini, A. Lanzini, and M. Santarelli. 'Co-Electrolysis of Water and CO2 in a Solid Oxide Electrolyzer (SOE) Stack'. International Journal of Energy Research 40, no. 2 (2016): 207–15. https://doi.org/10.1002/er.3450.

[44] Wang, Yao, Tong Liu, Libin Lei, and Fanglin Chen. 'Methane Assisted Solid Oxide Co-Electrolysis Process for Syngas Production'. Journal of Power Sources 344 (15 March 2017): 119–27. https://doi.org/10.1016/j.jpowsour.2017.01.096.

[45] 'Innovative Large-Scale Energy STOragE Technologies AND Power-to-Gas Concepts after Optimisation | STOREandGO Project | Fact Sheet | H2020 | CORDIS | European Commission'. Accessed 27 April 2022. https://cordis.europa.eu/project/id/691797.

[46] Zheng, Yun, Jianchen Wang, Bo Yu, Wenqiang Zhang, Jing Chen, Jinli Qiao, and Jiujun Zhang. 'A Review of High Temperature Co-Electrolysis of H2O and CO2 to Produce Sustainable Fuels Using Solid Oxide Electrolysis Cells (SOECs): Advanced Materials and Technology'. Chemical Society Reviews 46, no. 5 (6 March 2017): 1427–63. https://doi.org/10.1039/C6CS00403B.

[47] Wang, Yao, Tong Liu, Libin Lei, and Fanglin Chen. 'High Temperature Solid Oxide H2O/CO2 Co-Electrolysis for Syngas Production'. Fuel Processing Technology 161 (15 June 2017): 248–58. https://doi.org/10.1016/j.fuproc.2016.08.009.

[48] Buttler, Alexander, and Hartmut Spliethoff. 'Current Status of Water Electrolysis for Energy Storage, Grid Balancing and Sector Coupling via Power-to-Gas and Power-to-Liquids: A Review'. Renewable and Sustainable Energy Reviews 82 (1 February 2018): 2440–54. https://doi.org/10.1016/j.rser.2017.09.003.

[49] Rao, Megha, Xiufu Sun, and Anke Hagen. 'Durability of Solid Oxide Electrolysis Stack under Dynamic Load Cycling for Syngas Production'. Journal of Power Sources 451 (1 March 2020): 227781. https://doi.org/10.1016/j.jpowsour.2020.227781.

[50] A. Daza, Yolanda, and John N. Kuhn. 'CO 2 Conversion by Reverse Water Gas Shift Catalysis: Comparison of Catalysts, Mechanisms and Their Consequences for CO 2 Conversion to Liquid Fuels'. RSC Advances 6, no. 55 (2016): 49675–91. https://doi.org/10.1039/C6RA05414E.

[51] Rezaei, Ebrahim, and Stephen Dzuryk. 'Techno-Economic Comparison of Reverse Water Gas Shift Reaction to Steam and Dry Methane Reforming Reactions for Syngas Production'. Chemical Engineering Research and Design 144 (1 April 2019): 354–69. https://doi.org/10.1016/j.cherd.2019.02.005.

[52] Ostadi, Mohammad, Kristofer Paso, Sandra Rodriguez-Fabia, Lars Øi, Flavio Manenti, and Magne Hillestad. 'Process Integration of Green Hydrogen: Decarbonization of Chemical Industries'. Energies 13 (17 September 2020). https://doi.org/10.3390/en13184859.

[53] Du, Yingmeng, Yanzhou Qin, Guobin Zhang, Yan Yin, Kui Jiao, and Qing Du. 'Modelling of Effect of Pressure on Co-Electrolysis of Water and Carbon Dioxide in Solid Oxide Electrolysis Cell'. International Journal of Hydrogen Energy 44, no. 7 (5 February 2019): 3456–69. https://doi.org/10.1016/j.ijhydene.2018.12.078.

[54] PIERRE, BAURENS, BORGARD JEAN-MARC, and ZNAIGUIA RAJA. Catalyst for Reverse Water Gas Shift Reaction (rwgs), Associated Rwgs Reaction and Method for in-Situ Regeneration of the Catalyst. EP3375513, filed 14 March 2018, and issued 19 September 2018. https://www.freepatentsonline.com/EP3375513.html.

[55] V. K. Jayaraman and B. D. Kulkarni, CHEMICAL ENGINEEERING AND CHEMICAL PROCESS TECHNOLOGY –Vol. III -Catalytic Reactors: A Review, page 4/9

[56] Kai Sundmacher, Achim Kienle and, Andreas Seidel-Morgenstern. Integrated Chemical Processes, pp 203-232

[57] Parra, Alejandro A. Munera, Carsten Asmanoglo, and David W. Agar. 'Cyclic Steady-State Behavior of a Fixed-Bed Adsorptive Reactor for Reverse Water-Gas Shift Reaction'. Chemical Engineering Technology 40, no. 5 (May 2017): 915–26. https://doi.org/10.1002/ceat.201600611.

[58] Munera Parra, Alejandro A., Carsten Asmanoglo, and David W. Agar. 'Modelling and Optimization of a Moving-Bed Adsorptive Reactor for the Reverse Water-Gas Shift Reaction'. Computers Chemical Engineering 109 (4 January 2018): 203–15. https://doi.org/10.1016/j.compchemeng.2017.11.013.

[59] Dzuryk, Stephen, and Ebrahim Rezaei. 'Intensification of the Reverse Water Gas Shift Reaction by Water-Permeable Packed-Bed Membrane Reactors'. Industrial Engineering Chemistry Research 59, no. 42 (21 October 2020): 18907–20. https://doi.org/10.1021/acs.iecr.0c02213.

[60] Green Car Congress. 'Velocys Sells Its Second Commercial License for FT Renewable Diesel and Jet Technology to Red Rock Biofuels'. Accessed 27 April 2022. https://www.greencarcongress.com/2018/05/20180504-velocys.html.

[61] Cui, Xiaoti, and S. Kær. 'Thermodynamic Analyses of a Moderate-Temperature Process of Carbon Dioxide Hydrogenation to Methanol via Reverse Water–Gas Shift with In Situ Water Removal'. Industrial Engineering Chemistry Research, 2019. https://doi.org/10.1021/ACS.IECR.9B01312.

[62] Matsubu, John C., Vanessa N. Yang, et Phillip Christopher. « Isolated Metal Active Site Concentration and Stability Control Catalytic CO2 Reduction Selectivity ». Journal of the American Chemical Society 137, n 8 (4 mars 2015): 3076-84. https://doi.org/10.1021/ja5128133.

[63] Oshima, Kazumasa, Tatsuya Shinagawa, Yukako Nogami, Ryo Manabe, Shuhei Ogo, et Yasushi Sekine. « Low Temperature Catalytic Reverse Water Gas Shift Reaction Assisted by an Electric Field ». Catalysis Today, The 14th Japan-Korea Symposium on Catalysis, July 1-3, 2013, Nagoya, Japan, 232 (1 septembre 2014): 27-32. https://doi.org/10.1016/j.cattod.2013.11.035.

[64] Lu, Baowang, et Katsuya Kawamoto. « Preparation of Mesoporous CeO2 and Monodispersed NiO Particles in CeO2, and Enhanced Selectivity of NiO/CeO2 for Reverse Water Gas Shift Reaction ». Materials Research Bulletin 53 (1 mai 2014): 70-78. https://doi.org/10.1016/j.materresbull.2014.01.043.

[65] Wang, Luhui, Shaoxing Zhang, et Yuan Liu. « Reverse Water Gas Shift Reaction over Co-Precipitated Ni-CeO2 Catalysts ». Journal of Rare Earths 26, n 1 (1 février 2008): 66-70. https://doi.org/10.1016/S1002-0721(08)60039-3.

[66] Wang, Luhui, Hui Liu, Yuan Liu, Ying Chen, et Shuqing Yang. « Effect of Precipitants on Ni-CeO2 Catalysts Prepared by a Co-Precipitation Method for the Reverse Water-Gas Shift Reaction ». Journal of Rare Earths 31, n 10 (1 octobre 2013): 969-74. https://doi.org/10.1016/S1002-0721(13)60014-9.

[67] Kharaji, Abolfazl Gharibi, Ahmad Shariati, et Mohammad Ali Takassi. « A Novel -Alumina Supported Fe-Mo Bimetallic Catalyst for Reverse Water Gas Shift Reaction ». Chinese Journal of Chemical Engineering 21, n 9 (1 septembre 2013): 1007-14. https://doi.org/10.1016/S1004-9541(13)60573-X.

[68] Goguet, A., F. Meunier, J. P. Breen, R. Burch, M. I. Petch, and A. Faur Ghenciu. 'Study of the Origin of the Deactivation of a Pt/CeO2 Catalyst during Reverse Water Gas Shift (RWGS) Reaction'. Journal of Catalysis 226, no. 2 (10 September 2004): 382–92. https://doi.org/10.1016/j.jcat.2004.06.011.

[69] 'Fischer-Tropsch Process'. Accessed 27 April 2022. http://wiki.gekgasifier.com/w/page/6123715/Gas%20to%20Liquids

[70] 'Fischer-Tropsch Process'. Accessed 27 April 2022. http://large.stanford.edu/courses/2015/ph240/dodaro1/.

[71] LAAN, GERARD, and A. BEENACKERS. 'Kinetics and Selectivity of the Fischer–Tropsch Synthesis: A Literature Review'. CATAL. REV.—SCI. ENG. 41(3-4) (2 November 2011): 255–318. https://doi.org/10.1081/CR-100101170.

[72] Greener Fisher-Tropsch Processes for Fuels and Feedstocks; Edited by Peter M. Maitlis, Arno de Klerk

[73] Ghogia, Amel, Ange Nzihou, Philippe Serp, Katerina Soulantica, and Doan Pham Minh. 'Cobalt Catalysts on Carbon-Based Materials for Fischer-Tropsch Synthesis: A Review', n.d., 107.

[74] Bian, G., N. Koizumi, and M. Yamada. 'Recent Development of Fischer-Tropsch (FT) Synthesis Catalyst'. Nihon Enerugi Gakkaishi/Journal of the Japan Institute of Energy 81 (1 November 2002): 974–80.

[75] 'Kerosene'. In Wikipedia, 19 April 2022. https://en.wikipedia.org/w/index.php?title=Kerosene&oldid=1083622543.

[76] Kumabe, Kazuhiro, Takuya Sato, Kozo Matsumoto, Yasuyuki Ishida, and Tatsuya Hasegawa. 'Production of Hydrocarbons in Fischer–Tropsch Synthesis with Fe-Based Catalyst: Investigations of Primary Kerosene Yield and Carbon Mass Balance'. Fuel 89, no. 8 (1 August 2010): 2088–95. https://doi.org/10.1016/j.fuel.2010.02.018.

[77] Espinoza, R. L., A. P. Steynberg, B. Jager, and A. C. Vosloo. 'Low Temperature Fischer–Tropsch Synthesis from a Sasol Perspective'. Applied Catalysis A: General 186, no. 1 (4 October 1999): 13–26. https://doi.org/10.1016/S0926-860X(99)00161-1.

[78] Meurer, Andreas, and Jürgen Kern. 'Fischer–Tropsch Synthesis as the Key for Decentralized Sustainable Kerosene Production'. Energies 14, no. 7 (January 2021): 1836. https://doi.org/10.3390/en14071836.

[79] Sie, S.T., Senden, M.M.G., and Van Wechem, H.M.W. (1991) Catal. Today, 8, 371-394.

[80] Asinger, F. (1968) Paraffins Chemistry and Technology, Pergamon, Oxford.

[81] Tsakoumis, Nikolaos E., Magnus Rønning, Øyvind Borg, Erling Rytter, and Anders Holmen. 'Deactivation of Cobalt Based Fischer–Tropsch Catalysts: A Review'. Catalysis Today, Eleventh International Symposium on Catalyst Deactivation , Delft(The Netherlands,) October 25-28, 2009., 154, no. 3 (15 September 2010): 162–82. https://doi.org/10.1016/j.cattod.2010.02.077.

[82] Dieterich, Vincent, Alexander Buttler, Andreas Hanel, Hartmut Spliethoff, and Sebastian Fendt. 'Power-to-Liquid via Synthesis of Methanol, DME or Fischer–Tropsch-Fuels: A Review'. Energy Environmental Science 13, no. 10 (14 October 2020): 3207–52. https://doi.org/10.1039/D0EE01187H.

[83] Vázquez, Francisco Vidal, Joonas Koponen, Vesa Ruuskanen, Cyril Bajamundi, Antti Kosonen, Pekka Simell, Jero Ahola, et al. 'Power-to-X Technology Using Renewable Electricity and Carbon Dioxide from Ambient Air: SOLETAIR Proof-of-Concept and Improved Process Concept'. Journal of CO2 Utilization 28 (1 December 2018): 235–46. https://doi.org/10.1016/j.jcou.2018.09.026.

[84] Cao, Chunshe, Jianli Hu, Shari Li, Wayne Wilcox, and Yong Wang. 'Intensified Fischer–Tropsch Synthesis Process with Microchannel Catalytic Reactors'. Catalysis Today, Catalysis and Chemistry for the Synthesis of Fuels, Chemicals and Petrochemicals, 140, no. 3 (28 February 2009): 149–56. https://doi.org/10.1016/j.cattod.2008.10.016.

[85] Becker, W. L., R. J. Braun, M. Penev, and M. Melaina. 'Production of Fischer–Tropsch Liquid Fuels from High Temperature Solid Oxide Co-Electrolysis Units'. Energy, Asia-Pacific Forum on Renewable Energy 2011, 47, no. 1 (1 November 2012): 99–115. https://doi.org/10.1016/j.energy.2012.08.047.

[86] Fu, Qingxi, Corentin Mabilat, Mohsine Zahid, Annabelle Brisse, and Ludmila Gautier. 'Syngas Production via High-Temperature Steam/CO2 Co-Electrolysis: An Economic Assessment'. Energy Environmental Science 3, no. 10 (29 September 2010): 1382–97. https://doi.org/10.1039/C0EE00092B.

[87] Ali, Khozema Ahmed, Ahmad Zuhairi Abdullah, and Abdul Rahman Mohamed. 'Recent Development in Catalytic Technologies for Methanol Synthesis from Renewable Sources: A Critical Review'. Renewable and Sustainable Energy Reviews 44 (1 April 2015): 508–18. https://doi.org/10.1016/j.rser.2015.01.010.

[88] Dieterich, Vincent, Alexander Buttler, Andreas Hanel, Hartmut Spliethoff, and Sebastian Fendt. 'Power-to-Liquid via Synthesis of Methanol, DME or Fischer–Tropsch-Fuels: A Review'. Energy Environmental Science 13, no. 10 (14 October 2020): 3207–52. https://doi.org/10.1039/D0EE01187H.

[89] Din, Israf Ud, Maizatul S. Shaharun, Mshari A. Alotaibi, Abdulrahman I. Alharthi, and A. Naeem. 'Recent Developments on Heterogeneous Catalytic CO2 Reduction to Methanol'. Journal of CO2 Utilization 34 (1 December 2019): 20–33. https://doi.org/10.1016/j.jcou.2019.05.036.

[90] Navarro-Jaén, Sara, Mirella Virginie, Julien Bonin, Marc Robert, Robert Wojcieszak, and Andrei Y. Khodakov. 'Highlights and Challenges in the Selective Reduction of Carbon Dioxide to Methanol'. Nature Reviews Chemistry 5, no. 8 (August 2021): 564–79. https://doi.org/10.1038/s41570-021-00289-y.

[91] Anicic, B., P. Trop, and D. Goricanec. 'Comparison between Two Methods of Methanol Production from Carbon Dioxide'. Energy 77 (1 December 2014): 279–89. https://doi.org/10.1016/j.energy.2014.09.069.

[92] Köppel, René A., Carsten Stöcker, and Alfons Baiker. 'Copper- and Silver–Zirconia Aerogels: Preparation, Structural Properties and Catalytic Behavior in Methanol Synthesis from Carbon Dioxide'. Journal of Catalysis 179, no. 2 (25 October 1998): 515–27. https://doi.org/10.1006/jcat.1998.2252.

[93] Kung, Harold H. 'Deactivation of Methanol Synthesis Catalysts - a Review'. Catalysis Today 11, no. 4 (22 January 1992): 443–53. https://doi.org/10.1016/0920-5861(92)80037-N.

[94] Wu, Jingang, Masahiro Saito, Masami Takeuchi, and Taiki Watanabe. 'The Stability of Cu/ZnO-Based Catalysts in Methanol Synthesis from a CO2-Rich Feed and from a CO-Rich Feed'. Applied Catalysis A: General 218, no. 1 (25 September 2001): 235–40. https://doi.org/10.1016/S0926-860X(01)00650-0.

[95] Jun, K., W. Shen, and Kyu-Wan Lee. 'CONCURRENT PRODUCTION OF METHANOL AND DIMETHYL ETHER FROM CARBON DIOXIDE HYDROGENATION: INVESTIGATION OF REACTION CONDITIONS'. Undefined, 1999. https://www.semanticscholar.org/paper/CONCURRENT-PRODUCTION-OF-METHANOL-AND-DIMETHYL-FROM-Jun-Shen/9ef5d9f3b9ce239d618fe0379ee740556c2bccd9.

[96] Kim, Jun-Sik, Sang-Bong Lee, Min-Chul Kang, Kyu-Wan Lee, Myoung-Jae Choi, and Yong Kang. 'Promotion of CO2 Hydrogénation to Hydrocarbons in Three-Phase Catalytic (Fe-Cu-K-Al) Slurry Reactors'. Korean Journal of Chemical Engineering 20, no. 5 (1 September 2003): 967–72. https://doi.org/10.1007/BF02697307.

[97] Shen, Wen-Jie, Ki-Won Jun, Ho-Suk Choi, and Kyu-Wan Lee. 'Thermodynamic Investigation of Methanol and Dimethyl Ether Synthesis from CO2 Hydrogenation'. Korean Journal of Chemical Engineering 17, no. 2 (1 March 2000): 210–16. https://doi.org/10.1007/BF02707145.

[98] Qi, Gong-Xin, Xiao-Ming Zheng, Jin-Hua Fei, and Zhao-Yin Hou. 'Low-Temperature Methanol Synthesis Catalyzed over Cu/-Al2O3–TiO2 for CO2 Hydrogenation'. Catalysis Letters 72, no. 3 (1 April 2001): 191–96. https://doi.org/10.1023/A:1009049523210.

[99] Ahouari, Hania, Ahcène Soualah, Anthony Le Valant, Ludovic Pinard, Patrick Magnoux, and Yannick Pouilloux. 'Methanol Synthesis from CO2 Hydrogenation over Copper Based Catalysts'. Reaction Kinetics, Mechanisms and Catalysis 110, no. 1 (1 October 2013): 131–45. https://doi.org/10.1007/s11144-013-0587-9.

[100] An, Xin, Yizan Zuo, Qiang Zhang, and Jinfu Wang. 'Methanol Synthesis from CO2 Hydrogenation with a Cu/Zn/Al/Zr Fibrous Catalyst'. Chinese Journal of Chemical Engineering 17, no. 1 (1 February 2009): 88–94. https://doi.org/10.1016/S1004-9541(09)60038-0.

[101] A. G. Linde, The Linde-Variobars Process for the Production of Methanol with the New Isothermal Reactor, CEER, Chem. Econ. Eng. Rev., 1983, 15, 14–16.

[102] Hirotani, Kunio, Hitoshi Nakamura, and Kazuo Shoji. 'Optimum Catalytic Reactor Design for Methanol Synthesis with TEC MRF-Z® Reactor'. Catalysis Surveys from Asia 2, no. 1 (1 March 1998): 99–106. https://doi.org/10.1023/A:1019061921451.

[103] K. Kobayashi, H. Osora, H. Nagai and H. Ohira, US Pat., 7189379, 2001

[104] vdocument.in. 'CASALE COAL-BASED AMMONIA and METHANOL ... COAL-BASED AMMONIA and METHANOL SYNLOOPS By P. Moreo Ammonia Casale SA and Methanol Casale SA, Switzerland Abstract AMMONIA and METHANOL - [PDF Document]'. Accessed 27 April 2022. https://vdocument.in/casale-coal-based-ammonia-and-methanol-coal-based-ammonia-and-methanol-synloops.html.

[105] Haid, Jürgen, and Ulrich Koss. 'Lurgi's Mega-Methanol Technology Opens the Door for a New Era in down-Stream Applications'. In Studies in Surface Science and Catalysis, edited by E. Iglesia, J. J Spivey, and T. H. Fleisch, 136:399–404. Natural Gas Conversion VI. Elsevier, 2001. https://doi.org/10.1016/S0167-2991(01)80336-0.

[106] 'Liquid-Phase Methanol (LPMEOH) Process, Clean Coal Technology Compendium'. Accessed 27 April 2022. https://sites.science.oregonstate.edu/~hetheriw/energy/topics/doc/elec/coal/clean/Liquid-Phase_Methanol_(LPMEOH)_Process,_Clean_Coal_Technology_Compendium.htm.

[107] Ruokonen, Jenna, Harri Nieminen, Ahmed Rufai Dahiru, Arto Laari, Tuomas Koiranen, Petteri Laaksonen, Ari Vuokila, and Mika Huuhtanen. 'Modelling and Cost Estimation for Conversion of Green Methanol to Renewable Liquid Transport Fuels via Olefin Oligomerisation'. Processes 9, no. 6 (June 2021): 1046. https://doi.org/10.3390/pr9061046.

[108] Exxonmobil chemical. 'Methanol conversion to gasoline technology'. https://www.exxonmobilchemical.com/-/media/project/wep/exxonmobil-chemicals/chemicals/products/technology-licensing-and-services/methanol-to-gasoline-synthesis/methanol_to_gasoline_factsheet_enpdf.pdf

[109] Dieterich, Vincent, Alexander Buttler, Andreas Hanel, Hartmut Spliethoff, and Sebastian Fendt. 'Power-to-Liquid via Synthesis of Methanol, DME or Fischer–Tropsch-Fuels: A Review'. Energy Environmental Science 13, no. 10 (14 October 2020): 3207–52. https://doi.org/10.1039/D0EE01187H.

[110] Zaretskij, M.I. 'Production of Gasoline from Methanol', 1 January 2005, 29–31.

[111] Avidan, A. A. 'Gasoline and Distillate Fuels From Methanol'. In Studies in Surface Science and Catalysis, edited by D. M. Bibby, C. D. Chang, R. F. Howe, and S. Yurchak, 36:307–23. Methane Conversion. Elsevier, 1988. https://doi.org/10.1016/S0167-2991(09)60524-3.

[112] Tabak, S. A., and S. Yurchak. 'Conversion of Methanol over ZSM-5 to Fuels and Chemicals'. Catalysis Today 6, no. 3 (1 January 1990): 307–27. https://doi.org/10.1016/0920-5861(90)85007-B.

[113] Rolando Danesi, "Products – Peimar – A wide choice to meet every need," Peimar. (accessed May 13, 2022) https://www.peimar.com/us/home/products/

[114] « JRC Photovoltaic Geographical Information System (PVGIS) - European Commission ». Consulté le 23 mai 2022. https://re.jrc.ec.europa.eu/pvg_tools/en/#MR.

[115] Christensen, R. (2018). Na-S battery. In Technology Data for Energy storage: November 2018 (pp. 129-146). https://backend.orbit.dtu.dk/ws/files/163012494/Pages_NA_S_BATTERY.pdf

[116] NGK. « NAS Batteries ». Consulté le 28 mai 2022. https://www.ngk-insulators.com/en/product/nas.html.

[117] Cummins Inc. « Hydrogen Generation ». Consulté le 29 mai 2022. https://www.cummins.com/new-power/applications/about-hydrogen.

[118] Nel Hydrogen. « Atmospheric Alkaline Electrolyser », 31 mai 2018. https://nelhydrogen.com/product/atmospheric-alkaline-electrolyser-a-series/.

[119] Sunfire. « Sunfire - Renewable Hydrogen (HyLink) ». Consulté le 29 mai 2022. https://www.sunfire.de/en/hydrogen.

[120] Sunfire. « Sunfire - Renewable Syngas (SynLink) ». Consulté le 29 mai 2022. https://www.sunfire.de/en/syngas.

[121] Züttel, Andreas. « Hydrogen Storage Methods ». Die Naturwissenschaften 91, n 4 (avril 2004): 157-72. https://doi.org/10.1007/s00114-004-0516-x.

[122] Linde Gas. « H2 Fueling Technologies ». Consulté le 29 mai 2022. https://www.linde-gas.com/en/processes/hydrogen_energy_h2/h2_one_stop_shop/h2_fuelling_technologies/index.html.

[123] Simoes, Sofia G., Justina Catarino, Ana Picado, Tiago F. Lopes, Santino di Berardino, Filipa Amorim, Francisco Gírio, C. M. Rangel, et Teresa Ponce de Leão. « Water Availability and Water Usage Solutions for Electrolysis in Hydrogen Production ». Journal of Cleaner Production 315 (15 septembre 2021): 128124. https://doi.org/10.1016/j.jclepro.2021.128124.

Appendices

Reverse Water Gas Shift

CO2 Conversion:	0,55
CO Selectivity:	1

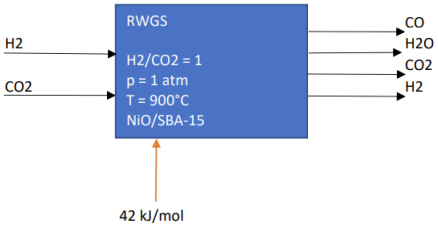

	CO2	+	H2	<=>	CO	H2O	ΔH (MJ/mol)	0,042	
mass flow in (kg/s)	4,4		0,2		0	0			
molar flow in (mol/s)	100		100		0	0			
mass flow out (kg/s)	1,98		0,09		1,54	0,99			
molar flow out (mol/s)	45		45		55	55			
									Sum
Energy flow in (MW)(HHV)	0		28,6		0	0		2,31	30,91
Energy flow out (MW)(HHV)	0		12,87		15,5782	0		0	28,45
									Sum
Energy flow in (MW)(LHV)	0		23,992		0	0		2,31	26,302
Energy flow out (MW)(LHV)	0		10,7964		15,5782	0		0	26,3746

molecules	Molar mass (kg/kmol)	HHV (MJ/kg)	LHV (MJ/kg)
H2	2	141,8	119,9
CO2	44	0	0
CO	28	10,1	10,1
H2O	18		

Efficiency (based on HHV without the gas enthalpy taken into account):	0,92035587
Efficiency (based on LHV without the gas enthalpy taken into account):	1,00276025

Figure 56: Efficiency calculation for the RWGS reactor

Methanol From Syngas

CO Conversion:	0,94	per pass (around 50%)
CH3OH Selectivity:	0,99	

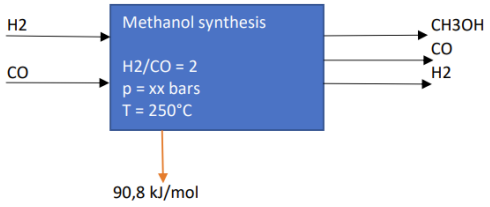

	CO	+	2 H2	<=>	CH3OH	ΔH (MJ/mol)	0,0906	
mass flow in (kg/s)	2,8		0,4		0			
molar flow in (mol/s)	100		200		0			
mass flow out (kg/s)	0,168		0,024		2,97792			
molar flow out (mol/s)	6		12		93,06			
								Sum
Energy flow in (kW)(HHV)	28,28		56,72		0		0	85
Energy flow out (kW)(HHV)	0		3,4032		67,598784		8,431236	79,43322
								Sum
Energy flow in (kW)(LHV)	28,28		47,96		0		0	76,24
Energy flow out (kW)(LHV)	0		2,8776		59,260608		8,431236	70,569444

Molecule	Molar mass (kg/kmol)	HHV (MJ/kg)	LHV (MJ/kg)
H2	2	141,8	119,9
CH3OH	32	22,7	19,9
CO	28	10,1	10,1
H2O	18		

HHV Efficiency:	0,93450847
LHV Efficiency:	0,9256223

Figure 57: Efficiency calculation for the methanol from Syngas synthesis

Methanol synthesis from CO2

CO2 Conversion:	0,94	per pass (around 21%)
CH3OH Selectivity (from CO2):	0,68	value found in :
CO Selectivity:	0,31	
CH3OH Selectivity (from CO):	0,99	

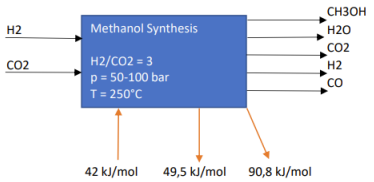

If CO reacts also in the reactor with 94% conversion, CO + 2H2 => CH3OH ΔH (MJ/mol) 0,0906

	CO2	+	3 H2	<=>	CO	H2O	CH3OH	ΔH (MJ/mol)	0,0495	0,042	0,0906	
mass flow in (kg/s)	4,4		0,6		0	0	0					
molar flow in (mol/s)	100		300		0	0	0					
mass flow out (kg/s)	0,264		0,1582		0,81592	1,67508	2,04544					
molar flow out (mol/s)	6		79,1		29,14	93,06	63,92					
after CO reacts (mol/s)	6		24,864632		1,7484	93,06	91,037684					
mass flow OUT final (kg/s)	0,264		0,04972926		0,0489552	1,67508	2,91320589					
												Sum
Energy flow in (kW)(HHV)	0		85,08		0	0	0		0	1,22388	0	86,30388
Energy flow out (kW)(HHV)	0		7,05160964		0,49444752	0	66,1297737		3,16404	0	2,45686217	79,296733
												Sum
Energy flow in (kW)(LHV)	0		71,94		0	0	0		0	1,22388	0	73,16388
Energy flow out (kW)(LHV)	0		5,96253875		0,49444752	0	57,9727972		3,16404	0	2,45686217	70,0506856

molecule	Molar mass (kg/kmol)	HHV (MJ/kg)	LHV (MJ/kg)
H2	2	141,8	119,9
CO2	44	0	0
CO	28	10,1	10,1
H2O	18		
CH3OH	32	22,7	19,9

(HHV)Efficiency when the reaction of CO to CH3OH is taken into account in the reactor:	0,91880844
(LHV)Efficiency when the reaction of CO to CH3OH is taken into account in the reactor:	0,95744903

Figure 58: Efficiency calculation for the methanol from CO_2 synthesis

MTO-MOGD process

		kg/h	HHV - MJ/kg	LHV - MJ/kg	
in	Methanol	3000	22,7	19,9	
in	H2	7,36	141,8	121	
out	Diesel	591	44,8	43,4	
out	Gasoline	224	47,3	44,4	
out	Kerosene	356	46,2	43	
out	LPG	59,1	49,3	45,5	
out	Fuel gas	98,1	52,22	47,1	assumed as natural gas (fuel gas = mixed of gaseous fuel so propane, methane, ...

HHV - energy flow in:	69143,65	MWh
HHV - energy flow out:	61555,61	MWh
HHV-based efficiency:	0,890256933	

LHV - energy flow in:	60590,56	MWh
LHV - energy flow out:	58212,56	MWh
LHV-based efficiency:	0,960753	

Fraction	Stream type	Mass Flow (kg/h)	Calculated Hydrocarbon Yield (wt%)	Reference Hydrocarbon Yield (wt%)
Methanol	Inlet	3000	-	-
Hydrogen	Inlet	7.36	-	-
Gasoline	Outlet	224	17	15
Diesel	Outlet	591	45	57
Kerosene	Outlet	356	27	25
Fuel Gas	Outlet	98.1	7.4	1
LPG	Outlet	59.1	4.5	2
Purges	Outlet	1.47	-	-
Water	Outlet	1679	-	-
Total			100	100

MTG process

By considering that the product of the MTG process contains 56wt% of water (correspond to value found in literature + above), the mass flow of product of a production plant utilising 3000 kg/h of methanol as inlet feed can be estimated as the following

		%	kg/h	HHV -MJ/kg	LHV - MJ/kg	
in	Methanol	0,997553	3000	22,7	19,9	
in	H2	0,002447	7,36	141,8	121	No futher information so considered equal to the value for the MTO-MOGD process
out	Water	56	1684,1216	0	0	
out	Light gas	0,616	18,5253376	52,22	47,1	assumed as natural gas (fuel gas = mixed of gaseous fuel so propane, methane, ...
out	Propane	2,42	72,778112	50,35	46,35	
out	Propene	0,088	2,6464768	48,82	45,8	
out	Isobutane	3,784	113,7985024	49,1	45,6	
out	n-Butane	1,452	43,6668672	49,5	45,75	value for butane
out	Butenes	0,484	14,5556224	48,33	45,33	
out	C5+ gasoline	35,156	1057,267482	47,3	44,4	
		100	3007,36			

HHV - Energy flow in:	69143,65	MWh
HHV - Energy flow out:	63222,21	MWh
HHV-based efficiency:	0,914360399	

LHV - energy flow in:	60590,56	MWh
LHV - energy flow out:	59156,47	MWh
LHV-based efficiency:	0,976331	

Figure 59: Efficiency calculation for the MtG and MTO-MOGD unit

UNIVERSITÉ CATHOLIQUE DE LOUVAIN
École polytechnique de Louvain
Rue Archimède, 1 bte L6.11.01, 1348 Louvain-la-Neuve, Belgique | **www.uclouvain.be/epl**